UNIVERSITY OF LATVIA
FACULTY OF PHYSICS, MATHEMATICS AND OPTOMETRY

UNIVERSITY
OF LATVIA

Ferrofluid thermophoresis in porous medium in dependence of surfactant concentration and temperature

Viesturs Šints

A thesis presented for the degree of
Doctor of physics and astronomy
Thesis advisor: Elmārs Blūms

Riga, 2020

Abstract

Results of experimental research into magnetic colloid non-isothermal mass transfer phenomena and characteristics are presented in this thesis. At focus of the research is effects of excess surfactant on surfactant stabilized colloid thermophoresis and physical characteristics, and temperature dependence of colloid mass transfer coefficients. Colloid thermophoresis and mass diffusion is investigated in free fluid conditions and in a porous medium, comparison between the two environments providing a third focal point for the research presented here. In addition, effect of an external magnetic field on ferrofluid thermophoresis and mass diffusion is investigated. Investigations carried out in a porous medium rely on magnetic properties of the colloidal nanoparticles, which enable measurement options not available for non-magnetic particles - specifically, Vibrating sample magnetometry. Mass transfer processes in free fluid conditions are measured by Forced Rayleigh scattering. Other measurement methods are employed for further characterization of the ferrofluids and cross confirmation of certain results. The results demonstrate that both temperature and amount of excess surfactant act to decrease ferrofluid Soret coefficient. In a porous layer, this reduction has been shown to change particle behavior from thermophobic to thermophilic, resulting in a negative Soret coefficient. Viscosity of a ferrofluid has been found to have a curious dependency on excess surfactant amount. Theoretical predictions on effect of an external magnetic field on Soret and mass diffusion coefficients have been confirmed.

Anotācija

Disertācijā izklāstīti eksperimentālu pētījumu rezultāti, kas apskata neizotermiskus magnētisku koloīdu masas pārneses procesus un ar šiem procesiem saistītus koloīdu raksturlielumos. Pētījumu uzmanības centrā ir papildus virsmaktīvās vielas pievienošanas ietekme uz ar virsmaktīvo vielu stabilizētu koloīdu termoforēzi un fizikālajiem raksturlielumiem, kā arī koloīdu masas pārneses koeficientu atkarība no temperatūras. Koloīdu termoforēze un masas pārnese tikusi pētīta gan brīvā šķidrumā, gan porainā vidē. Šo divu metožu salīdzinājums ir trešais no centrālajiem šī darba pētījumu aspektiem. Papildus tam, ticis izmeklēts arī ārēja magnētiska lauka iespaids uz magnētisko šķidrumu termoforēzi un masas difūziju. Pētījumos porainā vidē, mērījumu veikšanai tikušas izmantotas koloidālo nanodaļiņu magnētiskās īpašības, kas padarījušas iespējamas mērījumu metodes, kas nav pieejamas nemagnētisku koloīdu izpētē - proti, vibrējošu paraugu magnetometriju. Masas pārneses procesi brīvā šķidrumā tikuši veikti ar uzspiestās Releja izkliedes metodi. Vēl citas mērījumu metodes tikušas izmantotas tālākā šķidrumu raksturošanā un mērījumu rezultātu salīdzinājumam starp vairākām metodēm. Iegūtie rezultāti demonstrē Sorē koeficienta samazināšanos temperatūras un papildus virsmaktīvās vielas daudzuma ietekmē. Porainā slānī, šis samazinājums var novest pie negatīvām Sorē koeficienta vērtībām, kas iezīmē pāreju koloidālo daļiņu uzvedībā, no termofobas uz termofīlu. Ir tikusi atklāta neparasta magnētiskā šķidruma viskozitātes atkarība no pievienotā papildus virsmaktīvās vielas daudzuma. Gūts eksperimentāls apstiprinājums modelim, kas apraksta ārēja magnētiskā lauka ietekmi uz Sorē un masas difūzijas koeficientiem.

Acknowledgements

I would like to acknowledge the contributions of current and former colleagues, collaborators in research, coauthors of articles, general supporters and partners in discussions: Gunars Kronkalns, Michail Maiorov, Ansis Mezulis, Dmitry Zablotsky, Kaspars Erglis, Mitradeep Sarkar, Régine Perzynski, Jesse Riedl, Gilles Demouchy, Emmanuelle Dubois, Oksana Petricenko and Lasma Pukina. Special thanks to my thesis advisor Elmars Blums and to Guntars Kitenbergs for various means of support. I would also like to thank the kind people from University of Latvia for providing occasional funding for my research and Gints Rieksts for his help in attaining said funding. I further acknowledge the input of the anonymous reviewers of my rejected article and their extensive commentary. Writing of this thesis would not have been possible without support from my girlfriend Klinta, as well as from my mother.

Contents

Introduction

Context and motivation

In this thesis, experimental research results of processes and changes in characteristics of ferrofluids in non-isothermal conditions are presented. As such, the body of research given for readers' consideration here touches upon two intriguing subjects. One is the nature of magnetic fluids, understood here as fluids composed of single domain magnetic particles colloidally dispersed in a liquid carrier, alternatively (and seemingly more popularly) denoted as ferrofluids. This fascinating class of materials has been a source of research interest and applications since it's definition in the 1960s, see refs. [1] and [2] for historical context. Understanding of processes in ferrofluids driven by a temperature gradient is highly relevant to their thermal applications, both classical, like loudspeaker cooling, and an ever expanding list of novel ones, like in solar collectors[3], electrochemical thermal energy harvesters[4] and cooling of electronic devices[5].

The other point of interest here is colloidal particle thermophoresis. Thermodiffusion, the effect of mass flux induced by a temperature gradient, was first described by Ludwig and Soret in the 19th century (see ref. [6] for an introduction on the topic), and is hence sometimes referred to as Ludwig - Soret effect. This is a curious subject, as thermodiffusion in liquids is as of yet lacking a universally accepted theoretical interpretation[7] and colloidal particle thermophoresis is considered a challenging subject both theoretically and experimentally [8]. This lack of fundamental understanding makes this direction of research interesting from the perspective of insight into the physical phenomena concerned.

A source of interest in experimental research of role played by excess surfactant on physical characteristics of a surfactant stabilized colloid, looking from the perspective of field of magnetic fluids, concerns the possible

implications on manufacturing processes of these colloids for certain applications, where a role played by excess surfactant presence on certain ferrofluid properties should be considered. Investigation into peculiarities of ferrofluid viscosity as a function of surfactant concentration holds interest in contexts not limited to thermal applications. Interaction between surfactant and colloid might also hold some interest from the perspective of surfactant research, with their role in commercial applications like those related to cosmetics, and the less attractive importance as a pollutant[9] being potentially relevant to experimental results concerning surfactant effects on colloid properties.

Porous medium holds interest as an experimental system for thermally driven mass transfer research, be it due to the suppression of convective flow in such an environment, see for example ref. [10], interest in thermogravitational separation[11] or the related environmental and industrial processes[12]. It has been shown in previous experimental research[13] that thermophoretic ferrofluid transfer in a porous environment is much reduced compared to free fluid conditions. Authors of this work associated their observations with interaction between surfactant and the porous material. This finding has served as motivation for the research described in this thesis. Properly understood, this phenomena might expand the possibilities of tuning surfactant stabilized ferrofluid properties by altering their composition, thereby allowing optimization of them for certain applications, much like it is being successfully done with charged ferrofluids by varying ionic strength, see refs. [14] and [15].

Convection suppression provided by a porous environment holds an additional importance in magnetic systems, where thermomagnetic convection can affect mass transfer in the presence of a magnetic field and a temperature gradient, which provides a significant challenge to experimental research of thermophoresis in a magnetic field[16]. Introduction of a porous environment can solve the convection problem, however, new possible interactions between the porous material, mass flux and magnetic field can arise. These include microconvection induced by nonmagnetic grains[17] and magnetic pressure acting upon boundaries of a porous layer if such are exposed to mass flow and a magnetic field[18]. An experimental system that would exclude these possible interactions would provide the possibility of investigating effects of a high magnetic field on ferrofluid thermophoresis. A porous layer as used in the aforementioned research presented in ref. [13] could be employed as such a system, which provides additional motivation for deepening our understanding on thermophoresis in a porous layer.

Crucially, an opportunity has been taken to employ magnetic properties of ferrofluids as a tool for performing challenging measurements, such as those concerning colloidal particle transport within a porous medium.

Goal of thesis and set tasks

Goal

Demonstrate and investigate the effects of excess surfactant amount, temperature, porous medium and an external magnetic field on ferrofluid thermophoresis and physical characteristics and processes within a ferrofluid that are related to thermophoresis.

Tasks

1. Examine ferrofluid viscosity and particle size at multiple values of temperature and excess surfactant concentration; conclude if and how these ferrofluid parameters depend on temperature and amount of excess surfactant
2. Investigate ferrofluid thermophoresis and the influence of temperature and excess surfactant on thermophoretic and diffusive mass transfer of magnetic colloids; observe the effects of a porous medium on ferrofluid thermophoresis and mass diffusion
3. Characterize the influence of temperature and excess surfactant on carrier fluid (magnetic nanocolloid solvent) thermoosmosis; evaluate this influence in the context of thermophoretic particle transfer
4. Experimentally verify the effect of an external magnetic field on diffusive and thermophoretic transfer of magnetic nanoparticles in a porous environment

Thesis statement

Presence of excess surfactant, a porous environment and temperature all influence characteristics of ferrofluids in a way that significantly alters the properties and behavior of surfactant stabilized ferrofluid under a temperature gradient.

Structure of thesis

- In chapter 1, the theoretical basis employed in further sections is established
- Overview of ferrofluids used in experimental work is provided in chapter 2, along with select properties of the fluids. Other physical properties and their dependence on parameters related to experimental work described in this thesis are investigated in further chapters
- Experimental methods are described in chapter 3
- Investigation of ferrofluid properties and their dependence on temperature and amount of excess surfactant is described in chapters 4 (viscosity) and 5 (particle size and mass diffusion coefficient), both chapters therefore contributing to resolution of task 1. In ch. 5, measurements of mass transfer coefficients and experiments in a porous layer are introduced, which is the first contribution to task 2
- In chapter 6, ferrofluid thermophoresis is investigated. The results provided in this chapter are arguably the most curious in this thesis and cover the remainder of task 2
- Chapter 7 is dedicated to thermoosmosis experiments, conducted in an attempt to provide interpretation to results of ch. 6, this chapter covers task 3
- Effects of an external magnetic field on ferrofluid mass transfer coefficients are investigated in chapter 8, fulfilling task 4

A partial glossary

c	nanoparticle mass concentration
C	nanoparticle relative mass concentration
ϕ	nanoparticle volume concentration
Φ	nanoparticle relative volume concentration
c_s	surfactant mass concentration
X	relative distance (definition not fixed and given in each relevant section)
η	dynamic viscosity
ν	kinematic viscosity
γ	surface tension
S_T	Soret coefficient
D_m	mass diffusion coefficient
D_T	thermodiffusion coefficient
d_T	carrier fluid thermoosmosis coefficient
d_h	hydrodynamic diameter of a colloidal particle
τ	non-dimensional time
E_a	Arrhenius activation energy
δ	porous layer thickness
a	layer thickness parameter
τ_d	tortuosity of a porous medium
$S_{T,1}$, T_0, T^*	coefficients for an empirical model for $S_T(T)$, see sect. 6.4.2
A, B	coefficients for a linear model for $S_T(T)$, see sect. 6.4.2
α_{ij}	linear coefficient in Onsager equation system, see sect. 1.3
α	manometer incline angle
$\vec{j}$	mass flux of a component
$\vec{v}$	flow velocity
K	permeability of a porous medium

Chapter 1

Review of theoretical concepts and previous studies

1.1 Ferrofluids as colloids

Ferrofluids are colloids with single domain magnetic colloidal particles. The basic understanding of ferrofluids in this section comes from Rosensweig's fundamental book on the subject, "Ferrohydrodynamics", see ref. [19].

The matter of colloidal stability is a paramount aspect to consider in colloid physics, and it is for the reason of maintaining it that gives ferrofluids some of the structural properties investigated in this thesis. Indeed, as suggested by Doi[20], often in colloids it is in fact rate of agglomeration that should be looked at, rather than colloidal stability, due to unlikeliness of the latter to be achieved. In ferrofluids, colloidal stability is determined not only by sedimentation, and van der Waals attraction, but also by magnetic dipole - dipole interaction.

Both gravitational sedimentation and magnetic agglomeration are countered by thermal motion of the particles. Balances of thermal energy and that of gravitational and magnetic nature can both be expressed in terms of particle diameter, setting size limitations for the particles. Gravitational considerations yield:

$$d =\leq \left(\frac{6k_BT}{\pi\rho gL}\right)^{(1/3)} \tag{1.1}$$

where L is the height over which particle concentration would decrease

by a factor of e. Balance of magnetic and thermal energy gives:

$$d =\leq \left(\frac{72k_BT}{\pi\mu_0 M^2}\right)^{(1/3)} \tag{1.2}$$

where M is magnetization. Sedimentation would limit particle size to $d \approx 15-20\,nm$ and is of no real concern. Magnetism would give a maximum size for a magnetite particle of $d = 7.2\,nm$, and that is already on the verge of size for particles used in the research reported on in this thesis. Then, there is still the matter of van der Waals attraction.

To ensure colloidal stability, the particles are covered with a layer intended to prevent agglomeration. In sterically stabilized ferrofluids (also referred to as surfactant stabilized, or surfaced), molecules of surfactants are adsorbed on to surface of the particles. The polar head group is then fixed at the particle and the chain tails are pointed outwards, see fig. 1.1 for illustration. Another way to achieve colloidal stability is through electrostatic interaction. Agglomeration can be prevented by surface charge on the particles. This class of ferrofluids is referred to as "ionic". The concept is explained in ref. [21]. In citrated ferrofluids, the charged particle surfaces attract chain molecules that add steric repulsion to electrostatic one[22].

A note should be made that, because of the covering of the particles, a distinction between two characteristic "sizes" can be made - that of the magnetic core particle, and that of the colloidal particle, including the layer around it. Existing research, such as by Zhang *et al.*[23], has shown iron oxide nanoparticle size to increase by around $4\,nm$ as the particles are coated with oleic acid - that is, twice the OA molecule length, which is around $2\,nm$.

Incomplete surfactant covering of nanoparticles has been found by Susan-Resiga[24] *et al.* to lead to particle clustering. In the research mentioned, the source of imperfect covering was identified as presence of poorly stabilizing surfactant among the desired surfactant material. Buzmakov and Pshenichnikov[25] reported on NP aggregates in ferrofluids, noting a distinction between aggregates that are stable with respect to temperature alteration, and those forming in a reversible way under temperature variation. Hoell *et al.* looked at the nanoscale structure of magnetite nanoparticles by means of neutron scattering and found that, while a double layer of the surfactant, oleoylsarcosine, formed in a water based ferrofluid, it did not form in toluene, which is more relevant to the colloids used in research reported on in this thesis[26].

Figure 1.1: Visual representation of a sterically stabilized ferrofluid magnetite particle. The red circle represents the magnetic core made of magnetite. The size of this core is referred to as magnetic size. The dashed line represents the entire colloidal particle - magnetic core together with a layer of surfactant. The size of this particle is referred to as hydrodynamic size

1.2 Ferrofluid magnetic properties

Magnetic properties of a ferrofluid are determined by the structure of it - single domain particles made from a material with a known magnetization act as magnetic dipoles. Magnetic moment of a single nanoparticle is:

$$m = M_d V_p \tag{1.3}$$

where M_d is domain magnetization of particle material and V_p is particle volume. The particles are suspended in the carrier fluid. In the absence of a magnetic field, and with no agglomeration taking place, particle moments are not aligned to each other and there is no long range order, as thermal fluctuations reorient the magnetic moments in a random manner. When a magnetic field is applied to a ferrofluid, the particle moments align with the field, giving rise to ferrofluid magnetization. This kind of magnetic behavior is termed "superparamagnetism" (differing to paramagnetism in that low and medium field magnetization is much larger).

Ferrofluid magnetization is described by:

$$M(H) = M_S L(\xi) \tag{1.4}$$

where M_S is saturation magnetization of ferrofluid and $L(\xi)$ is the Langevin function, so that:

$$M(H) = M_S \left[\coth(\xi) - \frac{1}{\xi} \right] \tag{1.5}$$

with

$$\xi = \mu_0 \frac{mH}{k_B T} \tag{1.6}$$

where m is magnetic dipole moment of a particle. The full equation is, then:

$$M(H) = M_S \left[\coth\left(\mu_0 \frac{mH}{k_B T} \right) - \frac{k_B T}{\mu_0 m H} \right] \tag{1.7}$$

It may be beneficial to consider in stead of a single magnetic moment of a particle value, a distribution of magnetic moments, as particles in a ferrofluid cover a range of volumes and, therefore, magnetic moments. Then, eq. 1.7 becomes[27]:

$$M(H) = M_d \int_{m1}^{m2} f(m) \left[\coth\left(\mu_0 \frac{mH}{k_B T} \right) - \frac{k_B T}{\mu_0 m H} \right] dm \tag{1.8}$$

Here, m_1 and m_2 are the lower and upper boundaries for possible magnetic moment values and $f(m)$ represents distribution of particle sizes (in terms of volume density) and, therefore, dipole moments.

1.3 Thermodynamic processes in ferrofluids

Mass and energy transfer processes in colloids are viewed here in the context of non-equilibrium thermodynamics. The fundamental basis here is not a topic of this thesis, and is only touched upon briefly to provide context for equations directly employed in the work presented here, found at the end of this section. The understanding given here is largely based on books by Callen (ref. [28]) and Blundell and Blundell (ref. [29]).

The first law of thermodynamics can be rewritten for local entropy ds, taking into account that $dQ = TdS$, as:

$$ds = \frac{1}{T}du + \sum_j \frac{\mu_j}{T} dN_j \tag{1.9}$$

Here, du denotes internal energy density, N_j is number of particles for species denoted by j and μ_j is the chemical potential of said species. At this point, generalized densities are introduced, denoted by ρ_k (for example: du, dN_j), as well as generalized potentials, denoted Φ_k (for example: $\frac{1}{T}$). Then, eq. 1.9 becomes:

$$ds = \sum_j \Phi_k d\rho_k \tag{1.10}$$

For the generalized densities, continuity equation is true: $\frac{\partial \rho_k}{\partial t} + \nabla \vec{J}_k = 0$, where $\vec{J}_k$ are generalized current densities. For entropy current density, continuity is in the form $\frac{\partial s}{\partial t} + \nabla \vec{J}_s = \Sigma$, where Σ is local entropy production rate. Entropy current density can be related to other current densities by $\vec{J}_s = \sum_k \Phi_k \vec{J}_k$. It can then be shown that, then $\Sigma = \sum_k \nabla \Phi_k \vec{J}_k$.

By assuming for the response of a generalized current density J_i to a generalized force field $\nabla \Phi_j$ to be linear, a relation can be written, in general, as:

$$\vec{J}_i = \sum_j L_{ij} \nabla \Phi_j \tag{1.11}$$

Coefficients L_{ij} are known as kinetic coefficients. Onsager's reciprocal relations tell us that

$$L_{ij} = L_{ji}. \tag{1.12}$$

It should be pointed out that this relation is only true when the principle of microscopic reversibility is true. Mazur and de Groot[30] extended Onsager's reciprocal relations to systems with magnetic field, arriving at relation $L_{ij}(r', B'; r, B) = L_{ji}(r, B; r', B')$, where r and r' indicate spatial coordinates at two positions in the system and B and B' denote magnetic field at those positions.

If we recall how the generalized potentials were introduced, we see that the generalized current densities given by eq. 1.11 can be written out for a system of two components and energy as

$$\begin{cases} \vec{J}_u & = L_{uu}\nabla\frac{1}{T} + L_{uN1}\nabla\frac{\mu_1}{T} + L_{uN2}\nabla\frac{\mu_2}{T} \\ \vec{J}_{N1} & = L_{N1u}\nabla\frac{1}{T} + L_{N1N1}\nabla\frac{\mu_1}{T} + L_{N1N2}\nabla\frac{\mu_2}{T} \\ \vec{J}_{N2} & = L_{N2u}\nabla\frac{1}{T} + L_{N2N1}\nabla\frac{\mu_1}{T} + L_{N2N2}\nabla\frac{\mu_2}{T} \end{cases} \tag{1.13}$$

The three flows are thus expressed through generalized force fields for energy $\left(\nabla\frac{1}{T}\right)$ and the two species particle count $\left(\nabla\frac{\mu_j}{T}\right)$.

For a colloidal system[31], the system of equations 1.13 can be written for flows of solvent, solute (both in $\frac{mol}{m^2 s}$) and heat ($\frac{J}{m^2 s}$):

$$\begin{cases} \vec{J}_{fluid} & = \alpha_{11}\nabla\mu_1 + \alpha_{12}\nabla\mu_2 + \alpha_{13}\frac{\nabla T}{T} \\ \vec{J}_{particles} & = \alpha_{21}\nabla\mu_1 + \alpha_{22}\nabla\mu_2 + \alpha_{23}\frac{\nabla T}{T} \\ \vec{J}_{heat} & = \alpha_{31}\nabla\mu_1 + \alpha_{23}\nabla\mu_2 + \alpha_{33}\frac{\nabla T}{T} \end{cases} \tag{1.14}$$

The chemical potentials can be interpreted as $\nabla\mu_1 = -V_1\nabla p$, where V_1 is solvent molar volume, and $\nabla\mu_2 = \left(\frac{\partial\mu_2}{\partial\phi}\right)_p \nabla\phi$. Mass and heat flows of a colloid can thereby be described as driven by gradients of pressure, particle concentration and temperature.

A number of relations given by system 1.14 correspond to phenomenological laws of physics, for example, $\vec{J}_{fluid} = \alpha_{12}\nabla\mu_2$, which can be written as $\vec{J}_{fluid} = -d_p\nabla c$ (d_p being the osmotic coefficient), is osmosis and $\vec{J}_{particles} = \alpha_{22}\nabla mu_2$ written as $\vec{J}_{particles} = -D_m\nabla c$ is Fick's law of diffusion, with D_m being mass diffusion coefficient.

Equation for heat flux from system 1.14 describes the processes of convective enthalpy transport, Dufour effect and thermal diffusivity. As shown by Blums in ref. [32], for a ferrofluid with characteristics closely resembling the fluids used in experimental work described in this thesis, convective enthalpy transport and the Dufour effect both give a negligibly small contribution to the heat flow (it has been suggested by Würger that coefficients for thermal diffusion and Dufour effect do not satisfy Onsager's relations for colloid thermophoresis[33]). With these two cross effects, convective enthalpy transport and the Dufour effect, discarded, heat flow is driven solely by temperature gradient.

1.4 Colloid thermophoresis

Third term of particle flow equation in system 1.14 refers to species mass flux driven by a temperature gradient. This is called the Ludwig-Soret effect, or simply Soret effect. For mass transfer of particles under their own mass concentration gradient ∇c and temperature gradient, we can write mass flux of the particles as(here and up until the definition of Soret coefficient, approach given in ref. [34] is followed):

$$\vec{J}_{particles} = -D_m \nabla c - F(c) D_T \nabla T \tag{1.15}$$

Here, D_T is thermodiffusion coefficient. It is common to use $F(c) = c(1-c)$, c here being mass fraction of particles, and to assume that $c(1-c) \approx c_0(1-c_0)$, where c_0 is initial value of c. Under steady state conditions, when $\vec{J}_{particles} = 0$, concentration and temperature gradients can be related:

$$\nabla c = \frac{D_T}{D_m} c_0(1-c_0) \nabla T \tag{1.16}$$

The ratio

$$\frac{D_T}{D_m} = S_T \tag{1.17}$$

defines the Soret coefficient. If $S_T > 0$, particles move away from higher temperatures as a result of the Soret effect. Such behavior can be described as thermophobic. If $S_T < 0$, particles are said to be thermophilic, moving towards higher temperatures.

While a theoretical description exists for thermodiffusion in gases, there is no universally accepted description for liquids[7], and no generally accepted theoretical framework for the Soret coefficient exists[35]. Strength of Soret effect varies considerably among different systems. For example, S_T for ethanol in water can be $S_T = 0.0056 \frac{1}{K}$[6], while for $490\,nm$ polystyrene particles in water $S_T = 1.3 \frac{1}{K}$[36]. For ferrofluids (charged), S_T is shown to have a positive correlation with particle size[37]. Soret coefficient is also a function of temperature, which is elaborated upon in sect. 1.5.

Particle transport driven by a temperature gradient is referred to as thermophoresis, setting it apart from thermal diffusion in fluid mixtures. With relations between certain colloidal properties and particle thermal mobility in certain systems being known, such as those mentioned in previous paragraph, it should be said that strength of the thermophoretic effect is not

universally tied to any particle property[8]. While there is a lack of a fundamental theoretical basis, it would appear that this motion of particles is driven by microscopic processes in the layer around a particle that constitutes the interface between the particle and solvent[38]. Following is an overview of some of theoretical approaches proposed for thermophoresis.

Brenner, in his work "Navier–Stokes revisited"[39], presented an equation for thermophoretic velocity of a sphere, driven by temperature-induced density gradient:

$$\vec{U} = -\frac{\kappa\beta}{1 + (k_p/2k_s)}\nabla T \tag{1.18}$$

here, κ is thermal diffusivity, β is coefficient of thermal expansion, k_s and k_p are thermal conductivities of, respectively, solvent and particle. Semenov and Schimpf suggested[40] a hydrodynamic approach, where they related thermodiffusion of a molecule to the local temperature-induced pressure gradient in the liquid layer surrounding the molecule, and to a macroscopic pressure gradient in the system. Their model relies heavily on knowing Hamaker constants for components of the system.

Morozov[41] describes the colloidal particle thermophoresis as driven by interaction between the particles and smaller species, like surfactant molecules, relating thermal transfer of colloidal particles to molecule redistribution around the particle under the influence of temperature. In ref. [41], an analogy with a swimmer is used, describing how the particle forces the surrounding fluid to move and moves itself as a result. The equation given for S_T of surfactant coated colloidal particle is in the form:

$$S_T = \frac{P}{T_0} \tag{1.19}$$

where P is a microscopic characteristic of a colloid called the protective layer state parameter, being a function of microscopic parameters that characterize interaction between particle and carrier fluid, namely:

$$P = 6\pi\Gamma r_h l(1 - \kappa\iota)(\xi - 1) \tag{1.20}$$

Here, Γ is Gibbs excess surface concentration, r_h is hydrodynamic radius of the particle, l is solute - particle interaction length, κ is a parameter of thermal conductivities, ι is a parameter of particle and surfactant layer sizes,

$-\xi$ is the value of solute-particle potential when the surfactant molecule is attached to the surface of the grain.

Ruckenstein[42] considered both diffusiophoresis (motion driven by gradient of concentration of a chemical species) and the Marangoni effect as driving forces to particle motion, and points out an analogy between phoretic velocity of a particle and Marangoni effect. He gave a formula to thermophoretic velocity of a particle:

$$\vec{U} = -\frac{l}{\eta}\frac{d\gamma}{dT}\frac{dT}{dz} \tag{1.21}$$

Here, l is Debye length and γ is interfacial tension.

Derjaguin and Sidorenkov considered[43] thermodynamics near particle surface in terms of local enthalpy density $\hat{h}$ and arrived at an expression for the Soret coefficient:

$$S_T = \frac{4\pi r}{k_B T}\frac{\hat{h}}{T} \tag{1.22}$$

Another result of their research was an expression for fluid slip velocity in a membrane pore, driven by a similar mechanism, with excess enthalpy in the boundary layer resulting in flow towards colder temperatures, and negative enthalpy driving flow towards higher temperatures:

$$\vec{v_s} = -\frac{2}{T\eta}\frac{dT}{dz}\int_0^\infty dx \cdot xh(x) \tag{1.23}$$

Experimental results have shown thermoosmotic flow of water and ethanol mixtures through synthetic membranes to be directed towards higher temperatures[44], which is consistent with Derjaguin's findings. Bregulla *et al.* investigated[45] flow around a heated gold nanoparticle, driven by thermoosmosis resulting from a non-uniform heat content along the solid - liquid boundary. Their results were found to suggest a considerable contribution of thermoosmotic processes along solid - liquid interfaces to thermophoretic measurements in thin films. They also found slip velocities to be much stronger in interfaces covered with non-ionic polymers than those of bare charged glass.

Parola *et al.* presented[46] a microscopic description of thermophoretic phenomena in dilute suspensions of spherical colloids, relating thermophoresis to interfacial interaction between particle and solvent. Their expression for S_T is:

$$S_T = \frac{4\pi r}{k_B T} \frac{\partial(l\gamma)}{\partial T} \tag{1.24}$$

Here, γ is interfacial tension between particle and solvent, l is length scale of the colloid-solvent interaction and r is particle radius. This approach is also linked[47] to the empirical model for temperature dependence of S_T given in sect. 1.5.

1.5 The Soret coefficient depending on temperature

To characterize dependence of Soret coefficient S_T on temperature, an empirical model put forward by Iacopini and Piazza is employed. The model describes an exponential dependence of S_T on T, and claims that a temperature T^* exists for the system, at which particles change their behavior from thermophobic to thermophilic - "thermophobic" referring to particle motion away from higher temperatures, and "thermophilic" to motion towards higher temperatures. It was introduced in ref. [48]. Later, research by Iacopini *et al.*[47] affirmed validity of the model for a wider range of systems. A microscopic hydrodynamic model by Parola and Piazza (ref. [46], see also sect. 1.4), has been referred to in ref. [47] as a firmer theoretical base to the empirical model. The empirical fitting function is:

$$S_T(T) = S_T^{\infty}[1 - \exp(\frac{T^* - T}{T_0})] \tag{1.25}$$

Here, T^* is the temperature at which $S_T = 0$ - or, the temperature at which thermally induced particle transport changes direction. Parameter T_0 characterizes the strength of temperature effects on Soret coefficient. The authors refer to S_T^{∞} as a high temperature thermophobic limit for the Soret coefficient, in effect describing a sort of a plateau of S_T values reached as the temperature increases.

The Iacopini - Piazza model was originally developed to describe thermophoresis in protein solutions, but has since been employed in various systems, including polymers in aqueous solutions[49] and charged nanoparticles[50]. For polymers in ethanol, a Soret coefficient sign change has also been observed[51] - however, there S_T decreased as temperature increased.

1.6 Mass diffusion and Soret coefficients in a porous environment

To analyze mass diffusion and Soret coefficients in a porous environment, we need to introduce the parameter of tortuosity, denoted τ_d. As a particle travels, the very presence of a porous medium prevents it from taking a path it would travel in a free fluid. Therefore, to cover an effective distance l_{eff}, the particle needs to travel a longer path of length l_p, see Fig. 1.2.

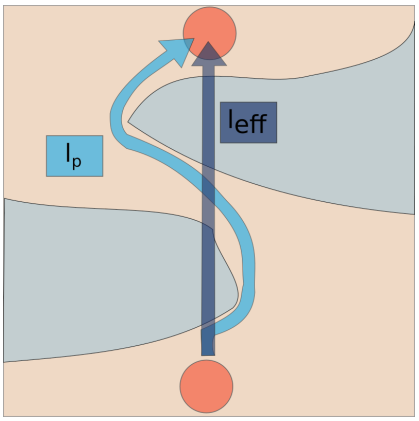

Figure 1.2: Visual representation of the two distances covered by a particle in a porous medium - effective one l_{eff} and the path traveled, l_p

The relation between these two parameters is called tortuosity:

$$\tau_d = \frac{l_p}{l_{eff}} \tag{1.26}$$

Effects of a granular porous medium through on mass diffusion and thermodiffusion coefficients for an electrolytic solution has been investigated experimentally by Costesèque *et al.* [10], finding relations for D_m:

$$\frac{D_m(free\ fluid)}{D_m(porous)} = \tau_d^2 \tag{1.27}$$

and D_T (note that the authors have introduced a separate tortuosity value for thermally induced transfer, τ_T, finding it to differ from τ_d by less than 1% of coefficient value):

$$\frac{D_T(free\ fluid)}{D_T(porous)} = \tau_d^2 \tag{1.28}$$

Davarzani *et al.* have investigate thermodiffusion of gas mixtures in a porous medium theoretically [52] and experimentally [53]. A decrease in mass diffusion and thermodiffusion coefficients was found. Relation between D_m and tortuosity has been given as:

$$\frac{D_m(porous)}{D_m(free\ fluid)} = \frac{1}{\tau_d} \tag{1.29}$$

and for D_T:

$$\frac{D_T(porous)}{D_T(free\ fluid)} = \frac{1}{\tau_d} \tag{1.30}$$

In either of these studies, no effect on Soret coefficient has been found. This is explained as a result from thermodiffusion coefficient having the same dependence on tortuosity as mass diffusion coefficient, leaving S_T unchanged.

Ahadi *et al.* investigated thermodiffusion of a hydrocarbon mixture in a thermodiffusion cell[54]. They found that the presence of a porous medium increased the time needed to reach steady state. A study by Colombani *et al.* found a decrease of Soret coefficient for a liquid mixture in a porous environment and associated it with adsorption of liquid in the porous medium[55].

Yasnou *et al.* conducted insightful experimental work in a fluid - porous layer - fluid system, measuring Soret, diffusion and thermodiffusion coefficients, and investigating thermal conductivity within the system[56]. In their research, they have found S_T to slightly increase in a porous medium, by around 5% of value, while also suggesting that changes in D_m correspond to tortuosity of porous material as given by eq. 1.27, rather than porosity of the material, as suggested in ref.[57].

Blums *et al.* showed that ferrofluids in a porous environment can present a decrease in thermally induced particle transport[13]. The authors associated their observations with slip velocity mechanisms, as described in [58], inducing flow through fluid - pore wall interaction. Later, a decrease in Soret coefficient of a ferrofluid was also found in thermophoresis through a layer formed by two permeable grid-like walls [59, Blums *et al.*], especially in an external magnetic field, where a reversal of particle flow direction was observed. In the latter study, influence of the permeable walls on particle

thermophoresis in an external magnetic field was associated with microconvective flow of the fluid and magnetophoretic transfer of the particles, both induced by the grid elements.

1.7 Effect of an external magnetic field on ferrofluid mass transfer, mass diffusion and thermophoresis

The Bernoulli equation for a ferrofluid contains an additional term to account for the effects of magnetism. The ferrohydrodynamic Bernoulli equation is[19]:

$$p + \frac{1}{2}\rho v^2 + \rho g h - \mu_0 M H = const \tag{1.31}$$

If we consider a setup of two regions adjacent to each other in way that gravitational and velocity terms of Bernoulli equation are in balance, we arrive at pressure difference between the regions[60]:

$$\Delta p = \mu_0 \left(M_1 H_1 - M_2 H_2 \right) \tag{1.32}$$

This is referred to as magnetic pressure. An example of a system where magnetic pressure could be expected to contribute to ferrofluid mass transfer is a porous layer placed between two ferrofluid volumes kept at different temperatures, such as described in ref. [18].

Effect of a magnetic field on ferrofluid mass diffusion has been described by Bacri *et al.*, see ref. [61]. Two geometries are considered - one where magnetic field is parallel to particle distribution gradient and the other where field is normal to the distribution gradient. In the first case, effect of a magnetic field on particle mass diffusion is predominantly caused by inhomogeneity of the magnetic field due to particle distribution. Then, mass diffusion coefficient becomes:

$$D_{m(H),\parallel} = D_{m,B=0} \left(1 + \frac{\gamma_M L^2(\xi)}{1 + \gamma_M L'(\xi)} \right) \tag{1.33}$$

where $L(\xi)$ denotes the Langevin function with $\xi = \mu_0 \frac{mH}{k_B T}$, see sect. 1.2, while γ_M is the reduced parameter of magnetic dipole - dipole interaction:

$$\gamma_M = \phi_0 M_d \frac{\mu_0 m}{k_B T} \tag{1.34}$$

In the second case, when magnetic field is perpendicular to particle concentration gradient, this inhomogeneity of particle distribution would have no contribution to D_m. Then, the principal mechanism through which magnetic field would influence mass diffusion would be through magnetic interaction between the particles. To characterize it, effective field constant λ is introduced. Calculation of λ with effective field model is described in ref. [62]. For the purposes of the work described here, λ is treated as a known constant of the ferrofluid that is used in mass diffusion experiments in magnetic field, see sect. 2.2. Diffusion coefficient D_m is, then:

$$D_{m(H),\perp} = D_{m,B=0}\left(1 - \frac{\lambda\gamma_M L^2(\xi)}{1 + \lambda\gamma_M L'(\xi)}\right) \tag{1.35}$$

For thermophoresis in a magnetic field, we are only looking at a case where temperature gradient and magnetic field are aligned. Principal mechanism of magnetic field influence on ferrofluid thermophoresis is expected to come from magnetic field gradients associated with particle distribution non-uniformity. Theoretical considerations for these circumstances are laid out in ref. [59]. The approach is based on employing equation 1.15 for particle mass transfer and writing out thermodiffusion coefficient according to definition of S_T, then applying to D_m dependence on H as given by eq. 1.33. Dependence of particle magnetization on temperature is taken into account through pyromagnetic coefficient α_T. The expression for $S_T(H)$ is, then:

$$S_{T,H} = S_{T,B=0}\left[\left(1 - \frac{\gamma_M L^2(\xi)}{1 + \gamma_M L'(\xi)}\frac{\alpha_T}{S_T}\right) / \left(1 + \frac{\gamma_M L^2(\xi)}{1 + \gamma_M L'(\xi)}\right)\right] \tag{1.36}$$

A mechanism of ferrofluid mass transport driven by microconvection induced by nonmagnetic grains is proposed in ref. [17]. This phenomenon, referred to as thermomagnetoosmosis, would induce not only additional mixing of the fluid, but also a macroscopic translation flow directed towards increasing temperatures. This corresponds to a decrease of Soret coefficient.

1.8 Ferrofluid viscosity

Rheology of a ferrofluid can be analyzed as that of a dilute or moderately concentrated suspension ([63]; ref. [63] has been used as the fundamental basis of understanding of rheology in this thesis). We are looking at all fluids concerned in experimental work as Newtonian liquids, with viscosity not dependent on shear stress. This means no shear thinning or thickening being present. For suspensions, shear thinning would be expected starting from particle volume concentration values of roughly around $\phi = 0.3$ and shear thickening from around $\phi = 0.4$. Both values of particle concentration are well above those found in the colloids used in the work described here, see sect. 2.2 (note that fluid compliance with Newton's law of viscosity has also been confirmed experimentally, see Sec. 4.2).

For dilute colloids, dynamic viscosity should change with particle volume concentration according to Einstein formula

$$\eta = \eta_s(1 + 2.5\phi) \tag{1.37}$$

However, for particle concentration exceeding $\phi = 0.03$ while still below $\phi = 0.1$, Batchelor formula would be more appropriate:

$$\eta = \eta_s(1 + 2.5\phi + 6.2\phi^2) \tag{1.38}$$

Temperature dependence of viscosity can be derived from comparing molecular motion induced by collisions arising from Brownian motion and by shearing motion. In terms of activation energy ν^* and activation barrier ΔH, the viscosity is given by

$$\eta = \frac{k_B T}{\nu^*} \tau_0 \exp\left(\frac{\Delta H}{k_B T}\right) \tag{1.39}$$

Here, $\tau_0 = \frac{1}{\Omega_0}\ 10^{-13} s$ is the average time between molecular collisions, as Ω_0 is the molecular collision rate and η_∞ is viscosity at "infinite temperature". Equation 1.39 describes Arrhenius type dependence of viscosity on temperature. The form of Arrhenius equation used in analysis of results presented in this thesis is:

$$\eta = \eta_\infty \exp\left(\frac{E_a}{RT}\right) \tag{1.40}$$

Here, R is the gas constant, T is temperature and E_a denotes activation energy. Existing research in similar physical systems, see for example [64] and [65], shows that ferrofluid viscosity decreases with temperature, driven by the viscosity of the carrier fluid.

Yang *et al.*[66] have looked at magnetic microparticles suspended in methyl silicone oil and mineral oil with oleic acid as surfactant. They observed that viscosity increases with an increase of excess oleic acid.

A mechanism is described in ref. [63], by which a colloid with sterically stabilized particles can have viscosity reduced through lubrication provided by the molecular layer around the colloidal particles. Lubrication is then provided by motion of molecules within the surfactant layer relative to the nanoparticles.

Chapter 2

Ferrofluids used in experimental work

Majority of ferrofluids used in this work were prepared in Institute of Physics, University of Latvia. Those include samples S-1, U5 and df105, which is the most thoroughly studied ferrofluid in the research described in this work. One sample, FF13-04, was prepared in Laboratory of Magnetic Soft Materials, University of Latvia. Oleic acid and lauric acid used as surfactants were provided by Sigma – Aldrich. Overview of all ferrofluids used in the work can be found in table 2.1.

Ferrofluids df105, S-1 and U5 are all surfactant stabilized. This means that the single domain magnetic core is coated in a layer of surfactant particles. Production of ferrofluids of this type is described in refs. [67], [68] and [69]. Particles are synthesized from ferric and ferrous salts by chemical coprecipitation and then coated with the surfactant layer. Advantages of this method, comparing to sol-gel, microemulsion and others, include being relatively simple and economical, and highly efficient[70]. Challenges of the method include insufficient dispersion, which can be countered by ultrasonic mixing, and uneven size distribution. In the ferrofluids concerned in this work, particle size is controlled by centrifugation at $7000g$ for a time of several hours. The particles are treated with high gradient magnetic separation - filtered through a wire matrix placed in an external magnetic field. Two of the three surfactant stabilized ferrofluids here use oleic acid as surfactant - it is a popular choice for ferrofluids of this type, providing good colloidal stability even compared to similar surfactants due to excellent wettability of oleic acid layers on surfaces by hydrocarbons[71].

Production of the ionic layer stabilized ferrofluid is described in ref. [72]. The particles were synthesized by coprecipitation, following the Massart method and stabilized by covering the nanoparticles with citrate ions.

2.1 Characteristics of ferrofluids used in experimental work

Materials and production methods of ferrofluids used in this work are summarized in table 2.1. Ferrofluid densities and volume and mass concentrations of the magnetic phase can be found in table 2.2.

ferrofluid	particle material	carrier fluid	method of stabilization	surfactant
df-105	Fe_3O_4	tetradecane	surfactant	oleic acid
S-1		di-(2-ethylhexyl) sebacinate		oleic acid + lauric acid
U5		undecane		oleic acid
FF 13 - 04	$\gamma - Fe_2O_3$	water + citrate	ionic double layer	citrate

Table 2.1: Overview of ferrofluids used in experimental work

ferrofluid	$\rho_p, \frac{kg}{m^3}$	$n_{p,V}, \%$ (magnetic phase)	$n_{p,m}, \%$ (magnetic phase)
df-105	1.037e3	4,75	24.05
S-1	1.062e3	1,48	7.34
U5	0.965e3	4,00	21.76
FF 13 - 04	1.043e3	0,87	4.37

Table 2.2: Physical parameters of the ferrofluids

2.2 Nanoparticle properties

In table 2.3, sizes of the magnetic phase of nanoparticles of the ferrofluids are characterized. Particle sizes are measured with Vibrating sample magnetometry, as described in ref. 3.7.

ferrofluid	particle size d, nm			dispersity Đ
	number average	mode	volume average	
df-105	8.8	9.7	11.6	2.3
S-1	5.0	4.8	5.6	1.4
U5	8.7	9.7	11.4	2.2
FF 13 - 04	24.2	27.6	32.3	2.4

Table 2.3: Nanoparticle size properties (magnetic phase)

Dispersity, Đ, is defined as:

$$Đ = \frac{M_w}{M_n} \tag{2.1}$$

M_w is weight average molar mass and M_n is number average molar mass. The formula used to calculate dispersity (sometimes called polydispersity index) Đ, assuming uniform density across particles and all particles having a spherical shape, is:

$$Đ = \frac{r(vol.average)^3}{r(numb.average)^3} \tag{2.2}$$

Nanoparticle hydrodynamic size measurements are performed for sample df105. Measurements and results are described in sect. 5.3. The determined mean apparent hydrodynamic diameter of a df105 particle is $d_h = 16.7\,nm$.

In figs. 2.1 and 2.2, particle magnetic phase size distribution of ferrofluid df105 are given relative to, respectively, particle number and volume. Magnetization measurements from which these were calculated are shown in fig. 2.3. Magnetic properties of the particles of all ferrofluids can be found in table 2.4. All ferrofluid size distributions are given in appendix A.

Effective field constant λ of ferrofluid df105 is $\lambda = 0.286$.

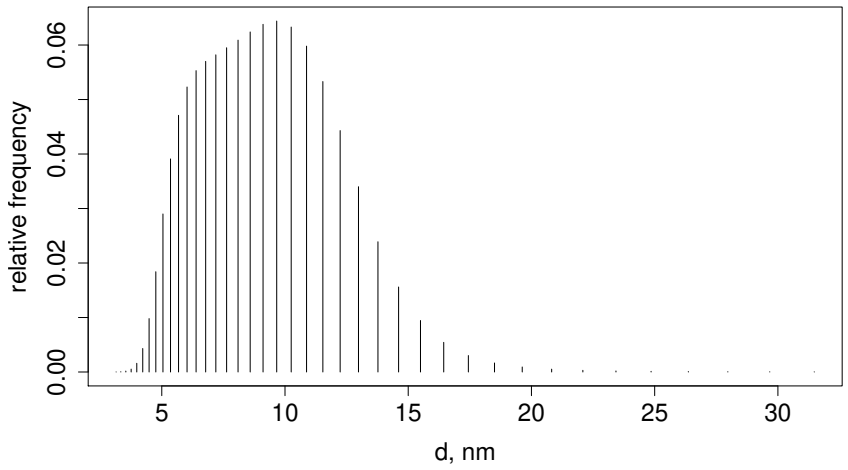

Figure 2.1: Nanoparticle size distribution (magnetic phase) in ferrofluid df105

ferrofluid	particle magnetic moment $m, A \cdot m^2$	particle material M_d, $\frac{kA}{m}$
df-105	$2.3 \cdot 10^{-19}$	490
S-1	$0.3 \cdot 10^{-19}$	490
U5	$2.2 \cdot 10^{-19}$	490
FF 13 - 04	$5.0 \cdot 10^{-18}$	430

Table 2.4: Nanoparticle magnetic properties

2.3 Addition of excess surfactant

In some experiments, an excess of surfactant being present in the colloid. The respective surfactant of each ferrofluid is used. Due to preparation procedures of the ferrofluid, all oleic acid present before the addition of excess surfactant is assumed to be bound to the nanoparticles, corresponding to 0% surfactant concentration. Surfactant volume concentration is consistently used as "concentration" value for surfactant, even when not specified. Preparation of fluids with excess surfactant consists of simply mixing the specified amount of surfactant in the fluid, so that a ferrofluid with say 2% excess surfactant would have 2% of volume taken by surfactant not bound to nanoparticles and

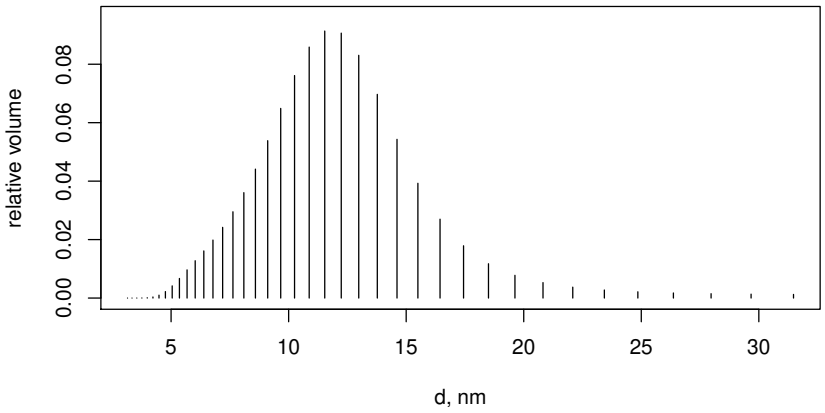

Figure 2.2: Nanoparticle size distribution (magnetic phase) in ferrofluid df105 as fraction of volume

98% of volume taken by the original ferrofluid, with volume concentration of each component reduced by 2%.

As tetradecane is non-polar, no micelle formation from surfactant molecules is expected. This is confirmed by Dynamic Light Scattering measurements, see sect. 5.3.

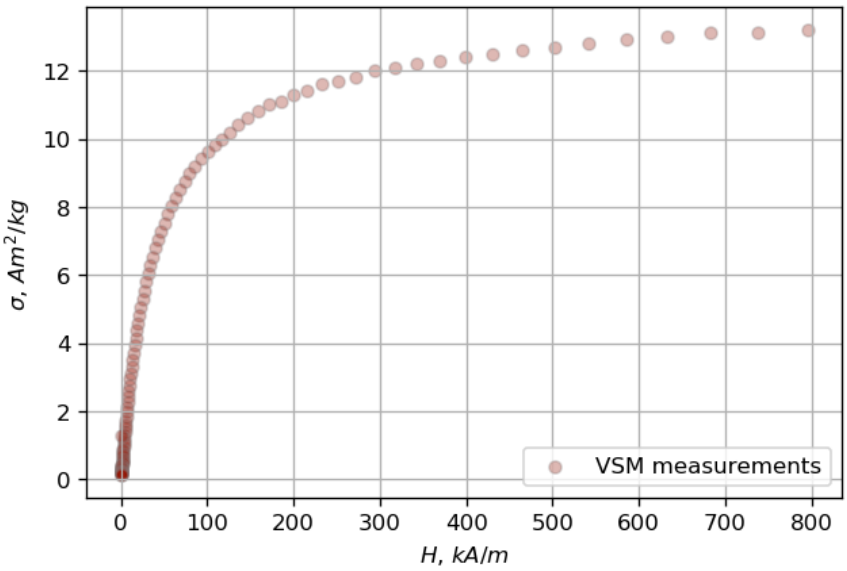

Figure 2.3: Magnetization of ferrofluid df105 - measurements by VSM that particle magnetic size is calculated from

Chapter 3

Experimental methods

Introduction

Experimental research methods described here can be divided into three categories. One describes the work carried out that concerns a porous medium, including two experimental setups, characterization of a porous medium and convective stability concerns. This category consists of sections 3.1 through 3.5. The second category describes the method of Forced Rayleigh Scattering as it is applied in the research presented in this thesis, given in sect. 3.6. The third category describes measurements performed with ready made experimental apparatus and includes sections 3.7 through 3.9.

3.1 Measuring thermophoresis in a porous layer

In porous medium thermophoresis experiments, illustrated in fig. 3.1, a flat cylindrical porous layer is placed in a temperature gradient. The layer is fully enclosed by walls, allowing for no mass transfer to or from the layer. Side walls are thermally insulated, having been made from a solid ring of polytetrafluoroethylene, more commonly referred to as teflon. Top and bottom walls are kept at a constant temperature through thermostatted fluid circulation, with top wall being heated and bottom wall being cooled.

The device can be seen in fig. 3.2. The porous layer is placed inside, between the two sides which are then pressed together. The layer itself is described in sect. 3.4 - it is formed of ten sheets of filter paper pressed together to form a continuous porous medium.

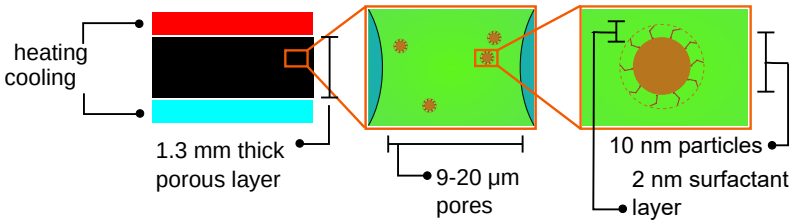

Figure 3.1: Schematic layout of thermophoresis experiments

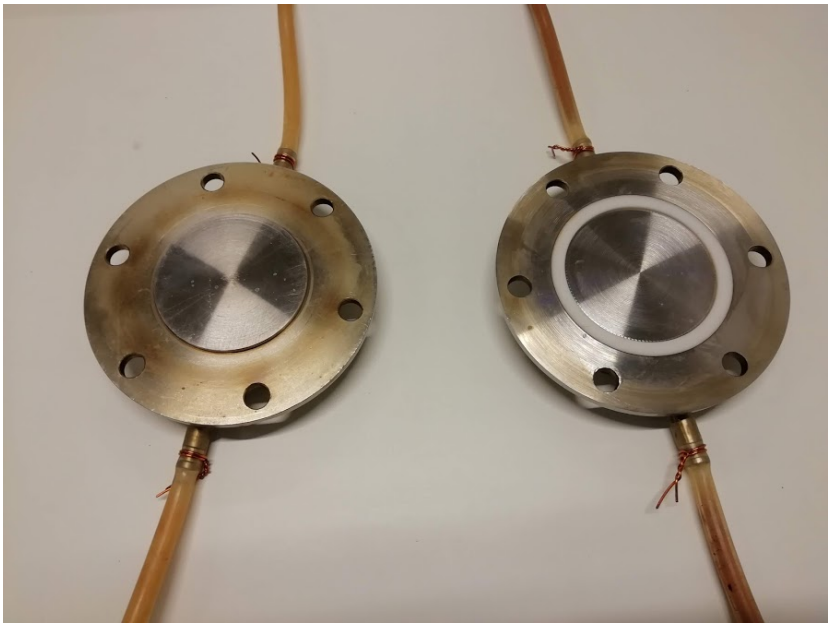

Figure 3.2: Experimental device for measuring thermophoresis in a porous layer. Top and bottom halves are thermoregulated with water circulation, see the tubes. Heat flux through side walls in prohibited by the teflon ring (white).

layer number	NP mass conc., ϕ_m		NP relative conc., ϕ		$\lvert\phi_m - \phi\rvert$
	rinsed	dried	rinsed	dried	
1	0.07%	5.00%	0.0475	0.0579	0.0103
2	0.07%	5.55%	0.0457	0.0643	0.0185
3	0.07%	6.25%	0.0457	0.0723	0.0267
4	0.10%	5.14%	0.0652	0.0595	0.0057
5	0.13%	7.80%	0.0835	0.0903	0.0068
6	0.14%	7.34%	0.0944	0.0849	0.0095
7	0.17%	9.55%	0.1109	0.1106	0.0004
8	0.20%	11.30%	0.1332	0.1308	0.0024
9	0.25%	13.48%	0.1649	0.1560	0.0090
10	0.32%	15.00%	0.2089	0.1736	0.0353

Table 3.1: Particle concentration measurements with two methods of sample preparation for VSM, ferrofluid df105

The porous layer is saturated with a ferrofluid. Diameter of the layer is 67 mm and the setup is positioned so that the axis of the flat cylindrical porous layer is aligned with the gravitational field. The temperature gradient is created at the start of the experiment and being kept constant throughout. Experiment is ended after 24 hours, which is a well sufficient time for Fourier time $\tau = \frac{D_m t}{\delta^2}$ to reach values of $\tau > 1$ (for D_m measured with Forced Rayleigh scattering, see Sec. 3.6) and therefore the particle distribution to reach a steady state.

After the experiment is ended, the ten layers are split apart and samples are extracted from each layer. Concentration of magnetic nanoparticles in each layer is measured with the method of vibrational magnetometry, see sect. 3.7.

For sample extraction, two approaches are evaluated. In one of them, the center of each layer is cut out after the experiment, and the fluid is rinsed out in a test tube. In the other approach, the layer is dried and a segment is cut out. The results for magnetic particle mass concentration are given in table 3.1. The resulting relative particle distribution is shown in fig. 3.3. It is found that no method provides an obvious advantage compared to the other in terms of result reliability.

The accuracy of vibrating sample magnetometry measurements is given by the manufacturer as better than 2% of value reading. There are, how-

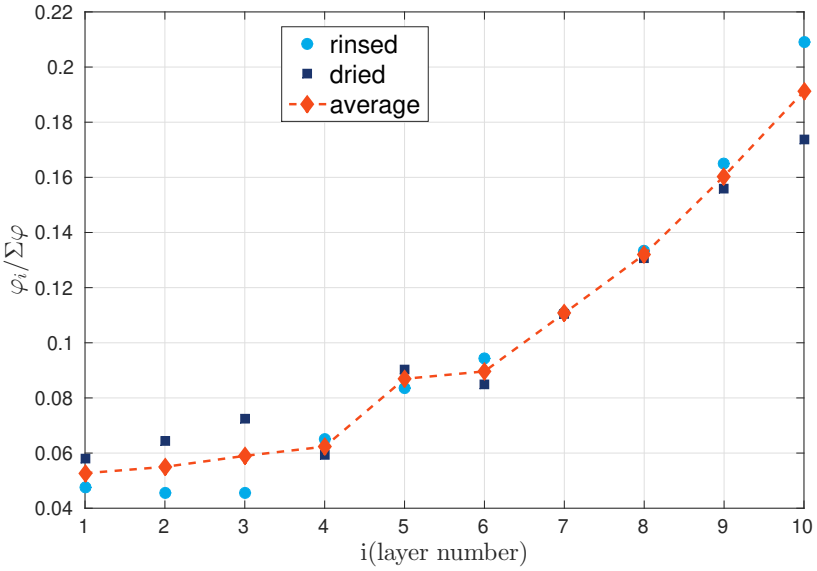

Figure 3.3: Example of relative particle distribution in the porous layer, measured from rinsed center cutout and a dried cutout section

ever, other sources of error, possibly the most prominent being associated with splitting apart the layers post experiment and possible parasitic mass transfer during that process. To better estimate the measurement error, an experiment is performed with no temperature gradient present and, therefore, an expected uniform distribution of particles. The deviation of particle concentrations in this experiment gives us a measurement error of 7 % of initial particle concentration.

Nanoparticle size distribution in each of the layers at the end of this isothermal test is given in fig. 3.4. No significant deviations in size distribution profiles are found between the layers.

3.2 Measuring mass diffusion in a porous layer

Diffusive transfer of the magnetic nanoparticles of a ferrofluid is investigated in a porous layer of the same geometry and composition than that used in thermophoresis experiments. The layer has a flat cylindrical shape and is composed of ten coaxial, tightly packed sub-layers. The mass diffusion coef-

layer number	relative particle concentration
1	0.987
2	0.906
3	0.991
4	1.074
5	0.889
6	0.984
7	1.080
8	0.981
9	1.032
10	1.075

Table 3.2: Particle distribution through sections of the porous layer with no mass transfer induced by temperature

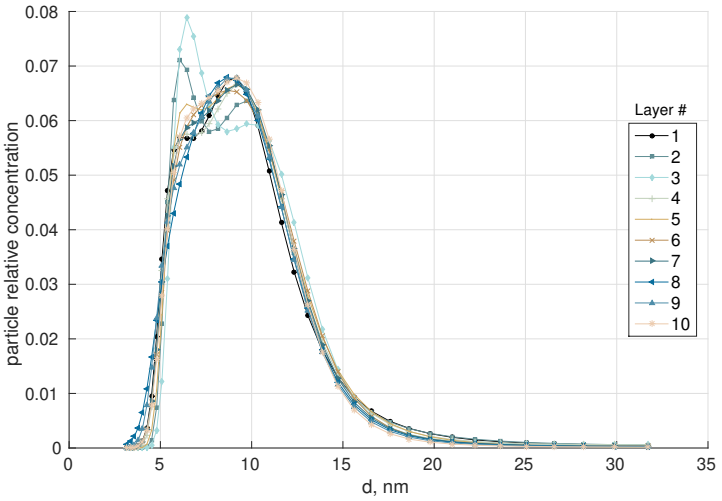

Figure 3.4: Particle size distribution in the ten layers that form the porous medium after 24 h long isothermal experiment

ficient is evaluated from measurements of particle concentration across the layer, where the mass transfer is driven by the development of concentration profile from initial step-vise distribution. The schematics of diffusion experiments and how they compare to thermophoresis experiments is given in fig. 3.5.

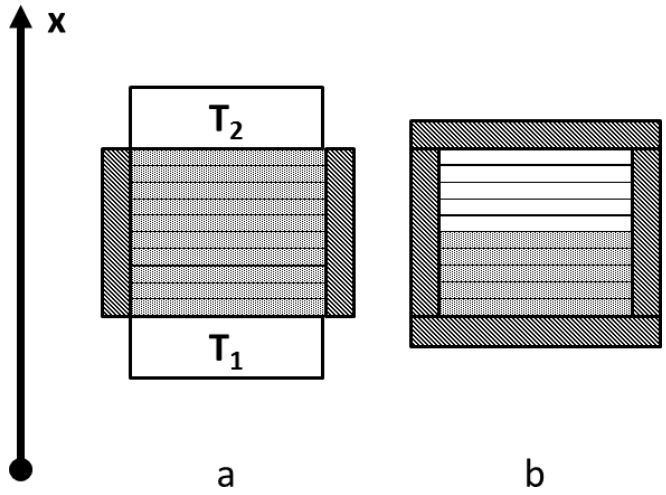

Figure 3.5: Schematic of porous layer arrangement in thermophoresis (a) and diffusion (b) experiments. Shading represents layers saturated with ferrofluid.

In diffusion experiments, no mass flux through any wall is present. No temperature gradient is present and no heat flux through top, bottom and side walls is allowed. At the starting point of an experiment, five of the ten sub-layers are homogeneously saturated with ferrofluid, while the other five are saturated with pure carrier fluid. Experiments are performed for 2 and 4 hours for each of samples df105 and FF 13-04, and 24 hours for samples S-1 and U5. After this time has passed, the layers are split apart and particle concentration within them measured with VSM, much like in thermophoresis experiments. Average of D_m from experiments of various time frames is given as the end result. It is from this averaging that measurement error of D_m is estimated, and is found to be 15 % of measurement value.

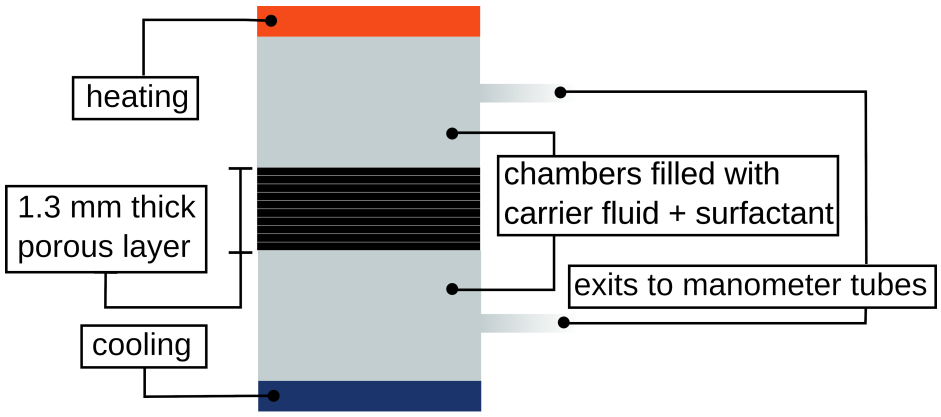

Figure 3.6: Schematic layout of thermoosmosis experiments

3.3 Measurements in a two volume thermoosmosis cell

Thermoosmosis experiments are illustrated in fig. 3.6. If colloid thermophoresis experiments investigate flow within a closed porous layer, in carrier fluid - surfactant thermoosmosis experiments that layer is "opened up", allowing for flow through it.

A porous layer with a diameter of $d_{layer} = 15\,mm$ is placed between two equal cylindrical volumes, forming an experimental cell that allows for both mass and heat transfer to and from the layer and the volumes. Axis of the cylinders are again aligned with gravitation field. Height of one volume is $15\,mm$. The device can be seen in fig. 3.7.

Both of the volumes have exits to a manometer, which is designed so that it's tubes run parallel and both at equal height from the ground at a point near the experimental cell, with the lower manometer tube being bent to meet the higher. From that point, the tubes can run either parallel to the ground (a setup that is referred to as "flow setup" in the article), or at an incline angle α (this setup is referred to as the "pressure setup"). Fluid levels in the manometer are monitored with a camera during experiments. The flow level is then determined from the pictures by an image analysis script written in Python. An example of a picture taken during the experiment is demonstrated in fig. 3.8.

The fluid used in thermoosmosis experiments is a mixture of tetradecane,

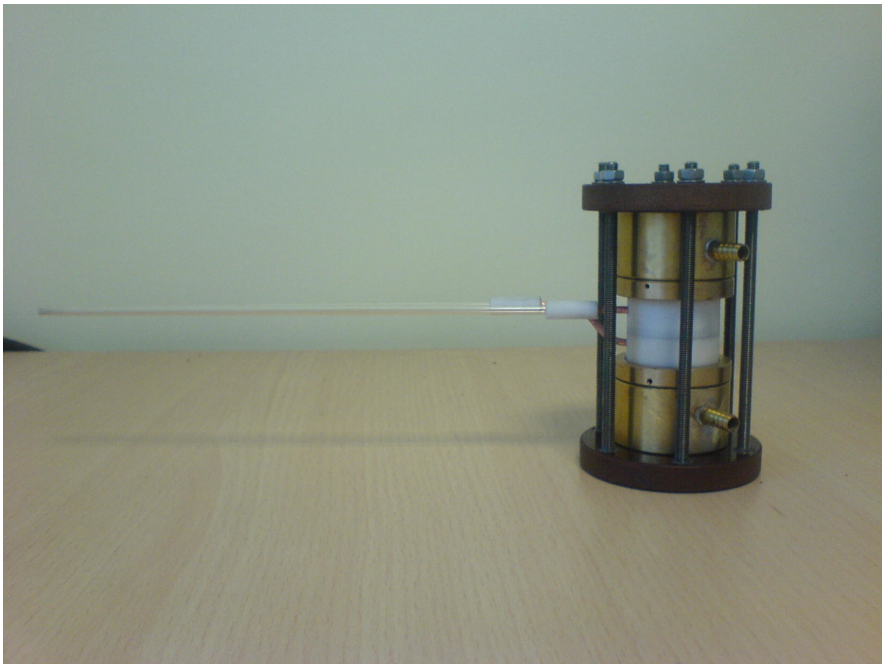

Figure 3.7: Experimental device used in two volume thermoosmosis experiments. Manometer tube endings on far left in the picture are where additional tubing is attached and raised at an incline angle if necessary

which is the carrier fluid of the ferrofluid used in thermophoresis experiments, and oleic acid - the surfactant of the ferrofluid. Volume concentration of oleic acid varies from 0 % to 2.5 %.

In isothermal experiments, temperatures are $T_{top} = 40\,^0C$ and $T_{bottom} = 40\,^0C$. In non-isothermal pressure experiments, end walls of both volumes are kept at constant temperatures, with $T_{top} = 60\,^0C$ and $T_{bottom} = 20\,^0C$. A series of flow experiments is also conducted at the same temperatures. Additionally, to examine the effect of using various temperatures and temperature differences, a series of flow experiments with $\Delta T = 20^0C$ is performed. The temperature combinations used in this series is $T_{top} = 40\,^0C/T_{bottom} = 20\,^0C$, $T_{top} = 50\,^0C/T_{bottom} = 30\,^0C$ and $T_{top} = 60\,^0C/T_{bottom} = 40\,^0C$.

Temperature within the volumes themselves is not measured, but we know from previous experimental work with cells of identical geometry and materials used for experiments (such as described in ref. [32]), that such a configuration, with temperatures $T_{top} = 60\,^0C$ and $T_{bottom} = 20\,^0C$, corresponds

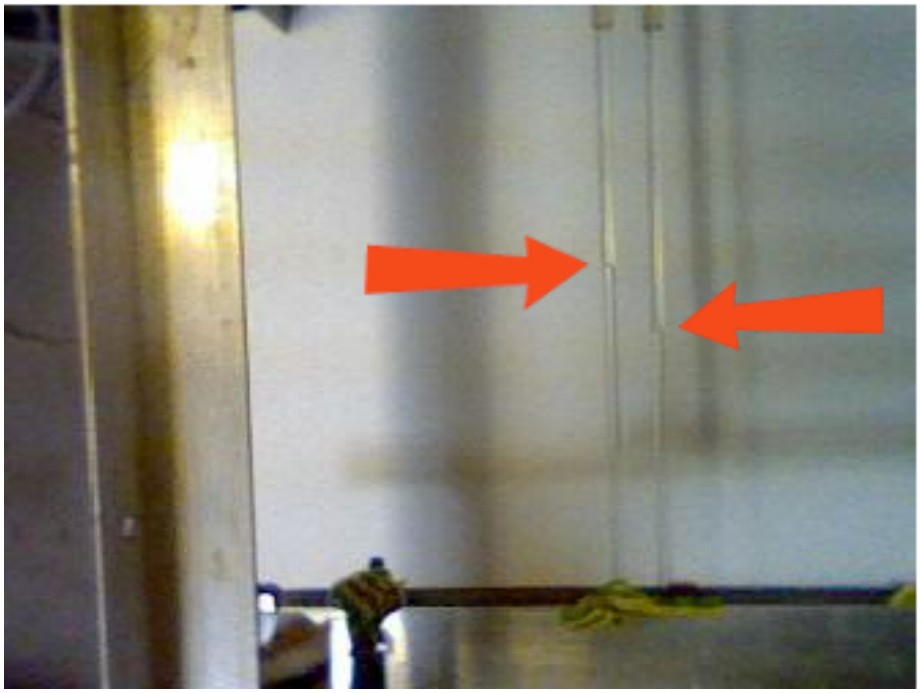

Figure 3.8: Example of a manometer picture taken during an experiment. The red arrows point at fluid levels in the tubes. Flow is measured by detecting these levels

thickness δ_{filter}	0.15	mm
minimum pore size $d_{pore,min}$	9	μm
maximum pore size $d_{pore,max}$	20	μm

Table 3.3: Parameters of filter paper used in formation of porous medium

to temperature gradient across the porous layer $\Delta T_{thermoosmosis} = 8\,^0C$.

Measurement error of the thermoosmosis series is discussed in sect. 7.3.2, and found to be approximately 20 % of value for coefficients obtained from the experiments.

3.4 The porous layer

In both thermophoresis and thermoosmosis experiments, a porous layer is used. In both cases, the layer is made of ten sheets of filter paper, tightly packed together to form a continuous porous environment.

The filter paper used is VWR Grade 410 with the relevant properties, as specified by the manufacturer, shown in Table 3.3.

The filters are found to be chemically inert to all the fluids used in experiments. The resulting layer then has thickness of $\delta = 1.5\,mm$. Porosity is determined experimentally by comparing the weight of a filter paper saturated with a fluid of known density to that of an "empty" one, and it is found that $\varepsilon = 0.328$.

To estimate permeability of the porous medium, we use the Kozeny-Carman relation in the form given in[73]:

$$K = \frac{d^2\varepsilon^3}{172.8(1-\varepsilon^2)} \tag{3.1}$$

and get $K = 5.149 \cdot 10^{-14}\,m^2$. It must be noted that this is only an initial estimation and the value of permeability used in calculations is obtained experimentally, as described in sect. 7.3.2.

3.5 Convective stability in the porous layer

For the research presented here, it is crucial that convective stability within the porous layer is ensured in non-isothermal conditions. This matter is

addressed in ref. [74, Sints et al.]. For our colloids, thermal diffusivity far exceeds mass diffusion coefficient, therefore the Lewis number $Le >> 1$, and for $N = \frac{S_T}{\beta_T}$, it is true for our case that $N >> 1$ (β_T is thermal expansion coefficient, see table 3.4). It is shown in ref. [75], that when $LeN > 10$, convective stability in a fluid saturated porous medium is determined by the solute Rayleigh number Ra_p:

$$Ra_p = Ra_\phi Da \tag{3.2}$$

Here, Ra_ϕ is the Rayleigh number and Da is the Darcy number:

$$Da = \frac{K}{\delta^2} \tag{3.3}$$

where K is permeability of the layer and δ is the thickness, see sect. 3.1. Magnetic and gravitational contributions for Ra_p are considered:

$$Ra_p = Ra_{pm} + Ra_{pg} \tag{3.4}$$

For a top heated layer, Ra_p is:

$$Ra_p = \mu_0 \frac{K\left(\varepsilon\phi_0 M_S L(\xi) S_T \Delta T\right)^2}{\eta D(1+\gamma_M L'(\xi))} - \frac{\delta\beta_\phi \rho g \phi_0 S_T \Delta T K}{\eta D} \tag{3.5}$$

In eq. 3.5, ϕ_0 is volume concentration of nanoparticles, ρ and η are density and viscosity of fluid, S_T and D are Soret and mass diffusion coefficients for ferrofluids, as measured by Forced Rayleigh scattering in Institute of Physics, University of Latvia (see values of those coefficients in sects. 6.2.3 and 5.2.2), and β_φ is defined as:

$$\beta_\phi = \frac{1}{\rho_0}\frac{\partial\rho}{\partial\phi} \tag{3.6}$$

Here, ρ_0 is initial density of the ferrofluid. Values of β_φ can be found in table 3.4.

Magnetic coefficients ξ and γ_M are those defined in sects. 1.2 and 1.7: $\xi = \mu_0 \frac{mH}{k_B T}$ and $\gamma_M = \phi_0 M_d \frac{\mu_0 m}{k_B T}$. $L(\xi)$ is the Langevin function. Values of solute Rayleigh number Ra_p, calculated for $\Delta T = 40^0 C$ at zero magnetic field and $B = 0.1\,T$ are shown in table 3.5. It can be seen that, for all fluids, Ra_p is lower than the critical value $Ra_{critical} = 4\pi^2$.

ferrofluid	β_T	β_ϕ
df-105	6,8e-4	5,8
S-1	6,8e-4	4,7
U5	6,8e-4	6,1
FF 13 - 04	2,1e-4	4,3

Table 3.4: Thermodynamic coefficients for ferrofluids used in experimental work

ferrofluid	$Ra_p, B = 0\,T$	$Ra_p, B = 0.1\,T$
df-105	-2.18	55.6
S-1	-0.18	0.33
U5	-0.75	2.65
FF 13 - 04	3.50	13.83

Table 3.5: Solute Rayleigh number Ra_p for ferrofluids used in experimental work

3.6 Forced Rayleigh scattering

Forced Rayleigh scattering (FRS) is described in ref. [15] - this article, along with correspondence with it's authors, has formed the base for the description of FRS method given here. Essence of the method is that a colloid is placed in a thin optical cell, within which a one-dimensional grid is created by a light source. This causes a spatial periodic temperature modulation ΔT, which, through the Ludwig-Soret effect, induces a volume fraction modulation of the nanoparticles $\Delta\phi$. Soret coefficient S_T can then be evaluated from these two modulations. When the light source - which is, effectively, a heat source - is switched off, volume fraction gradient undergoes a relaxation, driven by nanoparticle mass diffusion. From this, mass diffusion coefficient D_m can be evaluated. Measurements of the modulations are made with a non-absorbing laser, effectively investigating refractive index modulation.

In the experimental setup in Laboratorie PHENIX, a high power lamp, 500W- Hg Arc Lamp-240 Spectra Physics, is used as the light source to impose the one-dimensional grid. Period gratings Λ used are $92.5\,\mu m$, $110\,\mu m$ and $156\,\mu m$, each applied to every fluid sample at every temperature. The

cell is placed in a temperature regulated sample holder allowing measurements at controlled temperatures. In the work presented here, mass transfer coefficients are measured in temperature range $T = 20^0C$ and $T = 85^0C$, the upper temperature being determined by considerations about possible carrier fluid evaporation and measurement cell durability.

A number of results presented here have also been measured using the Forced Rayleigh scattering setup in Institute of Physics, University of Latvia. There, the grid in fluid is induced by a laser beam, instead of a high power lamp. The laser in use is a YAG laser with wavelength $532\,nm$. Laser used for measurements is a He-Ne laser with a wavelength of $633\,nm$. Period gratings are $50 - 100\,\mu m$. In these measurements, temperature has not been controlled. This experimental setup is described in detail in ref. [76].

3.7 Vibrating sample magnetometry

The working principle of Vibrating sample magnetometry (VSM) is described in ref. [77]. In brief - a sample with some magnetic properties is placed among a set of measuring, or receiver coils, and in a magnetic field generated by an electromagnet. This external field magnetizes the sample. A vibrating motion of the sample is then induced. According to Faraday law, this motion of a magnetic sample induces a current in the receiver coils. From that, magnetization of the sample at the corresponding magnetic field can be calculated.

Description of particle size distribution calculations, as used to characterize ferrofluids used in this work, can be found in refs. [78] and [27]. Magnetization of a ferrofluid in an external field is given by eq. 1.7 and depends on particle magnetic moment - therefore, magnetic moment can be calculated by knowing field and magnetization values, as provided by VSM measurements. Furthermore, a distribution of nanoparticle sizes can be attained by using eq. 1.8 instead of eq. 1.7.

VSM measurements in this thesis were performed in Institute of Physics, University of Latvia by using Lake Shore Cryotronics Co., model 7404 VSM vibrational sample magnetometer.

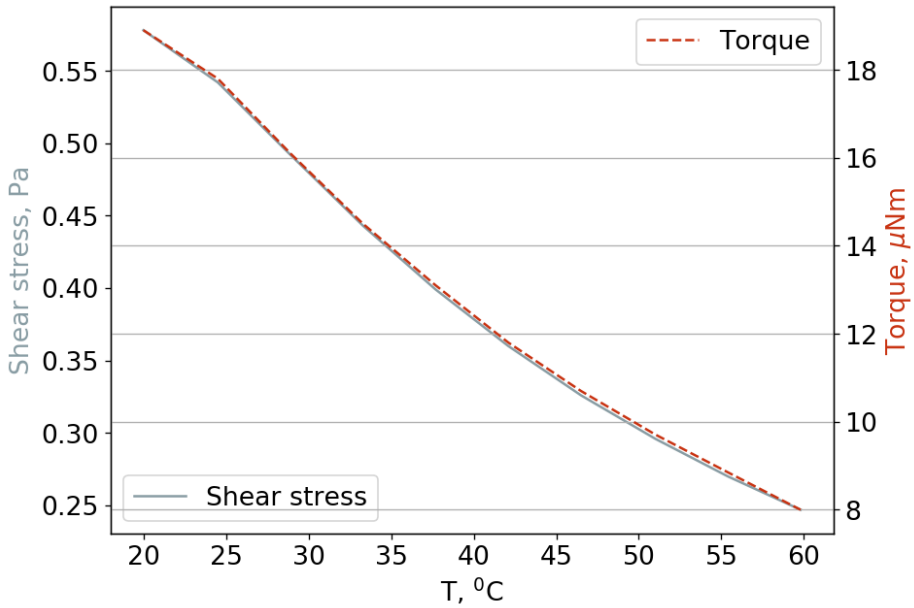

Figure 3.9: Stress rate and torque for ferrofluid df105 with 1% excess surfactant. Rotation is constantly at 13.4 1/min

3.8 Rheometry

Viscosity of fluid samples is measured with Anton Paar MCR 502 rheometer, in a cone - plate setup. In this setup, shear rate γ is determined from angular velocity Ω and angle between cone and plate, α, as:

$$\gamma = \frac{\Omega}{\tan(\alpha)} \tag{3.7}$$

Advantage of measuring viscosity with a cone - plate setup is having an even shear distribution. A disadvantage is inability to change the gap between cone and plate, which limits the chance to detect potential wall slip. The rheometer is equipped with a Peltier temperature control, which enables measurements at various temperatures. Measurements are done in a continuous rotational mode. Angular velocity is kept constant, while torque exerted on the rotating cone changes with viscosity. An example of torque changing with viscosity decrease as temperature increases, along with corresponding change in shear stress, at a constant shear rate, is given in fig. 3.9.

3.9 Dynamic light scattering

Method of Dynamic Light Scattering (DLS) is based on measuring fluctuations in light scattered by particles undergoing Brownian motion. Dynamic light scattering measurements were made with Vasco DLS Particle analyser from Cordouan Technologies, in Laboratorie PHENIX, Sorbonne Université. This apparatus works in back scattering. It is adapted for strongly absorbing colloidal dispersions and allows here the determination of the mass diffusion coefficient D_m of nanoparticles at room temperature. Nanoparticle apparent hydrodynamic size d_h is related to D_m through Stokes-Einstein formula:

$$d_h = \frac{k_B T}{3\pi\eta_0 D_m} \tag{3.8}$$

where η_0 is viscosity of pure carrier fluid.

Chapter 4

Viscosity measurements

4.1 Overview

Series of experiments are performed with ferrofluid df-105 and the corresponding carrier fluid, tetradecane. Measurements are made at several values of oleic acid concentration, and at temperatures ranging from $T = 20^0C$ to $T = 60^0C$. The results of viscosity measurements have been used in analysis of experimental work described in further sections. An unexpected effect of surfactant concentration on ferrofluid viscosity has been noted, with addition of more surfactant either decreasing or increasing viscosity of the colloid, depending on concentration value. Experimental methodology for viscosity measurements is described in sect. 3.8.

4.2 Newtonian fluid tests

Newtonian behavior at all relevant surfactant concentration values is confirmed for the ferrofluid by investigating the relation between shear rate and shear stress. All measurements are performed at 20^0C. The results are shown in fig. 4.1. In all investigated cases, the ferrofluid displays a behavior characteristic of a Newtonian fluid.

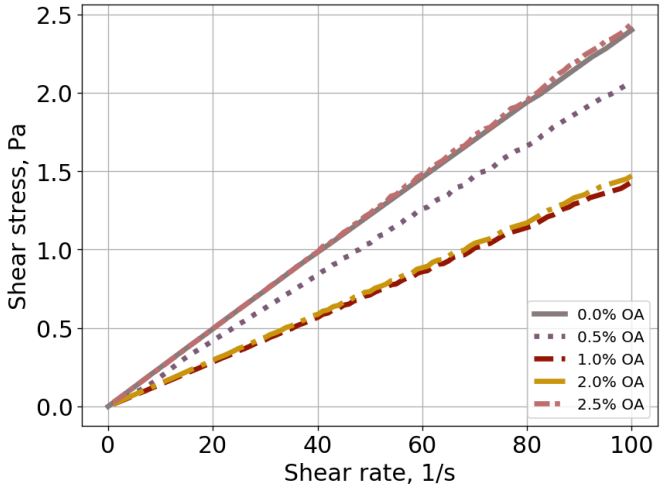

Figure 4.1: Shear stress depending on stress rate at $T = 20^0C$ for ferrofluid at various concentrations of OA

4.3 Dependence of ferrofluid and carrier fluid viscosity on surfactant concentration

Viscosity of tetradecane and oleic acid mixture depending on oleic acid concentration has been measured at different temperatures. The results are displayed in fig. 4.2.

Viscosity of ferrofluid and oleic acid mixture is plotted against oleic acid concentration in fig. 4.3. We can observe a marked difference in the viscosity characteristics compared to mixtures of pure tetradecane and oleic acid.

4.4 Dependence of ferrofluid and carrier fluid viscosity on temperature

The temperature dependence of ferrofluid viscosity is shown in fig. 4.5. As expected, the viscosity decreases with increasing temperature for both ferrofluid and tetradecane (with and without added surfactant). These measurements are analyzed within the Arrhenius model, as given by eq. 1.40.

By fitting eq. 1.40 to the data by a Python script, values of activation energy E_a are calculated and presented in table 4.1. We can see that, with

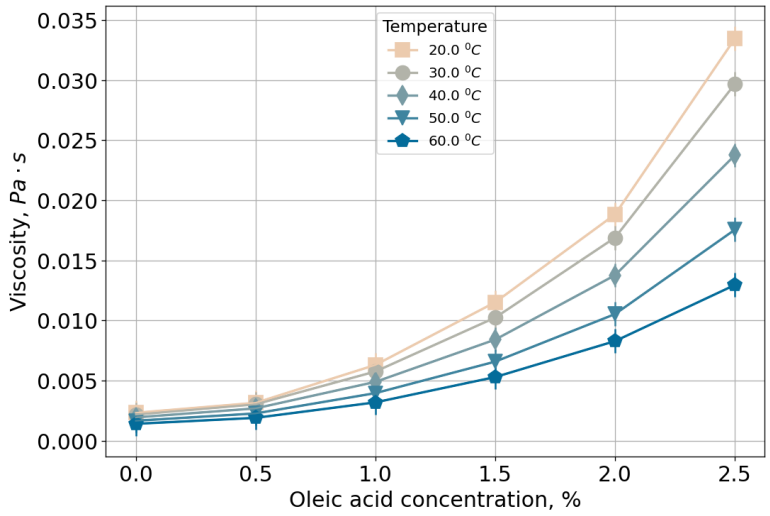

Figure 4.2: Viscosity of carrier fluid as a function of surfactant concentration at various temperatures between 20^0C and 60^0C

addition of oleic acid, the activation energy of ferrofluid initially presents a decrease by around 10%, before increasing at higher surfactant concentrations. Meanwhile, E_a for tetradecane consistently increases with the concentration of added oleic acid.

4.5 Analysis

Comparing viscosity values of carrier fluid and ferrofluid at 0% excess surfactant concentration, we see that viscosity of ferrofluid is higher than that of carrier fluid at corresponding temperature. The increase exceeds that predicted by eq. 1.38, which gives a value of $\eta = 0.0026\, Pa \cdot s$ at $T = 20^0C$. This would suggest that viscosity of a surfactant stabilized ferrofluid possesses characteristics not described by moderately concentrated colloid model, even when effects of magnetism are not in play.

For all inspected fluids, viscosity decreases with temperature in a manner than can be described by Arrhenius' law. An increase of carrier fluid viscosity following an increase of oleic acid concentration can be observed at all temperatures. The increase, higher than linear in proportion to surfactant amount, of tetradecane viscosity as more oleic acid is added, seems to suggest

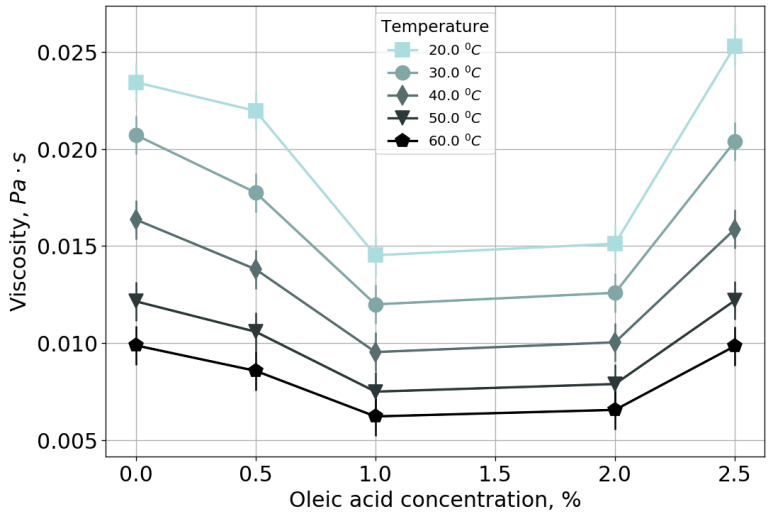

Figure 4.3: Viscosity of ferrofluid as a function of surfactant concentration at various temperatures between 20^0C and 60^0C

an interaction between oleic acid molecules. For ferrofluid, viscosity follows a curious trend, slightly decreasing at low oleic acid concentrations before increasing again. Then, at the highest investigated oleic acid concentrations, it reaches values similar to both ferrofluid at low oleic acid concentration and those of tetradecane with the same oleic acid concentrations.

Similarities of behavior between tetradecane and ferrofluid viscosity at high oleic acid concentration values seem to suggest that the pattern of ferrofluid viscosity changes is a result of two processes acting contrary and balancing each other at a temperature independent crossover point. Under this assumption, one of those processes, seen at high surfactant concentrations, would be a viscosity increase like that seen with tetradecane. The other, decrease of ferrofluid viscosity at lower, increasing surfactant concentrations, has no obvious explanation.

Potential explanations for the initial decrease of ferrofluid viscosity could involve either further adsorbtion of surfactant molecules, saturating the surfactant layer around nanoparticles, or some structure organization that could be compatible with the Newtonian regime of the rheological probing. Considering that no micelle formation is expected, nor, as briefly touched upon in sect. 1.1, is a surfactant double layer, the second explanation could be deemed unlikely.

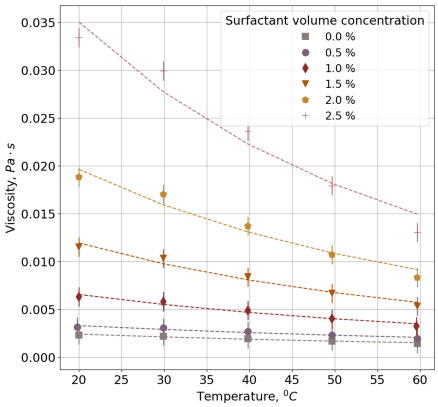

Figure 4.4: Tetradecane and oleic acid mixture viscosity depending on temperature, along with fitting results of eq. 1.40

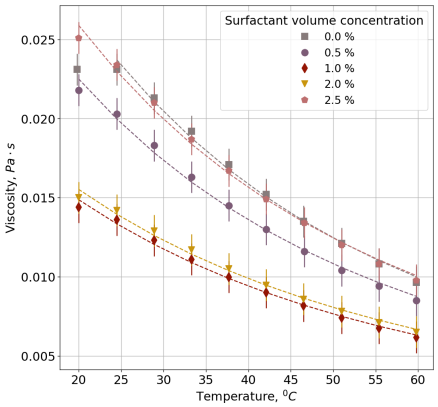

Figure 4.5: Ferrofluid and oleic acid mixture viscosity depending on temperature, along with fitting results of eq. 1.40

In the additional adsorbtion interpretation, we would be looking at a situation where the surfactant layer around the particles, while providing sufficient colloidal stability, is not saturated, and the added surfactant, in the initial steps, directly binds to the particles. Then, two mechanisms for viscosity reduction can be proposed.

In one scenario, structures of nanoparticles would form at lower surfactant concentrations (that would have to be compatible with the Newtonian regime seen throughout all surfactant concentrations) and dissolve as oleic acid concentration increases. The addition of surfactant would then lead to

$c_{oleic\,acid,vol.}, \%$	$E_a(tetradecane), \frac{J}{mol}$	$E_a(ferrofluid), \frac{J}{mol}$
0.0	$1.0 \cdot 10^4$	$2.0 \cdot 10^4$
0.5	$1.0 \cdot 10^4$	$1.9 \cdot 10^4$
1.0	$1.3 \cdot 10^4$	$1.8 \cdot 10^4$
1.5	$1.5 \cdot 10^4$	n/a
2.0	$1.6 \cdot 10^4$	$1.7 \cdot 10^4$
2.5	$1.7 \cdot 10^4$	$1.9 \cdot 10^4$

Table 4.1: Activation energy E_a for tetradecane and ferrofluid depending on amount of additional surfactant

progressive dissociation of weakly bound nanoparticle clusters into individual nanoparticles fully coated with surfactant. It will be demonstrated by size measurements performed with DLS (sect. 5.3), that this is indeed the case. Incomplete surfactant covering of nanoparticles leading to particle clustering has been previously reported by Susan-Resiga[24] – there, the source of imperfect covering was identified as presence of poorly stabilizing surfactant, while in our case, it is the apparent lack of surfactant on nanoparticles.

Additionally, it could be proposed that it is the saturation of surfactant layer itself that plays a role in viscosity reduction. Relevance could be suggested to a mechanism of lubrication provided by motion of molecules within the surfactant layer relative to the nanoparticles. As described in ref. [63], such lubrication can alter viscosity of colloid with sterically stabilized particles. The mechanism, as per the source, should apply to rotational oscillation mode of shear, which is not the case here. However, it does demonstrate the possibility of surfactant layer contributing to colloid viscosity decrease.

In order to provide an insight into dependence of viscosity on surfactant concentration, a parameter of relation between ferrofluid and carrier fluid viscosity η_{ff}/η_{td} is introduced, displayed in fig. 4.6.

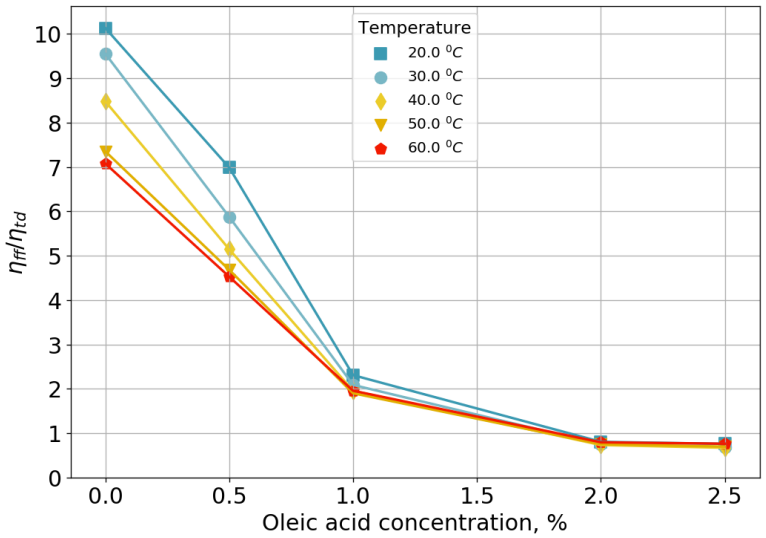

Figure 4.6: Ratio of ferrofluid and teradecane viscosities η_{ff}/η_{td} at various values of surfactant concentration and temperature

Three tendencies are immediately seen in fig. 4.6 - the ratio and spread

of ratio over temperatures both decrease as excess surfactant concentration increases, and the ratio is decreased by temperature increase. As suggested by the reduction of η_{ff}/η_{td} under T increase, temperature plays a role in agglomerate dissolution at lower surfactant concentration values. The vanishing temperature dependence of η_{ff}/η_{td} indicates that this role is diminished as more surfactant is adsorbed onto particles leading to increased colloidal stability - and less agglomerates to dissolve by temperature. A similarity could be seen between these temperature effects and nanoparticle aggregates in ferrofluids, forming in a reversible way under temperature variation, as described by Buzmakov[25]. This effect of temperature is in agreement with particle clusters being seen in DLS at room temperature, but not at FRS results, where ∇T is present. Reduction of the lowest ratio value at each surfactant concentration, reached at the highest temperature, could then be associated with surfactant layer saturation itself, reducing ferrofluid viscosity through particle lubrication.

As far as more mundane potential explanations of the observed phenomena are concerned, a possibility of wall slip of ferrofluid against rheometer plate can not be entirely denied, but it would have to be asked why it is not seen in carrier fluid measurements at the same surfactant concentrations, which renders this explanation unlikely.

Activation energy (characterizing the dependence of viscosity on temperature) shows a similar trend to that seen with viscosity. For tetradecane, activation energy increases with oleic acid concentration. For the ferrofluid, E_a decreases initially, before increasing again at higher oleic acid concentration values.

Chapter 5

Nanoparticle size and mass diffusion coefficient

5.1 Overview

In this chapter, measurements of nanoparticle size and mass diffusion coefficient, in both free fluid and a porous medium are given. Comparing D_m in the two environments comes as a part of the efforts to understand effects of a porous medium on nanoparticle transport properties. Apart from that, the purpose and effect of investigations into D_m and particle size measurements are twofold. Firstly, it is a way of characterizing the colloids by learning their mass diffusion coefficient and hydrodynamic size, to complement magnetic size measurements given in sect. 2.2. Secondly, several methods of particle size measurement have been employed, compared and their joint results used in context of mass diffusion coefficient measurements made with two FRS setups. Thus, the results reported in this section serve as a way to provide cross confirmation between several measurement methods employed in this thesis.

5.2 Mass diffusion coefficient

Mass diffusion coefficient of ferrofluids is determined in a free fluid and in a porous medium. In free fluid, D_m is measured by Forced Rayleigh scattering, as described in sect. 3.6 - by observing dissolution of particle concentration spatial modulation brought upon by spatial temperature modulation.

Here, mass diffusion coefficient measurements by FRS setup in Laboratorie PHENIX, Sorbonne Université are presented, while values of Soret coefficient determined in the same experiments are given in sect. 6.3. In a porous layer, mass diffusion coefficient is measured as described in sect. 3.2 - by saturating half (height wise) of a flat cylindrical porous layer with ferrofluid, the other half with the corresponding carrier fluid and measuring the developing particle concentration profile at various points in time.

5.2.1 Mass diffusion coefficient in free fluid

FRS has been used to measure mass diffusion coefficient of ferrofluid df105 at three values of oleic acid concentration and at several temperatures. Measurement results are given in fig.5.1, along with a curve representing D_m values calculated from Stokes-Einstein relation. It should be noted that results for 1% oleic acid concentration correspond to measurements performed with a measurement cell that was found to be leaking and could therefore be found to be less reliable.

$$D_m = \frac{k_B T}{3\pi\eta_0 d_h} \tag{5.1}$$

with the mean size value from all FRS and DLS measurements, given in sect. 5.3 as d_h and pure tetradecane viscosity as η_0.

5.2.2 Mass diffusion coefficient in a porous layer

Mathematical framework

The mathematical formulation used to calculate D_m in a porous layer is laid out in full in ref. [74, Sints et al.]. We are considering a flat cylindrical porous layer. Thickness of the layer is taken to be $\delta = 2a$, with half of layer where $a > x > 0$ saturated with ferrofluid and the other half of layer where $0 > x > -a$ saturated with carrier fluid. We introduce parameters for distance, X:

$$X = \frac{x}{a} \tag{5.2}$$

concentration, C, with c_0 denoting the initial concentration of particles, uniform across the ferrofluid-saturated half of layer:

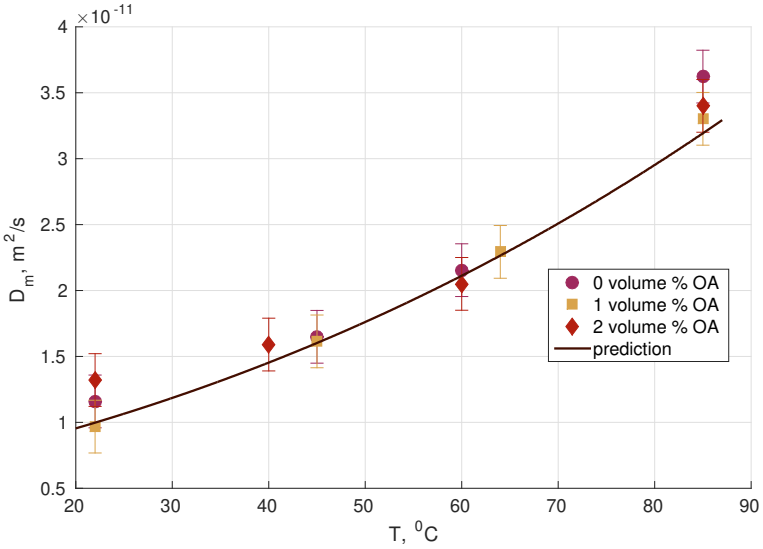

Figure 5.1: Mass diffusion coefficient D_m of sample df105 as a function of temperature T, as measured by FRS. The curve represents D_m calculated with eq. 5.1 from the average particle hydrodynamic diameter determined by FRS and pure tetradecane viscosity

$$C = \frac{c}{c_0} - 1 \tag{5.3}$$

and time, τ:

$$\tau = \frac{D_m t}{a^2} \tag{5.4}$$

The equation to be solved is, then:

$$\frac{\partial C}{\partial \tau} = \frac{\partial^2 C}{\partial X^2} \tag{5.5}$$

With boundary conditions representing no mass flux through top and bottom walls:

$$\frac{\partial C(X,\tau)}{\partial X}\Big|_{X=1} = \frac{\partial C(X,\tau)}{\partial X}\Big|_{X=-1} = 0 \tag{5.6}$$

It is shown that, at low values of τ, when the development of concentration profile may be described by employing the unsteady boundary layer approximation, the solution is:

$$C(X,\tau) = erf\left(\frac{X}{2\sqrt{\tau}}\right) \tag{5.7}$$

Results

Experimental setup is described in full in sect. 3.2. Experiments are performed for various time lengths and D_m is calculated from particle distribution in the layer, by fitting equation 5.7. The fitting is done with a MATLAB script. An example of experimental data and fitted curves for sample df105 is given in fig. 5.2.

Measurements from the porous layer are compared to FRS measurements of D_m performed in Institute of Physics, University of Latvia. The accuracy of D_m measurements by FRS is about 5%, the uncertainty being mostly due to particle polydispersity. It should be noted that these FRS measurements are not performed at a controlled temperature. The accuracy of measurements in porous layer is estimated in sect. 3.2 to be around 15 % of measurement value. Results from both methods are given in table 5.1.

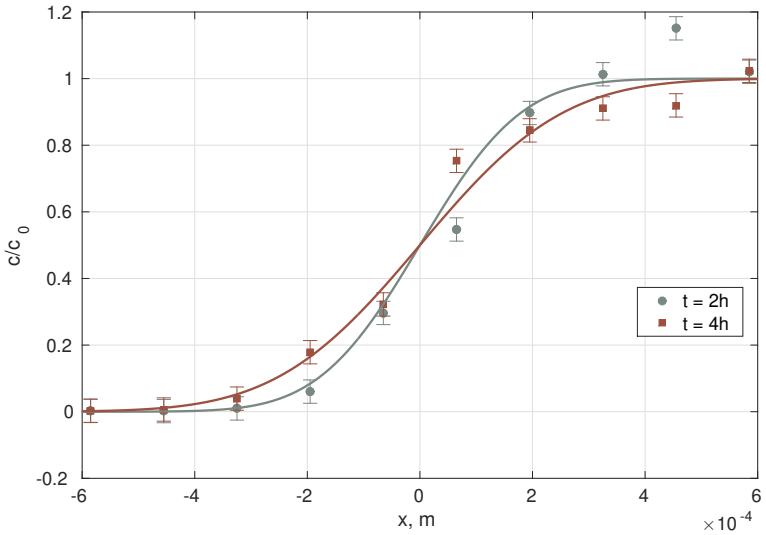

Figure 5.2: Particle distribution in a porous layer after 2h and 4h of diffusive transfer, corresponding to τ values of $\tau = 0.2$ and $\tau = 0.4$. The solid lines represent fitting of eq. 5.7

ferrofluid	$D_m, m^2/s(FRS)$	$D_m, m^2/s(porous)$
df105	$1.86 \cdot 10^{-11}$	$1.56 \cdot 10^{-12}$
S-1	$0.41 \cdot 10^{-11}$	$0.06 \cdot 10^{-12}$
U5	$3.50 \cdot 10^{-11}$	$2.85 \cdot 10^{-12}$
FF1304	$1.34 \cdot 10^{-11}$	$3.71 \cdot 10^{-12}$

Table 5.1: Mass diffusion coefficients in a free fluid and in a porous layer

$c_{oleic\,acid,vol.}, \%$	dh, nm
0.0	48
2.0	20

Table 5.2: Hydrodynamic diameter of particles in ferrofluid samples, measured by Dynamic light scattering at $T = 20^0 C$

5.3 Nanoparticle size

In this section, size measurements from Dynamic Light scattering and Forced Rayleigh scattering methods are presented and compared. Measurements have been made for sample df105 with 0 %, 1% and 2% excess oleic acid concentration. It would serve well to remind that number average particle diameter from magnetic measurements was $d = 8.8\,nm$ and volume average magnetic size is $d = 11.6\,nm$.

The DLS method is described in sect. 3.9 - particle size is calculated from mass diffusion coefficient, using pure carrier fluid viscosity. DLS measurements were performed in Lab. PHENIX, Sorbonne Université. Results of DLS measurements are given in table 5.2.

Another approach to particle size measurements is to calculate d_h from D_m measured with FRS. The procedure here is much like in case with DLS measurements. Viscosity value used in calculations is pure carrier fluid viscosity and temperature is known because the measurement cell is placed in a thermo-regulated chamber. Results are summarized in table 5.3.

OA conc.	0 %	1 %	2 %
$T, ^0 C$	dh, nm		
22	16.6	19.4	14.3
40			15.1
45	15.8	16.1	
60	15.7		16.5
64		15.8	
85	14.7	16.1	15.6

Table 5.3: Hydrodynamic diameter of particles in ferrofluid samples, measured by Forced Rayleigh scattering

ferrofluid	tortuosity
df105	3.4
S-1	8.3
U5	3.5
FF1304	1.9

Table 5.4: Tortuosity of the porous environment, calculated from experiments with different samples

5.4 Analysis

As seen from mass diffusion coefficient measurements in a free fluid, D_m increases with temperature, which is to be expected. Mass diffusion coefficient does not show a significant or consistent dependence on surfactant concentration. Calculations provide well fitting results if pure carrier fluid viscosity is used to relate particle size and D_m.

Mass diffusion coefficient in a porous layer is lower than in a free fluid for all tested samples, by about one order of magnitude. This is consistent with general expectation of D_m being reduced in a porous medium due to elongation of particle paths, characterized by the parameter of tortuosity τ_d, see sect. 1.6 for details. Table 5.4 shows values of tortuosity calculated from D_m using eq. 1.27 in the form:

$$\tau_d = \sqrt{\frac{D_m(free\ fluid)}{D_m(porous)}} \tag{5.8}$$

Average tortuosity across the samples would then be $\tau_d = 4.3$. This value is, however, skewed by the large tortuosity value for sample S-1. For this sample, D_m is considerably smaller than for the other samples, and it is possible that the 24 hour time allowed for diffusive mass transfer for the sample has been insufficient to get reliable results. If this measurement is discarded, a sufficient agreement can be seen between values for different samples, with an average of $\tau_d = 2.9$.

It is found that two methods of particle size determination provide significantly different results. Comparison to previous results[23], where iron oxide nanoparticle size was found to increase by around $4\,nm$, or about twice the oleic acid molecule size, as the particles are coated with oleic acid, lets us

conclude that hydrodynamic size determined by FRS is fairly consistent with magnetic size measurements given in sect. 2.2. Size measurements performed with DLS give higher size values, pointing at existence of agglomerates. A possible cause of this not being detected by FRS is that the agglomerates are weak, and the temperature gradient imposed during FRS measurements is enough to dissolve them. DLS, on the other hand, does not perturb the clusters and is able to detect them.

Chapter 6

Thermophoresis

6.1 Overview

This chapter of the thesis is devoted to results of experiment series characterizing ferrofluid thermophoresis. The first series of experiments investigates how Soret coefficient measured in a porous layer compares to that in a free fluid, experiments are done with four ferrofluid samples that include both surfaced and ionic ferrofluids. The other two series both investigate effects of temperature dependence and addition of excess surfactant on thermophoresis, one in a free fluid and the other in a porous medium. These series focus on sample df105, a surfactant stabilized ferrofluid.

It will be demonstrated in this chapter that surfaced ferrofluid Soret coefficient has an exponential dependence on temperature that can be described by the popular Iacopini - Piazza empirical model, and that, in a porous layer and beginning from certain values of excess surfactant concentration, temperature at which S_T changes sign from positive to negative can be lowered to almost room temperatures, resulting in an overall particle transfer towards higher temperatures for a ferrofluid with a positive S_T, as measured in a free fluid. It should be mentioned that another series of ferrofluid thermophoresis experiments, focusing on effects of an external magnetic field, is described in this thesis and can be found in chapter 8.

6.2 Thermophoresis in a porous medium compared to a free fluid

6.2.1 Overview

The first series of experiments to review is concerned with how the presence of a porous medium affects thermophoretic flow of ferrofluid particles. Soret coefficient is measured in two environments. In free fluid, S_T is measured by Forced Rayleigh scattering, as described in sect. 3.6. The FRS setup used is in Institute of Physics, University of Latvia. The accuracy of FRS S_T measurements here is estimated to be approximately 10% due to lack of detailed information about the colloid optical refractive index. Soret coefficient in a porous medium is measured as described in sect. 3.1 - in brief, a flat cylindrical porous layer is saturated with ferrofluid, which is then subjected to a temperature gradient. At the end of the experiment, the layer is split into ten along the axis that temperature gradient was aligned with and particle concentration in each is measured by Vibrating sample magnetometry.

6.2.2 Mathematical framework

The mathematical description of nanoparticle thermophoresis in a flat porous layer is given in ref. [74, Sints et al.], with only the points relevant to analysis of experimental results presented in this work given here. We look at a layer of thickness $\delta = 2a$, with a temperature gradient along x axis, so that temperature difference $\Delta T = T(a) - T(-a)$. It should be noted that this effectively gives x axis direction opposite to that in diffusion experiments. We introduce relative concentration of particles C (with c_0 being the initial, uniform particle distribution):

$$C = \frac{c}{c_0} \tag{6.1}$$

distance, X:

$$X = \frac{x}{a} \tag{6.2}$$

time, τ:

$$\tau = \frac{D_m t}{a^2} \tag{6.3}$$

and parameter k as:

$$k = \frac{S_T \Delta T}{2} \tag{6.4}$$

Then, particle mass transfer by thermodiffusion is given by:

$$\frac{\partial C}{\partial \tau} = \frac{\partial^2 C}{\partial X^2} + k \frac{\partial C}{\partial X} \tag{6.5}$$

With boundary condition, representing no mass flux through top and bottom walls:

$$\frac{\partial C}{\partial X}\Big|_{X=\pm 1} + kC\Big|_{X=\pm 1} = 0 \tag{6.6}$$

and initial condition, expressing the uniform relative distribution of particles:

$$C\Big|_{t=0} = 1 \tag{6.7}$$

It is shown in ref. [74] that the solution to eq. 6.5 at a stationary state is:

$$C(X) = \frac{k \exp(-kX)}{\sinh(k)} \tag{6.8}$$

6.2.3 Results

Thermodiffusion experiments are conducted in a porous layer for 24 hours. Experimental values of Soret coefficient are attained by fitting eq. 6.8 to experimental data of particle distribution in the layer. The results are shown in table 6.1, where S_T in a porous layer is compared to values in free fluid measured by Forced Rayleigh scattering.

Two examples of particle distribution (ferrofluids df-105 and FF 13-04) with the respective approximation functions from eq. 6.8 are presented in fig. 6.1. It should be noted that, for the ferrofluid sample FF 13-04 with $S_T = 0$ in free fluid, the particle flow within the porous layer is directed toward higher temperatures, with a negative S_T.

$c_{oleic\,acid,vol.}$, %	$S_{T,1}(FRS)$, $\frac{1}{K}$	$S_{T,1}(porous)$, $\frac{1}{K}$
df-105	0.15	0.048
S-1	0.20	0.006
U5	0.15	0.062
FF13-04	0.00	-0.030

Table 6.1: Soret coefficient in free fluid, measured by FRS, and in a porous medium

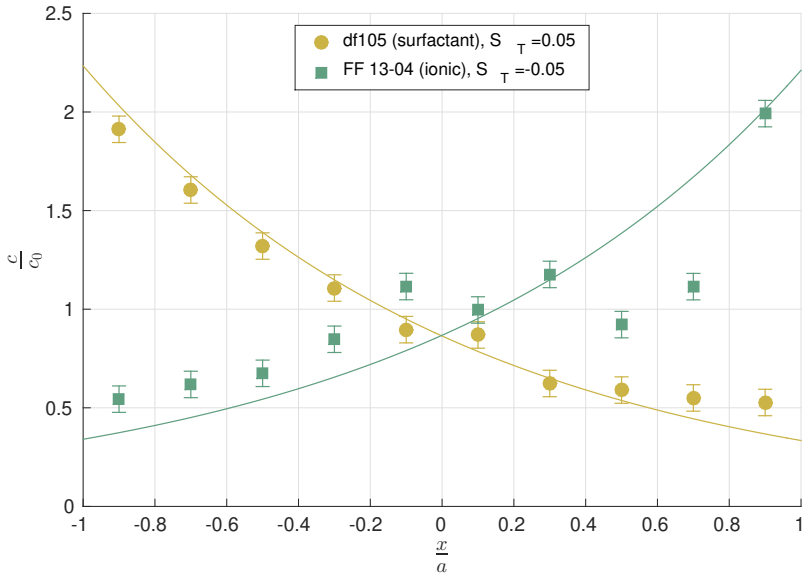

Figure 6.1: relative concentration profiles for surfaced (df-105) and ionic (FF 13-04) ferrofluid in a porous layer, along with fitting results of eq. 6.8. Temperature gradient is directed toward positive distance values, opposite to direction of gravitation force. In the case of ionic ferrofluid, nanoparticle concentration has increased at higher temperatures, which corresponds to negative S_T, while $S_T = 0$ in free fluid.

6.2.4 Analysis

A conclusion can immediately be drawn from these results, that both diffusion and Soret coefficients measured in the porous environment are significantly lower than in free fluid. It should be highlighted that decrease of transfer coefficients does not always correspond to the absolute values of S_T decreasing, which would correspond to particle transfer being hampered or, potentially, a stationary state not having been reached. This is demonstrated by Soret coefficient for ferrofluid FF 13-04, that has turned negative in the porous layer. No particle transfer induced by a temperature gradient was observed in free fluid for FF 13-04, corresponding to Soret coefficient of zero. In this case, particle transfer has appeared, instead of being diminished.

No immediate explanation for the decrease in S_T is apparent. It is known that mass diffusion and thermodiffusion coefficients can both be reduced in a porous environment. However, they are expected to both decrease by the same proportion to tortuosity of the porous environment, leaving S_T unchanged, see sect. 1.6 for a more detailed look. A possible interpretation that has been considered draws parallels to the very nature of particle thermophoresis as described by some of the models listed in sect. 1.4. According to this proposed interpretation, elements of the porous medium would induce a temperature gradient driven flow of ferrofluid through a mechanism comparable to that responsible for thermally induced motion of nanoparticles - consider an analogy with the slip velocity mechanism described by Anderson, or the fluid slip velocity through a membrane pore given by Derjaguin and Sidorenkov. Attempts to interpret the results given in this section are revisited in the summary section for ferrofluid particle thermophoresis measurements, sect. 6.5.

6.3 Effects of surfactant concentration and temperature on ferrofluid thermophoresis in a free fluid

6.3.1 Overview

Ferrofluid thermophoresis has been investigated in free fluid, as opposed to a porous environment, with particular attention paid to effects of excess surfactant added to the colloid, and of temperature dependence. All experi-

ments are done with ferrofluid sample df105. The experimental methodology of Forced Rayleigh scattering (FRS) has been employed, the methodology is described in sect. 3.6. Measurements are performed with FRS setup in Lab. PHENIX, Sorbonne Université and come from the same experimental work that is described in sect. 5.2.

6.3.2 Results

Soret coefficient is measured by FRS for ferrofluid df105 with 0%, 1% and 2% excess oleic acid concentration at temperatures in range from $T = 20^0C$ to $T = 85^0C$. Due to a leaking fluid cell, 1% surfactant concentration measurements have been deemed unreliable and been discarded. Results of the measurements are given in table 6.2.

0% OA volume conc.		2% OA volume conc.	
$T,^0C$	$S_T, 1/K$	$T,^0C$	$S_T, 1/K$
22	0.27	22	0.20
45	0.25	40	0.19
60	0.20	60	0.18
85	0.14	85	0.14

Table 6.2: Soret coefficient depending on temperature, measured by FRS at two values of excess surfactant concentration

6.3.3 Analysis

Soret coefficient as a function of temperature has been analyzed in the framework of the Iacopini - Piazza empirical model given by eq. 1.25, see ref. [48] and sect. 1.4. However, a need for a slight difference from the model as originally presented is apparent from the results, see table 6.2 and fig. 6.2 for a visual representation. The original model contains a coefficient S_T^∞ referred to as a high temperature limit for the Soret coefficient. However, for the ferrofluid used here, S_T decreases with temperature. To acknowledge this, S_T^∞ is replaced by $S_{T,1}$. With that, the coefficients are T^* (the temperature at which $S_T = 0$), T_0 (characterizing the strength of temperature effects on Soret coefficient) and $S_{T,1}$ (a "low temperature limit" for S_T). The math-

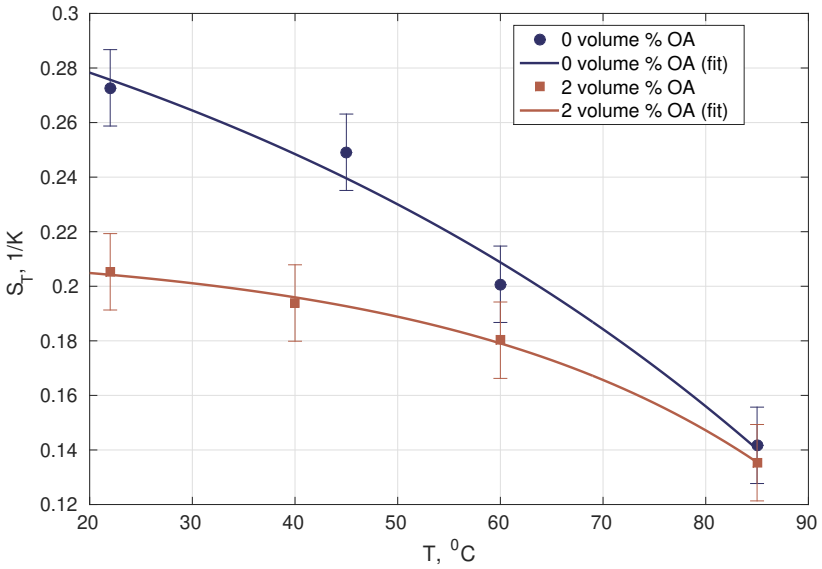

Figure 6.2: Soret coefficient depending on temperature, measured by FRS, along with fitting results of eq. 6.9

$c_{oleic\,acid,vol.}, \%$	$S_{T,1}, \frac{1}{K}$	$T^*, {}^0C$	$T_0, {}^0C$
0.0	0.37	118.60	70.22
2.0	0.22	116.27	31.40

Table 6.3: Parameters of Iacopini-Piazza model fitted to Soret coefficient measurements

ematical notation of the model has been slightly modified to reflect these peculiarities:

$$S_T(T) = S_{T,1}[1 - \exp(\frac{T - T^*}{T_0})] \tag{6.9}$$

Results of the measurements are given in fig. 6.2 as S_T plotted against temperature, along with fitting results of eq. 6.9. Fitting is done via a Matlab script. Parameters attained by fitting eq. 6.9 to experimental data are shown in table 6.3.

It can be seen already from fig. 6.2 that the addition of excess oleic acid decreases S_T. At room temperature, the decrease in S_T between 0 % and 2 %

excess oleic acid concentration appears to be around a quarter of the initial value. The values of $S_{T,1}$ quantify this observation.

The decrease of parameter T_0 shows that, by adding more surfactant, the Soret coefficient has become less dependent on temperature. Values of T^* reinforce what an observation of fig. 6.2 would also suggest - that it appears possible to reduce S_T into negative values by further increasing temperature.

6.4 Effects of surfactant concentration and temperature on ferrofluid thermophoresis in a porous medium

6.4.1 Overview

Experiments series of thermophoretic particle transfer of ferrofluid sample df105 in a closed porous layer are reported on in this section, the results have originally been published in [79, Sints *et al.*]. A series of experiments is done at different values of excess surfactant concentration, showcasing a dependence on this parameter with fundamental consequences to thermophoretic characteristics of the colloid. Two approaches to modeling temperature dependence of S_T have been employed. Experiments at several values of temperature difference are done to compare the two approaches.

6.4.2 Mathematical framework

The significance of temperature dependence displayed by S_T in measurements presented in sect. 6.3 suggest that equation 6.8 used hitherto to describe particle distribution in a porous layer is not sufficient to describe the thermophoretic mass transfer process, and that the Soret coefficient must be viewed as dependent on temperature. For the mathematical description of colloidal particle distribution as a result of thermophoresis in a layer with $S_T = S_T(T)$, equation 1.16, describing particle flux as a result of concentration and temperature gradients, is used, assuming $1 - c \approx 1$, so that, along the axis of temperature gradient:

$$\frac{dc}{dx} = -c_0 S_T \frac{dT}{dx} \tag{6.10}$$

We strive here to define concentration relative to initial particle concentration, uniform across the layer: $C = \frac{c}{c_0}$. A linear temperature gradient within the layer is assumed:

$$\frac{dT}{dx} = \frac{\Delta T}{2a} \tag{6.11}$$

Two models for $S_T(T)$ are considered. One of them is the Iacopini - Piazza model, given in eq. 1.25, in the form given by eq. 6.9, taking into account that the ferrofluid used in research presented displayed a low temperature "plateau" of Soret coefficient, followed by a decrease as temperature increases, see sect. 6.3. Then, eq. 6.10 becomes

$$\frac{dc}{dx} = -c_0 S_{T,1}[1 - \exp(\frac{T - T^*}{T_0})]\frac{dT}{dx} \tag{6.12}$$

which, upon integration, yields particle distribution:

$$c = \exp[-S_{T,1}(x_*\Delta T - T_0 \exp[\frac{T_{x_*=0} + x_*\Delta T - T^*}{T_0}])] \tag{6.13}$$

To arrive at relative concentration of particles, it is recalled that c is initially uniform, so that $c = c_0$ across a layer of thickness $2a$, an there is no mass flux to or from the layer. Then, with relative distance defined as (note that this definition of X differs from that used before, in sect. 6.2):

$$X = \frac{x}{2a} \tag{6.14}$$

c_0 is given by:

$$c_0 = \frac{1}{\Delta X}\int_{-1/2}^{1/2} \exp[-S_{T,1}(X\Delta T - T_0 \exp[\frac{T_{X=0} + X\Delta T - T^*}{T_0}])]dX \tag{6.15}$$

And relative particle concentration distribution is:

$$\frac{c}{c_0} = \frac{\exp[-S_{T,1}(X\Delta T - T_0 \exp[\frac{T_{X=0}+X\Delta T - T^*}{T_0}])]}{\int_{-1/2}^{1/2} \exp[-S_{T,1}(X\Delta T - T_0 \exp[\frac{T_{X=0}+X\Delta T - T^*}{T_0}])]dX} \tag{6.16}$$

The other model for $S_T(T)$ is a loose interpretation of theoretical model found in a work by Morozov[41], following the expression for the Soret coefficient given as $S_T = \frac{P}{T_0}$, see sect. 1.4. With the parameters of colloid used in

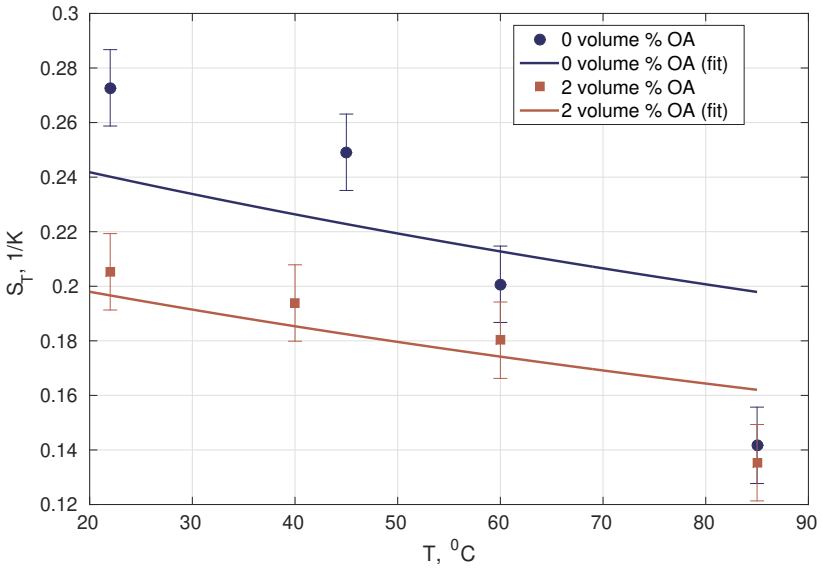

Figure 6.3: Soret coefficient depending on temperature, measured by FRS, along with fitting results of eq. 1.19

our experiments, the temperature dependence of eq. 1.19 can be linearized to get:

$$S_T(T) = S_{T,0} + \frac{dS_T}{dT}(T - T_0) \tag{6.17}$$

where $S_{T,0} = S_T(x = 0)$. Figure 6.3 is presented both as an argument for the possibility of $S_T(T)$ linearization, and as a demonstration of how well, or rather ill fitting the model is for our situation. In fig. 6.3, the data points are the same as given in sect. 6.3.2 and the lines correspond to best fit of $S_T = \frac{P}{T_0}$ to said data.

The poor fit of the model to experimental results is no surprise if one recalls the general shape of function $y = \frac{1}{x}$, and compares that to layout of the data. It should be highlighted that the approach presented here is indeed an approximate take on Morozov's model, as all the physical parameters constituting the protective layer state parameter P are assumed to be temperature independent. It could also be recalled that a similar conundrum presented itself with implementation of the Iacopini - Piazza model, solved by reconsidering values of some of the parameters while keeping the mathematical

formulation. With lack of knowledge regarding the microscopic thermodynamic parameters constituting P, neither such manipulations, not expansion of P as $P(T)$ are viable options. With this in mind, the interpretation of $S_T(T)$ presented here should not be considered as an implementation of Morozov's model, but rather a comparative analysis on how a linear model for $S_T(T)$ compares to the exponential one described previously.

Carrying on from eq. 6.17, the stationary particle concentration distribution for thermophoretic transfer is:

$$\frac{dc}{dx} = -c(S_T + \frac{dS_T}{dT}\frac{dT}{dx}x)\frac{dT}{dx} \tag{6.18}$$

From this, we get an expression for particle concentration distribution:

$$c(x) = \exp[-S_{T,0}\frac{\Delta T}{2a}x - \frac{dS_T}{dT}(\frac{\Delta T}{2a})^2\frac{x^2}{2}] \tag{6.19}$$

Or, after introducing parameters $A = S_{T,0}\frac{\Delta T}{2}$ and $B = \frac{dS_T}{dT}(\frac{\Delta T}{2})^2$:

$$c = \exp[-2(AX + BX^2)] \tag{6.20}$$

For relative particle concentration $\frac{c}{c_0}$, following a similar approach as before, we get:

$$\frac{c}{c_0} = \frac{\exp[-2(AX + BX^2)]}{\int_{-1/2}^{1/2}\exp[-2(AX + BX^2)]dX} \tag{6.21}$$

This approach is referred to throughout this section as the linear approach due to the linearized temperature dependence of S_T, while the approach based on Iacopini - Piazza model is referred to as exponential.

6.4.3 Particle distribution in a porous layer at different surfactant concentration values

Eight thermophoresis experiments have been performed with temperatures $T_{top} = 60\,^0C$ and $T_{bottom} = 20\,^0C$, with the amount of excess surfactant concentration ranging from $c_{surfactant} = 0\,\%$ to $c_{surfactant} = 3.75\,\%$. Experimental setup has been described in sect. 3.1 and is the same as in experimental work comparing S_T in a free fluid and a porous layer, see sect. 6.2.

Particle concentration distributions within the porous layer after 24 hours of the layer being subjected to temperature gradient are summarized in fig.

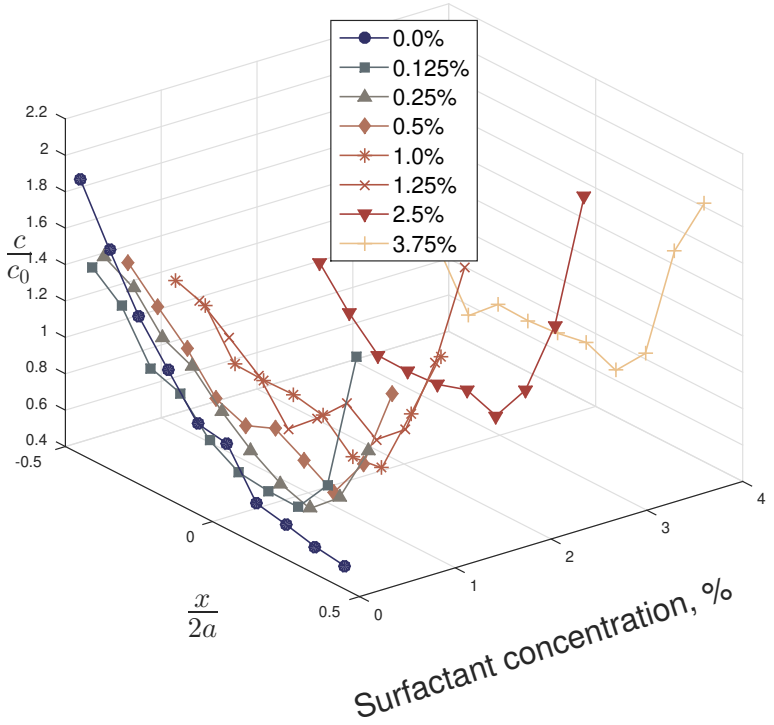

Figure 6.4: Nanoparticle concentration profiles from thermophoresis experiments. Values in legend correspond to surfactant volume concentration

6.4. Here and throughout this section, $X = \frac{x}{2a} = -0.5$ corresponds to T_{bottom}, or the lower temperatures, and $X = 0.5$ corresponds to T_{top}, the higher temperatures.

As was already seen in previous sections, with no excess surfactant added, particles demonstrate a thermophobic behavior, as their concentration near higher temperatures has decreased, and concentration near lower temperatures has increased. What is demonstrated in fig. 6.4 is that an increase in excess surfactant concentration leads to a decrease in the tendency of magnetic nanoparticles to move away from higher temperatures. As the excess surfactant concentration increases, the thermophobic behavior of the particles diminishes and a thermophilic one emerges and becomes dominant, with a net particle flux towards higher temperatures at higher values of excess surfactant concentration.

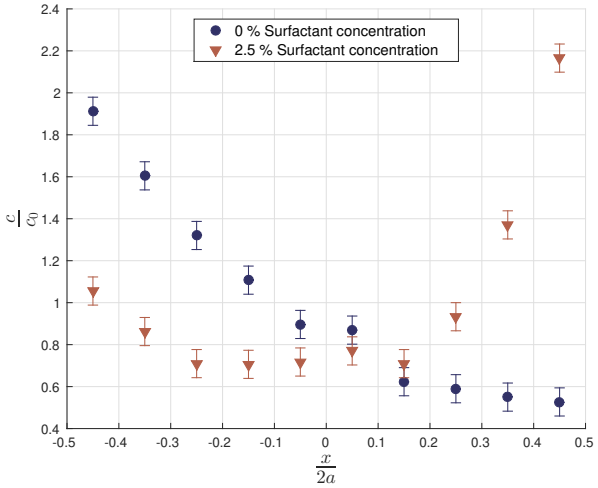

Figure 6.5: Comparison of nanoparticle distribution profiles at high and low values of surfactant concentration

For a more transparent comparison, two concentration profiles are highlighted in fig. 6.5, showcasing all but a full reversal in profile, achieved by increasing volume concentration of excess oleic acid from 0 % to 2.5 %.

6.4.4 Particle distribution in a porous layer at different temperatures

In order to evaluate the ability of two models for Soret coefficient dependence from temperature introduced in sect. 6.4.2 to describe and predict $S_T(T)$, thermophoresis experiments are performed at various temperatures and results compared to predictions made with the two models. Equations 6.21 and 6.16 to the experimental data shown in fig. 6.4 to obtain coefficients A and B for the linearized temperature dependence model, and $S_{T,1}$, T^* and T_0 for the Iacopini model, for different values of excess surfactant concentration. These are used to predict the distribution of relative particle concentrations at different temperatures, to be compared with experimental data.

Two experiments are performed at temperatures $T_{top} = 60\,^0C$ and $T_{bottom} = 40\,^0C$, with excess surfactant concentrations of $c_s = 0.25\,\%$ (results and model predictions given in fig. 6.6) and $c_s = 1\,\%$ (results and predictions given in fig. 6.7).

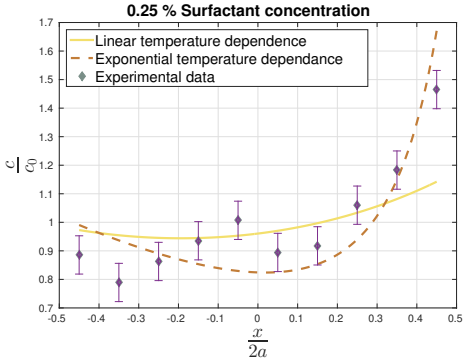

Figure 6.6: Particle distribution profile at surfactant concentration 0.25 %; $T_{top} = 60\,^0C$, $T_{bottom} = 40\,^0C$, along with predictions made by the two models

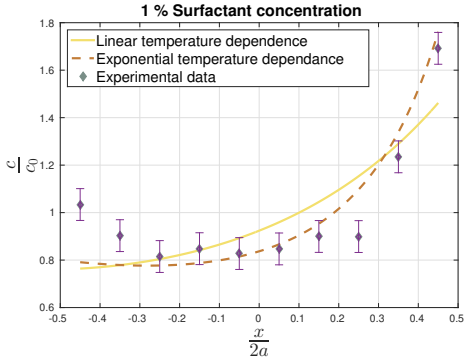

Figure 6.7: Particle distribution profile at surfactant concentration 1.00 %; $T_{top} = 60\,^0C$, $T_{bottom} = 40\,^0C$, along with predictions made by the two models

A single experiment is performed with temperatures $T_{top} = 40\,^0C$ and $T_{bottom} = 20\,^0C$, and $c_{surfactant} = 2.5\,\%$, results and model predictions are presented in fig. 6.8. An unusually high scattering of measurement points may prevent any clear conclusions from being drawn.

6.4.5 Analysis

The immediate and obvious takeaway from thermophoresis experiments in a porous layer is that addition of excess surfactant contributes to turning behavior of nanoparticles from thermophobic towards thermophilic, up to the point where particle flow at certain values of additional surfactant concentration is as strong towards higher temperatures as it was towards lower temperatures prior to any additional surfactant being added.

Before any analysis of S_T as a function of temperature has been carried out, it can be noticed that in majority of the concentration profiles, slope of the profile is inverted at $X = 0.5$ compared to $X = -0.5$. This would suggest that a positive Soret coefficient is observed where fluid temperature is lower, and is diminished or even inverted where fluid temperature is higher, particularly at larger surfactant concentrations.

While none of the two models for $S_T(T)$ described in sect. 6.4.2 fail completely in describing the general shape and direction of particle transfer in

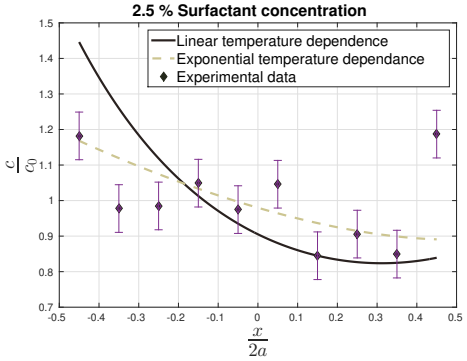

Figure 6.8: Particle distribution profile at surfactant concentration 2.5 %; $T_{top} = 40\,^0C$, $T_{bottom} = 20\,^0C$, along with predictions made by the two models

experiments at various temperatures, predictions made with the exponential model seem to be more accurate in predicting the concentration profiles. This can be seen particularly in the high particle concentrations near higher temperatures.

Soret coefficient as described by both models is plotted against temperature in fig. 6.9 for select values of surfactant concentration. A decrease of the Soret coefficient as the temperature increases is observed, as it was in a free fluid. This effect is stronger at higher values of surfactant concentration. Values of S_T are consistently lower than in free fluid and, unlike in FRS experiments, cross the value of $S_T = 0$, Soret coefficient becoming negative within the investigated temperature range.

Coefficients from both models that correspond to a form of the Soret coefficient itself are presented in fig. 6.10. The coefficient $S_T(T = 40\,^0C)$ is obtained using the linearized temperature dependence model described in eq. 6.21 and describes S_T at temperature $T = 40^0C$. We can see a decrease and a change in sign of the coefficient, also giving a hint on eventual saturation of the effect. The coefficient $S_{T,1}$, obtained from eq. 6.16, demonstrates a similar dynamic. The magnitude of decrease of $S_{T,1}$ and $S_T(T = 40\,^0C)$, compared to Soret coefficient measured in free fluid in the case of no excess surfactant reaffirm the results of ref. [13] and is comparable to that reported for Soret coefficient of another surfaced ferrofluid in a different experimental

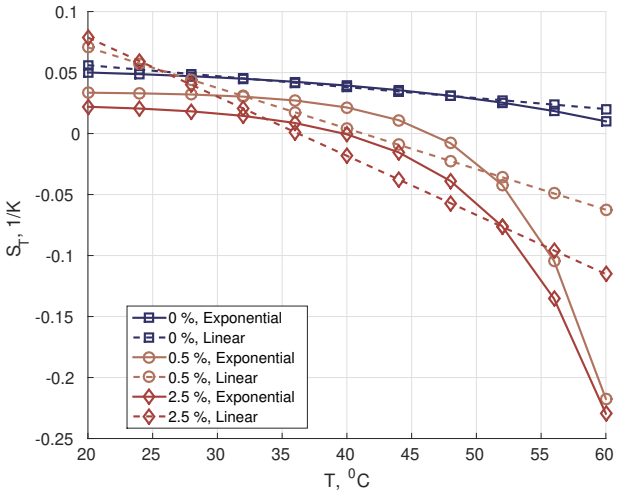

Figure 6.9: Dependence of Soret coefficient on temperature at various values of surfactant volume concentration, as described by the two models

system, as described in ref. [59].

Interpretation of coefficient T^*, from the Iacopini - Piazza model, is very straightforward, as the temperature at which the colloidal particles change their behavior between thermophilic and thermophobic. As fig. 6.11 demonstrates, for the colloid used in our experiments and in a porous medium, addition of excess surfactant can bring the change-of-sign temperature down to almost room temperature levels. Once again, we observe what appears to be a saturation of the effect.

It can be observed that a saturation of the effects caused by addition of excess surfactant seems to set in at certain values of surfactant concentration. Approximation with a simple exponential decay of coefficients presented in figs. 6.10 and 6.11 suggests that saturation should be reached at volume concentration values of less than 10 %.

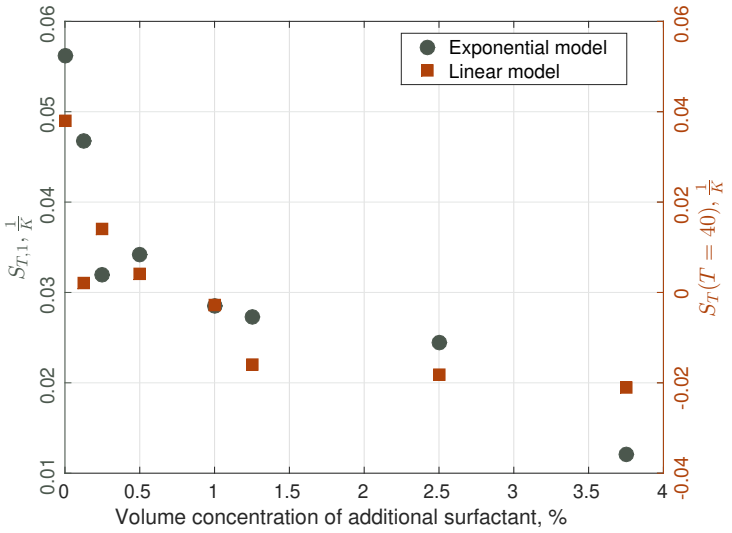

Figure 6.10: Dependence of coefficients $S_T(T = 40^0C)$ (linear model) and $S_{T,1}$ (highest attainable value of S_T, from the exponential model) on the amount of surfactant volume concentration

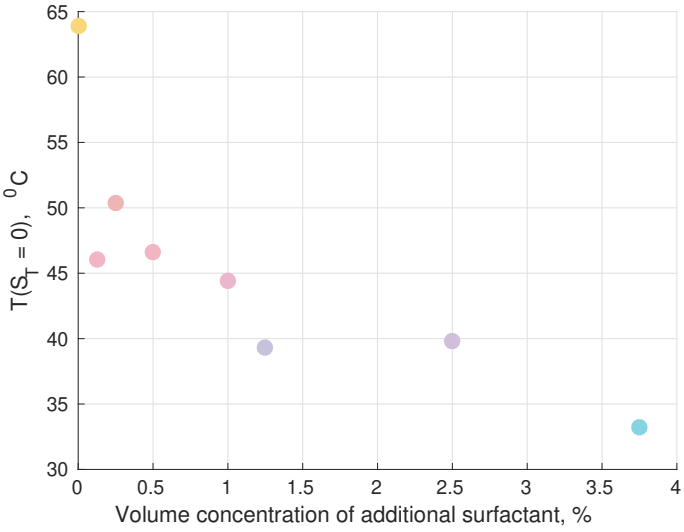

Figure 6.11: Dependence of particle thermophoretic transfer direction inversion temperature on the amount of surfactant volume concentration

6.5 Summary and discussion of thermophoresis experiments

Effect of excess surfactant on thermophoresis

Addition of excess surfactant (beyond the amount necessary to ensure colloidal stability that is added in manufacturing process) to a surfactant stabilized ferrofluid decreases the value of Soret coefficient for that ferrofluid. In free fluid, decrease of positive S_T to smaller positive values has been observed. In a porous layer, at large enough excess surfactant concentrations, a decrease from positive to negative S_T values has been demonstrated. The effects of a porous medium on colloid thermophoresis will be discussed separately further on.

The physical mechanism through which this influence is exerted has not been determined. Generally speaking, the mechanism would have to involve interaction either through the bulk of carrier fluid, or with the colloidal particles. As far as bulk of the carrier fluid is concerned, we can refer to results presented in Ch. 4, where no effect of excess surfactant concentration on mass diffusion coefficient of the ferrofluid examined here was observed. In sect. 6.2, it is shown that S_T is the same for two ferrofluids (df105 and U5) with very similar particle size and oleic acid as surfactant, but with different carrier fluids (tetradecane and undecane). This could be taken as a hint that S_T is predominantly determined by interaction of the surfactant layer and the particle, like the thermophoresis models reviewed in Sec. 1.4 would suggest anyway. There is, however, an intriguing possibility of a spatial inhomogeneity of surfactant concentration being induced under temperature gradient. Then, the colloidal particles would move in a gradient of surfactant concentration, as well as ∇T. In free fluid, this inhomogeneity would have to be induced by thermal diffusion of surfactant in carrier fluid. In a porous layer, a contribution of additional flow induced by the pore walls could be considered. Regrettably, we lack information on transport coefficients in such a system that would be necessary to evaluate this possibility.

Possible interaction of surfactant molecules in the fluid with the surfactant layer around colloidal particles could mean either interaction "from the outside" - surfactant layer interacting with surfactant molecules outside of the layer, or a sort of a double layer forming - or adsorption of the additional surfactant molecules onto the particles themselves. In sect. 5.3, it has

been shown that addition of excess surfactant does not increase particle size. Adsorbtion of additional surfactant on surface of the particles would imply that the surface is not saturated with surfactant after the synthesis process. Curiously, this has also been offered as an interpretation for effects of excess surfactant on ferrofluid viscosity in chapter 4. Alteration of S_T through such mechanism could be compatible with the models proposed for colloid thermophoresis given in sect. 1.4, as adsorbtion of surfactant molecules from the fluid onto the particles would have an impact on Gibbs excess surface concentration (relevant to Morozov's model for S_T), local enthalpy (Derjaguin's model) and surface tension (models proposed by Parola and Ruckenstein). An association could perhaps be made between this proposed explanation and the retardation of droplet thermophoresis as described in ref. [80]. Evaluation within framework of any specific model would require microscopic characteristics of particle surface, and such are not available.

Soret coefficient as a function of temperature

Soret coefficient of a surfactant stabilized ferrofluid has been found to decrease with temperature in both free fluid and a porous medium. The dependence of S_T on temperature can be described with a modified Iacopini - Piazza model in both cases. The modifications are necessitated by S_T decreasing from a low temperature plateau, instead of reaching one at high temperatures. In a free fluid, change of sign for S_T has been predicted at temperatures higher than the experimentally covered range. In a porous medium, a change of sign for S_T has been observed.

Both a porous medium and addition of excess surfactant reduce the dependence of S_T on temperature. This is shown in table 6.4, where values of Iacopini - Piazza model coefficient T_0 are given.

Effect of a porous medium on thermophoresis

The Soret coefficient measured in a porous medium has been found to be lower than that measured in a free fluid. This has been found to be true for four samples of ferrofluid, including both surfactant stabilized and ionic. For the three surfaced colloids, S_T has reduced from a positive value to a lower positive value. For the ionic ferrofluid, Soret coefficient has reduced from $S_T = 0$ to a negative value.

$c_{oleic\ acid,vol.}$, %	T_0,^0C (FRS)	T_0,^0C (porous)
0.0	70.2	19.8
1.25		10.1
2.0	31.4	
2.5		8.6

Table 6.4: Parameter T_0 of Iacopini-Piazza model, measured by FRS and in a porous layer

A slight review of these results is made necessary by some of the observations presented in this thesis. In sect. 5.2, it is reported that mass diffusion coefficient D_m is much reduced in a porous medium compared to a free fluid. This poses a problem, because in the equation 6.5 used to describe thermophoresis in a porous layer, we have used non-dimensional time $\tau = \frac{D_m t}{a^2}$, which involves D_m. In fact, it has been shown in ref. [74] that a stationary state is reached at $\tau = 1$. Using the value of D_m from sect. 5.2, we arrive at $\tau = 0.13$. The situation is not a straightforward one - the porous layer does not change D_m, it affects the effective value of D_m by elongation of the paths that particles travel, see sect. 1.6. Along with S_T being a proportion of two coefficients affected by porous environment to the same extent, we have to ask if it is the fundamental value of D_m or the effective one that we have to use for τ. A further investigation is therefore carried out.

We return to eq. 6.5 and accommodate certain findings of our research. We formulate S_T as a function of temperature according to results of Soret coefficient measurements with FRS given in sect. 6.3, using coefficients from free fluid measurements. The equation for particle concentration then becomes:

$$\frac{\partial C}{\partial \tau} = \frac{\partial^2 C}{\partial X^2} + \frac{\Delta T}{2}\left(S_{T,1}[1 - \exp(\frac{T - T^*}{T_0})]\right)\frac{\partial C}{\partial X} \tag{6.22}$$

Equation 6.22 is then solved numerically, using coefficients from FRS measurements for df105 and temperature values used in experimental work. The result for $\tau = 0.13$ is shown in fig. 6.12 along with experimental data and fitting results for eq. 6.8 that returned a reduced value for S_T.

It can be seen that the solution with reduced τ and unchanged S_T does not correctly predict characteristics of particle distribution. Another argument for a stationary state having been reached can be seen in results presented

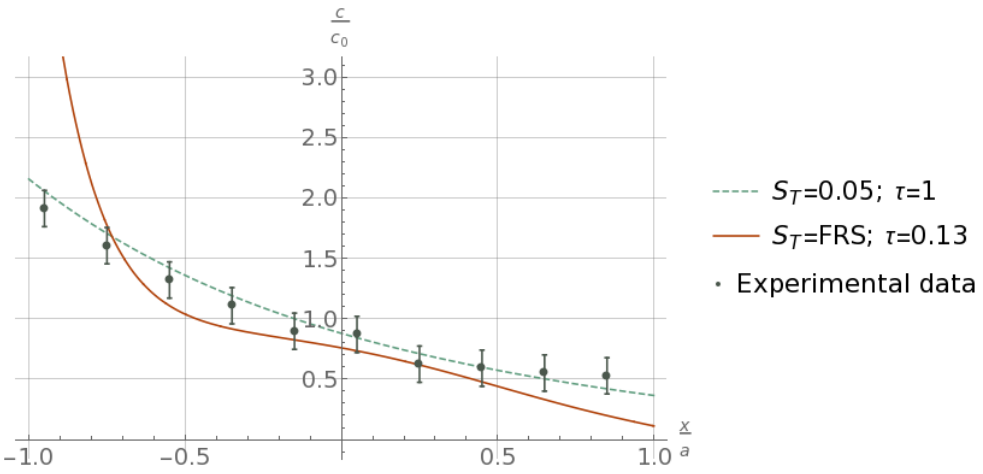

Figure 6.12: Particle concentration calculated for a non-stationary state at free fluid value of S_T and at a stationary state for a reduced S_T, along with experimental data

in sect. 8.2. There, the effect of an external magnetic field upon ferrofluid thermophoresis is investigated. Theoretical values are calculated from the framework given in sect. 1.7, where a stationary state is assumed. Experimental and theoretical values are found to have a good agreement. It could therefore be asked, if the stationary state is not reached, why does the theory still provide accurate predictions? Results of ionic ferrofluid sample FF 13-04 could also be brought up - there, a negative S_T is observed from a free fluid value of $S_T = 0$, which can not be explained by measurements being made in a transient state.

Nevertheless, only experimental results could answer the question decisively, and such we do not have. Therefore, implications of the possibility of a stationary state having not been reach must also be discussed. An obvious one is that the values for S_T could be questioned, as well as values for fitting coefficients in temperature dependence models. Relations for those coefficients when comparing different surfactant concentration values are more on the safe side, as it has been demonstrated (see sect. 5.2) that surfactant concentration does not affect D_m and, therefore, τ - meaning that, even if a stationary state wouldn't be reached, measurements would still be performed at the same value for τ. An important result that is also not under question regardless of stationary state being reached or not is the inversion of parti-

cle thermophoresis direction at certain values of surfactant concentration - we see an increase of particle concentration at higher temperatures, which lower values of τ can not account for. Furthermore, in FRS measurements, an excess surfactant concentration of 2 % does not lead to change of sign for S_T (fig. 6.2), while in a porous medium, we see particle concentration increasing near higher temperatures at surfactant concentration values lower than 2 % (fig. 6.4) - this demonstrates that the effect of a porous medium on particle thermophoresis goes beyond an increase of time needed to achieve a stationary state (if the latter is true at all), certainly when excess surfactant is present.

To discuss potential mechanisms for a porous medium to reduce the observed thermophoretic mobility of colloidal particles, we must consider two cases. In one case, particle thermophoresis is not affected at all, instead, a flux of carrier fluid is induced, and particles move with it, leading to an apparent decrease in thermophoretic mobility. In the other case, porous medium would interact with the particles.

An interpretation of how a porous medium could induce a flow can be found in work of Derjaguin and Sidorenkov[43], see also article by Anderson[58]. Under a temperature gradient, the lyophilic interface of pore walls would drive a slip velocity transfer of molecules toward higher temperatures. This could also be identified as driving force of particle thermophoresis - then, flow induced in the same direction around the particles would drive them towards the lower temperatures. See fig. 6.13 for illustration.

Combined effects of temperature and porous environment on thermophoresis - change of sign for Soret coefficient

In a porous medium and at a sufficiently high concentration of excess surfactant, Soret coefficient can become negative in temperatures not much in excess of room temperature (at $T \approx 30 - 60^0\, C$). This is arguably the most curious result among those reviewed in this chapter.

We have again several questions regarding the nature of our observations. Carrying over from thermophoresis experiments with no additional surfactant is the question of whether we are seeing an influence on particle phoresis, or on bulk fluid motion. An additional important division is on whether the effects of excess surfactant act to increase the strength of porous medium

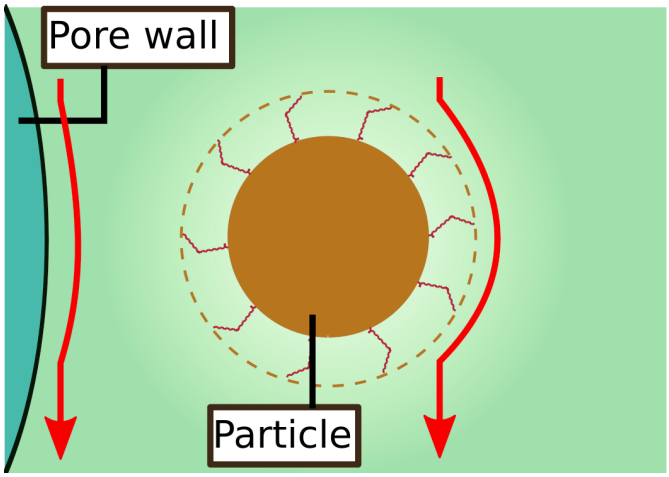

Figure 6.13: A schematic representation of a proposed interpretation on fluxes driven by similar mechanisms along colloidal particles and pore walls

effects, or do they represent a separate mechanism of interacting with particle thermophoresis. The answer to that would be closely related to another question: is the considerable decrease of change of sign temperature for S_T a combination of porous medium and additional surfactant both reducing the Soret coefficient through their separate mechanisms, or is there a more intricate interplay at work. A glance at results presented in sections 6.2 and 6.3 suggests that a linear combination of the two effects could not explain the observed phenomena, assuming that porous medium effect on thermophoresis remains the same. Verifying the validity of this assumption merely loops us back to the questions asked previously in this paragraph.

It is tempting to offer an interpretation where the porous medium would induce surfactant flow. Then, the colloidal particles would be moving in gradients of both temperature and surfactant concentration. The latter could then interact with the particles through any of the mechanisms suggested in the discussion regarding effects of excess surfactant on thermophoresis, be it particle motion induced by surfactant concentration gradient itself, or surfactant interacting with thermophoresis driving mechanism within the layer around a colloidal particle (the oleic acid concentration gradient then playing the role of varying the amount of surfactant in bulk fluid at different points within the layer). The latter mechanism would be compatible with interpretations for suggested effects of additional surfactant both on particle

thermophoresis in free fluid, and on viscosity. However, to confirm or discard this theory, insights on surfactant distribution would be necessary. Regrettably, experimental capacity needed for such measurements goes beyond the scope of this thesis.

As an attempt to simplify the system at hand and make some conclusions on surfactant behavior in a porous medium and effect on carrier fluid flow, thermoosmosis experiments with a tetradecane and oleic acid mixture in a porous medium are conducted, and are described in the next chapter. Aims of the research presented there are establishing an understanding of surfactant influence on carrier fluid thermoosmosis in a porous medium and, if possible, make conclusions about implications it would have on particle thermophoresis. It is concluded there that additional surfactant is unlikely to induce bulk flow of carrier fluid. Effects of excess surfactant on carrier fluid thermoosmosis are found to exceed those of increased viscosity. It is concluded that an investigation of the microscopic processes of surfactant and porous medium interaction would be necessary to make claims about surfactant redistribution within the system.

Chapter 7

Thermoosmosis of surfactant and carrier fluid mixture

7.1 Overview

In thermoosmosis experiments, we are investigating thermal transport of carrier fluid mixed with surfactant, moving through a porous layer. Motivation for this series of experiments is provided by the need to interpret results of nanoparticle thermophoresis experiments in a porous layer - the system investigated here is indeed much like the one described in chapter 6, with the colloidal particles removed. The experimental setup is described in section 3.3. General idea is that a porous layer like that used in thermophoresis experiments described in sections 6.2 and 6.4 is placed between two volumes of fluid which are heated or cooled. The cylindrical volumes have exits through manometer tubes, the manometers are leveled and fluid flow in them is measured.

In the context of particle thermophoresis experiments, an influence of surfactant on mass transfer is expected. To be more precise, we could expect to be looking at either significant changes to fluid flow characteristics that could let us correlate observations of thermophoresis experiments to changes of bulk flow of the fluid induced by porous medium and surfactant, or more subtle phenomena that would hopefully let us draw some conclusions on interactions between the porous medium, surfactant and carrier fluid. For theoretical basis, the slip velocity interpretation laid out in Anderson's work, see sec. 1.4 and ref. [58], could be considered. Within this interpretation, the

slip velocity caused by interaction between surfactant molecules and lyophilic pore walls would result in a flow of surfactant particles towards higher temperatures. A redistribution of surfactant molecules, driven by this or another mechanism, like a process comparable to Marangoni effect, would then drive either bulk flow of the fluid, corresponding to the aforementioned significant changes in flow characteristics, or interact with the colloidal particles in thermophoresis experiments - since the particles are not present in thermoosmosis experiments described in this chapter, more subtle changes to flow, as it is observed here, would be expected.

7.2 Mathematical framework

In thermoosmosis experiments, we are looking at a two phase system involving carrier fluid and the surfactant. For the mathematical description, we mimic the approach introduced in sect. 1.3 and look at carrier fluid flow as driven by pressure, surfactant concentration (c_s) and temperature gradients:

$$\vec{j} = \alpha_{11}\nabla p + \alpha_{12}\nabla c_s + \alpha_{13}\nabla T \tag{7.1}$$

Contributions of these driving forces are again associated with phenomenological laws. In a flow through a porous medium, mass flux is related to pressure gradient by the Darcy equation, as given in ref. [81] and written for pressure gradient, with K being permeability of a porous medium:

$$\nabla p = \frac{-\nu}{K}\vec{j} \tag{7.2}$$

Thermoosmosis is accounted for as:

$$\alpha_{13}\nabla T = d_T\rho\nabla T \tag{7.3}$$

where d_T is thermoosmotic coefficient of carrier fluid. We make an assumption that any significant deviations from a uniform concentration distribution of surfactant particles stems from the influence of temperature gradient - that is, that ∇c_s is proportional to ∇T. The basis of this assumption is the difference in scale between pore sizes and the length of an oleic acid molecule (around $2\,nm$), which should make noticeable filtration processes unlikely. Then, flow equation becomes:

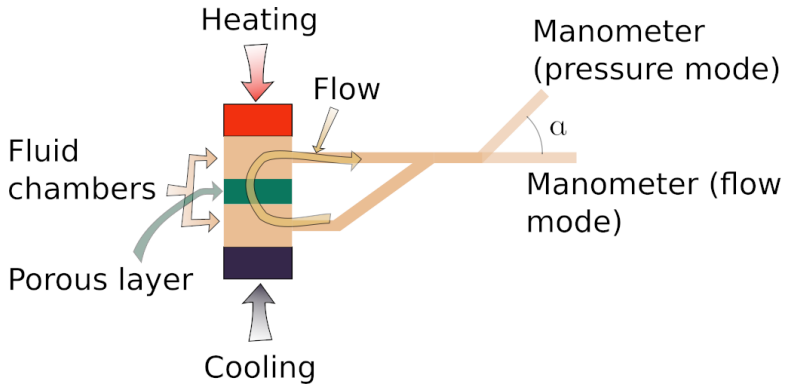

Figure 7.1: Schematic view at experimental device used in thermoosmosis experiments. The two manometer tubes are both placed at either flow mode (parallel to the ground for their entire length) or pressure mode (end sections raised at an incline angle α)

$$\vec{j} = -\frac{K}{\nu}\nabla p + (d_T + d_T^*)\rho\nabla T \tag{7.4}$$

Here we claim that all effects on fluid transfer caused by a gradient in surfactant concentration are embodied in the purely empirical coefficient d_T^*. We define effective thermoosmotic coefficient as:

$$d_{T,eff} = d_T + d_T^* \tag{7.5}$$

It is here that we introduce the specifics of our experimental device, see fig. 7.1. We are looking at a flow that goes through a porous medium, two surrounding volumes and a manometer tube for each volume. The tubes reach an equal height at a point some distance from the volumes. Moving further away still, we arrive at a point when the manometer tubes can either continue running parallel to the ground, or be raised at an incline angle α.

Pressure gradient can be determined from height difference Δh in a manometer raised in an incline angle α by:

$$\nabla p = \frac{-\rho g \sin\alpha \Delta h}{\delta} \tag{7.6}$$

Considering that we measure the flow rate and pressure with manometer tubes, we also try to account for capillary pressure, a difference of which could

arise from surface tension or fluid in the tubes changing with temperature. Denoting capillary pressure as Δp_c, we use Young-Laplace equation:

$$\Delta p_c = \frac{2\gamma \cos \Theta}{r} \tag{7.7}$$

Where γ denotes surface tension, Θ stands for contact angle between liquid and tube wall, and r is radius of the tube. Written for difference between the two tubes, the pressure becomes:

$$\Delta p_c = \left(\frac{2\gamma_{hot} \cos \theta}{r_{hot}} - \frac{2\gamma_{cold} \cos \theta}{r_{cold}} \right) \tag{7.8}$$

we can write eq. 7.4 as:

$$\vec{j} = -\frac{K}{\nu\delta} \left(-g\rho \sin \alpha \Delta h + \Delta p_c \right) + (d_{T,eff})\rho \nabla T \tag{7.9}$$

Analysis of thermoosmosis experiments is based on eq. 7.9. The only measured quantity in experiments is height difference in manometer tubes Δh, which is related to fluid flow as:

$$\vec{j} = -\frac{d\Delta h}{dt} \frac{s}{2S} \rho \tag{7.10}$$

Here, S is area of the porous layer and s is cross section area of the manometer. Combining eqs. 7.9 and 7.10 yields:

$$\frac{d\Delta h}{dt} = \frac{2S}{s} \left(\frac{K}{\nu\delta} \left(-g \sin \alpha \Delta h + \frac{\Delta p_c}{\rho} \right) + d_{T,eff} \nabla T \right) \tag{7.11}$$

7.3 Results

7.3.1 Three experimental regimes

All experiments are done with tetradecane, which is the carried fluid for ferrofluid df105, with additional oleic acid, up to 2.5 % volume concentration. For each sample, measurements are performed in three experimental regimes:

- isothermal experiments, where $\Delta T = 0$ and manometer tubes are raised to an angle of $\alpha = 30^0$

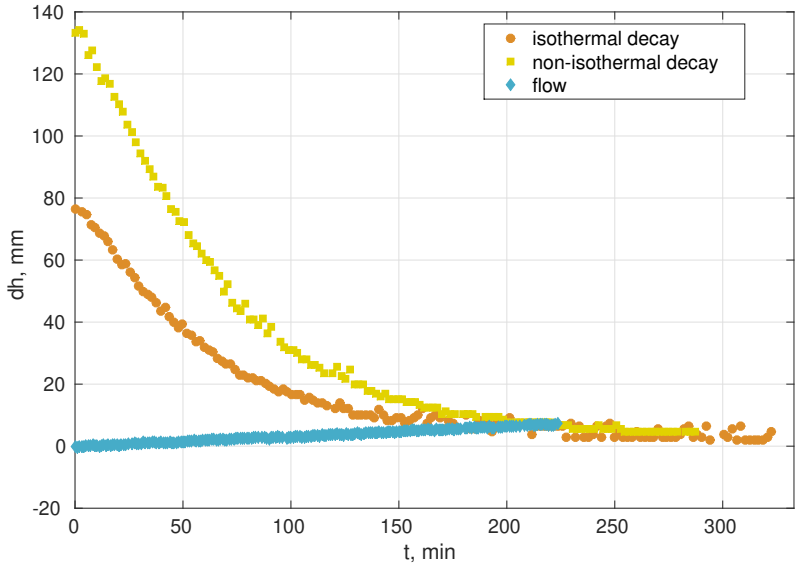

Figure 7.2: Fluid level difference development in manometer in different flow regimes, tetradecane with 1 % volume concentration additional oleic acid

- non-isothermal pressure experiments, where manometer tubes are raised to $\alpha = 30^0$ and a temperature gradient is imposed
- non-isothermal flow experiments, where manometer tubes run parallel to the ground, therefore $\nabla p = 0$, and a temperature gradient is imposed.

Following the considerations mentioned in sect. 7.2, we assume surfactant concentration gradient to be $\nabla c = 0$ in isothermal experiments. In isothermal and non-isothermal pressure experiments, relaxation from a set height difference is observed. Examples of fluid level difference measurements in all three regimes are given in Fig. 7.2.

The capillary pressure difference Δp_c is determined by measuring thermostated capillary rise in the manometer tubes at different temperatures and with different surfactant concentrations.

$c_{surf,vol.}, \%$	K, m^2
0.0	$1.05 \cdot 10^{-15}$
0.5	$0.66 \cdot 10^{-15}$
1.0	$1.21 \cdot 10^{-15}$
1.5	$1.28 \cdot 10^{-15}$
2.5	$1.24 \cdot 10^{-15}$

Table 7.1: Permeability parameter K of the porous layer at different values of surfactant volume concentration

7.3.2 Isothermal experiments

The series of isothermal experiments allows the measurements of pressure driven flow through the system, enabling determination of Kozeny coefficient. Solution of eq. 7.11 with $\Delta T = 0$ is:

$$\Delta h(t) = \frac{2}{g}(\exp\left[-\frac{0.5gKS}{\delta\nu s}t\right](0.5g\Delta h_0 - \frac{\Delta p_c}{\rho}) + \frac{\Delta p_c}{\rho}) \tag{7.12}$$

Here and throughout this chapter, measurements of viscosity presented in sect. 4 are used. As first estimate for Kozeny coefficient, the value given in 3.4 is used. We can then fit eq. 7.12 to experimental data and obtain adjusted values of K. The results are shown in table 7.1. From those, we can calculate K, obtaining the average value $K_{experimental} = 1.09 \cdot 10^{-15}$.

The deviation of $K_{experimental}$ is used to estimate the accuracy of measurements for the thermoosmosis series of experiments. It is concluded that the relative error is approximately 20 % of measurement value.

7.3.3 Non-isothermal experiments

The full solution to eq. 7.11 is:

$$\Delta h(t) = \frac{2\nu}{gK}(\exp\left[-\frac{0.5gKS}{\delta\nu s}t\right](\frac{0.5gK\Delta h_0}{\nu} - \\ - d_{T,eff}\Delta T - \frac{K\Delta p_c}{\nu\rho}) + d_{T,eff}\Delta T + \frac{K\Delta p_c}{\nu\rho}) \tag{7.13}$$

$c_{surf}, \%$	$d_T + d_T^*, \frac{m^2}{s\,K}$	$d_T^*, \frac{m^2}{s\,K}$	$\pm(d_T^*), \frac{m^2}{s\,K}$
0.0	$1.70 \cdot 10^{-12}$	0.00	$3.6 \cdot 10^{-13}$
0.5	$1.14 \cdot 10^{-12}$	$-5.6 \cdot 10^{-13}$	
1.0	$-0.8 \cdot 10^{-13}$	$-1.77 \cdot 10^{-12}$	
1.5	$-5.8 \cdot 10^{-13}$	$-2.27 \cdot 10^{-12}$	
2.5	$-1.3 \cdot 10^{-13}$	$-1.83 \cdot 10^{-12}$	

Table 7.2: Effective thermoosmotic coefficients from pressure experiments at different values of surfactant volume concentration

Pressure mode

In nonisothermal pressure experiments, fitting eq. 7.13 to experimental results gives us $d_{T,eff}$. The values of $d_T + d_T^*$ and d_T^* (calculated assuming $d_T^* = 0$ at $c_{surfactant} = 0$), according to our definition of $d_{T,eff}$ in eq. 7.5, are presented in table 7.2.

Flow mode

In thermoosmotic flow experiments, gravitational pressure alone would give $\nabla p = 0$. Following eqs. 7.2 and 7.8, capillary flow in the manometer tubes themselves can be accounted for in the form:

$$\vec{j} = -\frac{K}{\nu\delta}\left(\frac{2\gamma_{hot}\cos\theta}{r_{hot}} - \frac{2\gamma_{cold}\cos\theta}{r_{cold}}\right) \tag{7.14}$$

Like with Δp_c, the necessary parameters can be determined by capillary rise experiments. This contribution to flow is treated as a correction term and subtracted from the observed flow measurements. Then, eq. 7.4 reduces to

$$\vec{j} = (d_T + d_T^*)\rho\nabla T \tag{7.15}$$

Combining eqs. 7.15 and 7.10, we can calculate the effective thermoosmotic coefficient from

$$-\frac{d\Delta h}{dt}\frac{s}{2S}\rho = \rho d_{T,eff}\nabla T \tag{7.16}$$

Results of $d_{T,eff}$ from flow experiments are presented in table 7.3.

$c_{surf}, \%$	$d_{T,eff}, \frac{m^2}{s\,K}$	$\pm(d_{T,eff}), \frac{m^2}{s\,K}$
0.0	$1.733 \cdot 10^{-12}$	$3.65 \cdot 10^{-13}$
0.5	$1.134 \cdot 10^{-12}$	$2.39 \cdot 10^{-13}$
1.0	$7.26 \cdot 10^{-13}$	$1.53 \cdot 10^{-13}$
1.5	$5.81 \cdot 10^{-13}$	$1.22 \cdot 10^{-13}$
2.5	$6.5 \cdot 10^{-14}$	$1.4 \cdot 10^{-14}$

Table 7.3: Effective thermoosmotic coefficient from flow experiments at different values of surfactant volume concentration

$T, {}^0C$	$20^0C/40^0C$	$30^0C/50^0C$	$40^0C/60^0C$
$c_{surf}, \%$	$d_{T,eff}, \frac{m^2}{s\,K}$		
0.0	$-6.8 \cdot 10^{-13}$	$3.31 \cdot 10^{-12}$	$3.34 \cdot 10^{-12}$
1.0	$-0.3 \cdot 10^{-13}$	$6.1 \cdot 10^{-13}$	$3.1 \cdot 10^{-13}$
1.5	$-1.3 \cdot 10^{-13}$	$3.8 \cdot 10^{-13}$	$8.0 \cdot 10^{-13}$

Table 7.4: Effective thermoosmotic coefficient $d_{T,eff}, \frac{m^2}{s\,K}$ from flow experiments at different values of surfactant volume concentration. The header line represents bottom and top temperatures

Values of $d_{T,eff}$ measured with pressure and flow methods are compared in fig. 7.3. A reasonable agreement between the two methods can be seen, especially with lower surfactant concentration values. In both cases, values of the effective thermoosmotic coefficient decrease as surfactant concentration increases. A change of sign for $d_{T,eff}$ at higher values of c_s and saturation at low positive effective thermoosmotic coefficient values both look possible. Surfactant concentration can not be increased further due to the exponential increase of viscosity, as seen in chapter 4 - resistance within the highly capillary experimental system renders it practically inoperable.

To help understand the effect of temperature on $d_{T,eff}$, thermoosmotic flow experiments with $\Delta T = 20^0C$ are performed at different average temperatures and surfactant concentration values. Results are summarized in table 7.4 and visualized in figure 7.4.

We can see that, with the exception of an outlier result at $c_s = 0\%$ and $T_{average} = 30^0C$, dependence of the thermoosmotic coefficient on surfactant concentration seems to follow much the same pattern as in experiments with

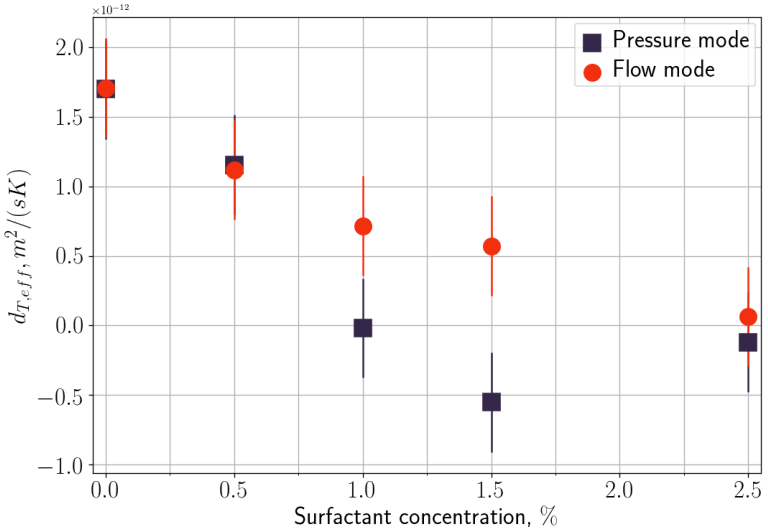

Figure 7.3: Effective thermoosmotic coefficients from pressure and flow experiments depending on surfactant volume concentration

$\Delta T = 40^0C$, with average temperature changes bringing relatively insignificant differences. Reduction of temperature difference from $\Delta T = 40^0C$ to $\Delta T = 20^0C$ doesn't result in changes to values of $d_{T,eff}$ beyond those of error boundaries.

7.4 Analysis

As seen in fig. 7.3, the measured effective thermoosmotic coefficients decrease from an initial positive value as the amount of excess surfactant increases. This corresponds to an decreasing tendency of the fluid to move towards higher temperatures. The range of surfactant concentration values that are viable for experimental use prevents us from concluding if an inversion of flow direction could be attained - limiting factor here is fluid viscosity.

The effective thermoosmotic coefficient is shown in fig. 7.4 to have a positive correlation with temperature, $d_{T,eff}$ increasing as T increases. Magnitude of ∇T has not been found to have an effect on $d_{T,eff}$.

Fluid viscosity is known and accounted in for in the equations governing flow within the experimental system. This means that an addition of surfactant has an influence on mass transfer in such a system beyond that of

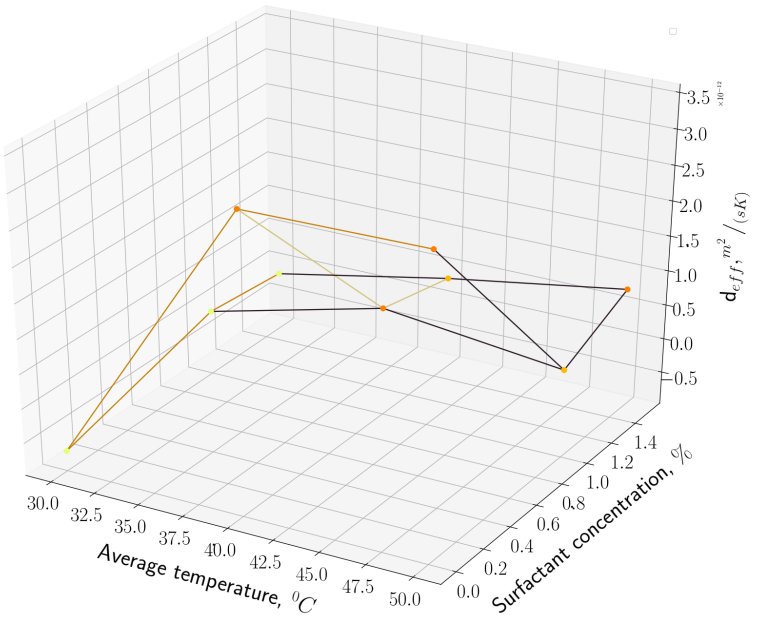

Figure 7.4: Effective thermoosmotic coefficients from flow experiments at different combinations of surfactant volume concentration and average temperature at $\Delta T = 20^0C$

viscosity increase.

Before considering the nature of this influence, let us review some immediate conclusions in the context of our main interest in the system, which is the possible implications for colloidal particle thermophoresis, if such were present. The first thing to notice is that thermoosmotic flow does not at any point reverse direction, remaining directed towards higher temperatures. Surfactant concentration used in experimental work reach values where, in a corresponding system with colloidal particles present, S_T had reached negative values as seen in Chapter 6. This allows us to discard a suggestion that the observed changes in particle behavior would stem from a changing nature of carrier fluid flow that would merely carry the particles with it - simply put, no fluxes of the bulk fluid emerging as surfactant is added have been discovered.

For a more detailed analysis, let us consider system of equations given by eqs. 1.14, considering chemical potentials to be $\nabla\mu_1 = -V_1\nabla p$, where V_1 is solvent molar volume ($\vec{J}_{fluid}$ and $\vec{J}_{particles}$ are given in $\frac{mol}{m^2 s}$), and $\nabla\mu_2 = \left(\frac{\partial\mu_2}{\partial\phi}\right)_p \nabla\phi$:

$$\begin{cases} \vec{J}_{fluid} & = \alpha_{11}(-V_1)\nabla p) + \alpha_{12}\left(\frac{\partial\mu_2}{\partial\phi}\right)_p \nabla\phi + \alpha_{13}\frac{\nabla T}{T} \\ \vec{J}_{particles} & = \alpha_{21}(-V_1)\nabla p) + \alpha_{22}\left(\frac{\partial\mu_2}{\partial\phi}\right)_p \nabla\phi + \alpha_{23}\frac{\nabla T}{T} \\ \vec{J}_{heat} & = \alpha_{31}(-V_1)\nabla p) + \alpha_{23}\left(\frac{\partial\mu_2}{\partial\phi}\right)_p \nabla\phi + \alpha_{33}\frac{\nabla T}{T} \end{cases}$$

In ref. [32], ferrofluid thermophoresis in an analogous experimental setup is considered. The system of equations can be rewritten as presented there, expressing flow velocities. The coefficients used are as follows: V_p denotes particle volume, ζ is filtration coefficient defined as $\zeta = \alpha_{11}V_1^2\rho g\delta$; δ is layer thickness and α_{11} is kinetic coefficient describing solvent flux under a pressure gradient. From this definition, ζ is positive. Nanoparticle concentration is expressed in terms of volume concentration ϕ. The resulting equations describing fluid and particle flow velocities are:

$$\begin{cases} \vec{v}_{fluid} & = -\frac{\zeta}{\rho g\delta}\nabla p + d\frac{\nabla\phi}{\phi} + d_T\nabla T \\ \vec{v}_{particles} & = \frac{1}{\phi}\left(-\frac{V_p d}{k_B T}\nabla p - D\nabla\phi - D_T\phi\nabla T\right) \end{cases} \tag{7.17}$$

Here, "fluid" denotes the mixture of carrier fluid and surfactant, while "particles" refer to the colloidal particles and $d_{T,eff}$ is embodied in d_T in

system 7.17. To be entirely clear - system of equations 7.17, as analyzed here, does not refer to actual experimental results. Instead, it provides a framework to discuss implications of results presented in this section on colloidal particle phoresis, if such particles were present, in a system like that seen in previous chapter.

Let us now assume that no convective flux of the fluid is present, or $\vec{v}_{fluid} = 0$ (no flux through the layer, as in the closed layer experiments of Ch. 6), and try to assess how the observed changes in d_T following addition of surfactant would affect colloidal particle thermophoresis. As seen from the first equation of system 7.17, a positive d_T would contribute to a pressure gradient directed the same as ∇T. Inserting this pressure in the particle flow equation would yield a contribution to $\vec{v}_{particles}$ directed opposite to ∇T, the same as particle thermophoresis. Therefore, as long as values of d_T remain positive, thermoosmosis may contribute to thermophobic behavior of the colloidal particles, and decreasingly so as d_T is reduced by addition of surfactant, but not, at any value of oleic acid concentration in the examined range, to the thermophilic colloidal particle behavior we are trying to explain. As seen in the experiments measuring $d_{T,eff}$ depending on temperature, low negative values are reached, but only with system temperature $T = 30^0\,C$, while colloidal particles in thermophoresis experiments only display thermophilic behavior in higher temperatures, including in systems where $T > 30^0\,C$ at all points of the system, see sect. 6.4.4.

We can regardless conclude that addition of surfactant has an effect on thermoosmosis of carrier fluid - surfactant mixture in a porous medium and that this effect goes beyond the influence of increased viscosity. Trying to analyze possible implications that the observed changes to effective thermoosmotic coefficient would have in the context of a ferrofluid thermophoresis in a porous layer shows that the effects of surfactant on fluid thermoosmosis alone can not be translated to the thermophilic behavior observed in colloidal particles. It could be claimed that, instead, the physical process, involving surfactant, responsible for the reduction of $d_{T,eff}$ is also linked to the reduction of S_T in thermophoresis experiments. Attempt of an analysis is provided in appendix B, it is heavy on assumptions and fails short of delivering a conclusion. The reason for this is lack of information regarding interaction of the porous medium, surfactant and carrier fluid.

Let us consider some of the physical processes that could be associated with the observed phenomena. Flow of carrier fluid along pore walls could be induced by a Marangoni effect, either solutocapillary, if temperature gradient

would induce a redistribution of surfactant molecules, or thermocapillary, if surface tension gradient would be induced by the temperature gradient. The two mechanisms would be associated with different characteristics of concentration gradient and, therefore, different implications to colloidal particle thermophoresis, should such particles be introduced in the system. A thermally induced flow in pores, as described by Derjaguin (see ref. [43] and sect. 1.5) would drive flow along a lyophilic wall towards higher temperatures[58], which coincides with the observed thermoosmotic flow direction. If such is the case, the analysis presented in this section can largely be disregarded. Then, the reduction of colloid S_T in a porous media could be explained by the flow phenomena described by Derjaguin, but lacking an explanation would be the further decrease of S_T following the addition of surfactant. We can also consider the possibility of an osmotic flow driven by surfactant concentration gradient in bulk fluid. Lack of information on the nature of interaction between the three elements of the system (the porous medium, carrier fluid and surfactant) under non-isothermal conditions prevents us from providing a clear interpretation of the results.

Chapter 8

Soret and mass diffusion coefficients in a magnetic field

8.1 Overview

Measurements of Soret coefficient and mass diffusion coefficient in a porous layer are done in a magnetic field. Both series of experiments are variations of experimental work reviewed in previous chapters - thermophoresis in a porous layer, see section 3.1 for experimental setup and sec. 6.4 for mathematical framework and results, and mass diffusion in a porous layer, see section 3.2 for description of setup and 5.2.2 for mathematical framework and results. Magnetic field is $B = 0.1T$ in all experiments viewed here. Theoretical values for S_T and D_m in an external field are calculated as described in section 1.7. As is shown in sec. 3.5, convective stability is not expected to be an issue even in the presence of a magnetic field.

8.2 Results

Results of Soret coefficient measurements in a magnetic field are given in table 8.1. Orientation of the magnetic field is parallel to temperature gradient. Experimental results are compared to theoretical predictions, which are calculated from eq. 1.36. The value of Soret coefficient in a porous layer in the absence of magnetic field, $S_{T,B=0}$, is known from measurements of S_T in sect. 3.1 to be $S_{T,B=0} = 0.048$.

Mass diffusion is investigated in a porous layer with an external magnetic

ferrofluid	$S_T, 1/K(B = 0.0T)$	$S_T, 1/K(B = 0.1T)$	
		experiment	theory
df-105	0.048	0.023	0.023
S-1	0.06	0.002	0.002
U5	0.062	0.027	0.029
FF 13 - 04	-0.030	-0.035	-0.015

Table 8.1: Soret coefficient in a porous layer under external magnetic field $B = 0.1T$ parallel to temperature gradient, experimental and theoretical values. Zero field values given for comparison

field, with field orientation parallel and normal to the initial concentration distribution gradient. Measurements are done with sample df105. For theoretical value calculations, value for D_m in a porous medium $D_{m,B=0}$ is taken from results given in sect. 5.2.2: $D_{m,B=0} = 1.56 \cdot 10^{-12} m^2/s$. For parallel orientation, theoretical values are calculated with eq. 1.33 and for normal field orientation, with eq. 1.35. The results of measurements and calculations are shown in table 8.2.

field orientation rel. to $\nabla\phi$	$D_m, m^2/s$	
	experiment	theory
no field	$1.56 \cdot 10^{-12}$	
parallel	$2.10 \cdot 10^{-12}$	$3.16 \cdot 10^{-12}$
normal	$1.44 \cdot 10^{-12}$	$1.26 \cdot 10^{-12}$

Table 8.2: Diffusion coefficient of sample df105 in a magnetic field $B = 0.1T$, parallel and normal to particle concentration gradient, experimental and theoretical values. Zero field value given for comparison

8.3 Analysis

For Soret coefficient, a fine agreement between predicted and measured values for the coefficient in an external magnetic field can be seen for all ferrofluid samples. The same can be said about mass diffusion coefficient in normal field arrangement. For D_m in magnetic field parallel to initial concentration

gradient, we see a predicted increase in D_m compared to zero field value, with difference between experimental and theoretical values slightly exceeding that expected by error boundaries, which give 15 % of measurement value. Even so, across the range of the two series, experimental results agree well with the description of mass diffusion coefficient for ferrofluids in a magnetic field given in ref. [61], from which the description of Soret coefficient in a magnetic field has also been derived.

The fact that Soret coefficient in an external magnetic field can be expressed from effects of field inhomogeneity resulting from particle distribution non-uniformity upon particle transfer indicates lack of other field-related transfer mechanisms being present. Specifically, magnetic pressure and microconvective flow induced by elements of the porous medium can be said to have no considerable influence in this experimental system.

If a reason for the comparatively large deviation from theoretical values in the diffusion experiments was to be given, it would concern the way these experiments are conducted - at the start of each experiment, ten saturated layers of filter paper are assembled to form a continuous porous medium, see sect. 3.2. During this assembly, pressure is exerted upon the stack of layers. On the boundary between the last carrier fluid saturated layer and the first ferrofluid saturated layer, it would be possible for this pressure and the sharp concentration gradient to contribute to induce a motion of the colloid components significant enough to distort nanoparticle distribution. As all layers are saturated with ferrofluid in the thermoosmosis experiments, they would not suffer from this parasitic transfer.

In the context of research presented in this thesis, agreement between experiment and theory here can be seen as validation for measurements of D_m and S_T in a porous medium. The predicted effects of a magnetic field being numerically true act as a form of confirmation that measurements have been performed correctly and the observed mass transfer effects indeed correspond to those described my mass diffusion and thermodiffusion, rather than some other, unaccounted for process.

Conclusion

Confirmation of thesis statement

Thesis statement can be concluded to be fulfilled, as it has been shown that addition of surfactant lowers the Soret coefficient and that a reversal of sign for the Soret coefficient can be achieved, signifying change in particle behavior from thermophobic to thermophilic. Effects of surfactant on ferrofluid viscosity and temperature dependence of Soret coefficient and viscosity have been investigated and findings are detailed in individual conclusions.

Conclusions

1. Ferrofluid viscosity has been found to have a non-monotonous relation to surfactant amount increase, exhibiting viscosity decrease at lower surfactant concentrations and increase at higher concentration values. This is associated with saturation of surfactant layers around particles and the effects that incomplete surfactant covering of particles and temperature have on reversible formation of weak clusters of nanoparticles

2. Effects of surfactant and temperature on ferrofluid thermophoresis can be described as:

   (a) Soret coefficient of a ferrofluid decreases, as temperature is increased. This process can be described by a modified Iacopini - Piazza model

   (b) Soret coefficient of a ferrofluid is decreased by an increase of surfactant concentration. Two mechanisms potentially involved in this process are saturation of the surfactant layer around colloidal

particles, which is central to the process of thermophoresis, and redistribution of surfactant within the fluid

(c) Soret coefficient of a ferrofluid is reduced in a porous medium. This is a result of pore walls inducing surfactant transport, which leads to the colloidal particles being subjected to inhomogeneity of surfactant concentration in addition to that of temperature

(d) Combination of the aforementioned effects can lead to sign change of the Soret coefficient

It is out of these results that confirmation of thesis statement follows.

3. Addition of surfactant reduces thermoosmotic flow of carrier fluid through a porous layer to an extent that cannot be explained by viscosity increase. The proposed explanation relates this to flow driven by interaction of surfactant and pore walls. Carrier fluid thermoosmosis is not the reason for effect of porous medium on ferrofluid thermophoresis

4. Influence of an external magnetic field on ferrofluid thermophoresis can be described by an effect of the field on ferrofluid mass diffusion and an effect of temperature on magnetization of colloidal particles

Accomplishment of thesis tasks and other remarks

Ferrofluid properties and mass transfer coefficients have been investigated with a number of measurement methods and both in free fluid conditions and in a porous medium, characterizing effects of excess surfactant concentration and temperature.

Following first of the tasks set for research described here, ferrofluid particle size and viscosity have been investigated as functions of temperature and surfactant concentration. Measurements of nanoparticle hydrodynamic size performed with Forced Rayleigh scattering are found to be compatible with magnetic size measurements performed with Vibrating sample magnetometry. Dynamic light scattering measurements have found weak agglomerates of nanoparticles to be present in the ferrofluid. Detection of these clusters should be credited to the noninvasive nature of DLS method, with the clusters assumed to be destroyed by temperature gradients imposed by FRS.

Rather unsurprisingly, viscosity of ferrofluid is found to decrease with temperature. Effects of excess surfactant on ferrofluid viscosity are less expected, as an initial decrease is followed by an increase as more surfactant is added. The latter is similar to viscosity increase of carrier fluid by surfactant addition. This leads to an assumption of two processes working in parallel - an increase of ferrofluid viscosity like that of the carrier fluid, and a phenomena leading to viscosity decrease that initially overshadows the former process before saturating. The latter is interpreted as a result of saturation of surfactant layer around particles as more surfactant is added to the colloid. This process, along with temperature increase, would reduce the number of weak nanoparticle clusters in the colloid.

Effects of surfactant concentration, temperature and the presence of a porous medium on ferrofluid thermophoresis and mass diffusion are investigated according to second of the set tasks. Soret coefficient of a surfactant stabilized ferrofluid has been found to decrease with temperature in an exponential manner that can be described with a modified version of an empirical model referred to as the Iacopini - Piazza model. The modifications are necessitated by the nature of Soret coefficient as a function of temperature, exhibiting relatively stable values at lower temperatures, before decreasing rapidly as the temperature rises. This is at odds with the empirical model as it is originally described, and also other models for Soret coefficient, which tend to predict a rapid decrease followed by saturation at lower values. The same form of dependence on temperature is displayed by Soret coefficient measured in free fluid as well as in a porous medium. In a free fluid, an inversion on sign for the Soret coefficient, from positive to negative, is predicted, but not observed within the experimentally covered range of temperatures. In a porous medium, Soret coefficient is observed to change sign. This marks a shift in particle behavior, switching from being thermophobic to thermophilic. With addition of excess surfactant, Soret coefficient sign change temperature can be reduced to values of about ten degrees Kelvin above room temperature.

Addition of excess surfactant lowers the value of Soret coefficient in ferrofluids. In free fluid conditions, this corresponds to positive values of Soret coefficient reduced to lower positive values. In a porous medium, Soret coefficient has been reduced to negative values at sufficiently high temperatures. Ferrofluid mass diffusion coefficient is found to increase with temperature and to have no significant dependence of excess surfactant concentration. Mass diffusion coefficient is found to decrease in a porous layer. This has

been linked with tortuosity of the porous medium.

Investigation of carrier fluid and surfactant mixture thermoosmosis through a porous medium has been carried out, motivated by a possibility of correlating thermoosmotic phenomena to observations made in thermophoresis experiments. This corresponds to the third task. It has been found that addition of excess surfactant does not lead to an additional flux of carrier fluid in non-isothermal conditions, from which it can be concluded that the influence of surfactant on ferrofluid mass transfer in porous media is unlikely to be related to carrier fluid bulk flow. It has also been found that excess surfactant has an effect on decreasing thermoosmotic flow that goes beyond viscosity increase.

An interpretation offered for the observed effects involves adsorption of excess surfactant onto the particles, which could explain the nature of ferrofluid viscosity and Soret coefficient as functions of excess surfactant concentration, along with surfactant redistribution aided by the porous medium, which would then be related to the influence of excess surfactant upon thermophoresis and thermoosmosis in porous medium. However, for this or any other interpretation to be verified or discredited, a microscopic scale investigation of surfactant interaction with surfaces of particles and pore walls would be necessary.

Following fourth of the tasks set for the research presented in this thesis, measurements of Soret and mass diffusion coefficients in a porous medium have both been found to depend on an external magnetic field as predicted by theoretical considerations. The theory, including that for Soret coefficient, relies on field effects upon the mass diffusion coefficient, and using the effective, tortuosity modified values for this coefficient yields predictions that prove to be a good fit for experimental values. It can therefore be concluded that a porous medium does not affect the influence that an external magnetic field exerts over ferrofluid mass diffusion and thermophoresis.

Contributions

It goes without saying that the research presented here is the result of effort from multiple people, more complete lists of whom can be found in the acknowledgments section and in the authors lists of publications associated with this thesis. Given here is a list of clear and measurable contributions to the data and results presented in thesis.

Ferrofluids produced in Institute of Physics, University of Latvia, were synthesized by Gunars Kronkalns. Ferrofluid produced in Laboratory of Magnetic Soft Materials, Faculty of Physics, Mathematics and Optometry, University of Latvia, was synthesized by Oksana Petricenko.

Ferrofluid characterization measurements by Vibrating Sample Magnetometry were performed by Michail M. Maiorov, particle concentration in porous layer samples VSM measurements were performed by the author. In all VSM measurements, software courtesy of M. M. Maiorov was used to arrive to particle size distribution.

Forced Rayleigh scattering measurements in Institute of Physics, University of Latvia were performed by Ansis Mezulis, and in Laboratorie PHENIX, Sorbonne Université, by Mitradeep Sarkar together with Jesse Riedl and Gilles Demouchy.

Viscosity measurements were performed by the author together with Kaspars Erglis and Dmirty Zablotsky.

Dynamic Light Scattering measurements were performed by Amandine Anfry and Emmanuelle Dubois.

A share of mathematical descriptions is the contribution of thesis advisor Elmars Blums.

Appendix A

Ferrofluid nanoparticle size distributions

Particle magnetic size distributions for all four ferrofluids used in the research presented in this thesis are given here. Ferrofluids df105, S-1 and U5 were synthesized in Institute of Physics, University of Latvia, by Gunars Kronkalns. Ferrofluid FF 13-04 synthesized in Laboratory of Magnetic Soft Materials, Faculty of Physics, Mathematics and Optometry, University of Latvia, by Oksana Petricenko. Particle magnetic sizes measured with Vibrating sample magnetometry by Michail M. Maiorov.

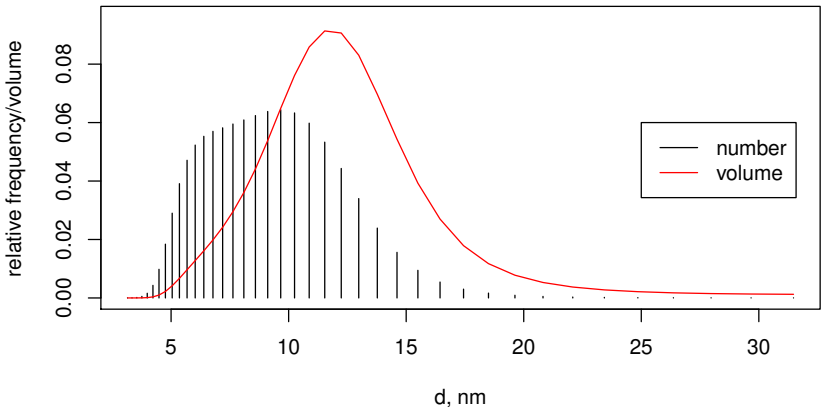

Figure A.1: Nanoparticle size distribution (magnetic phase) in ferrofluid df105 as relative frequency and fraction of volume

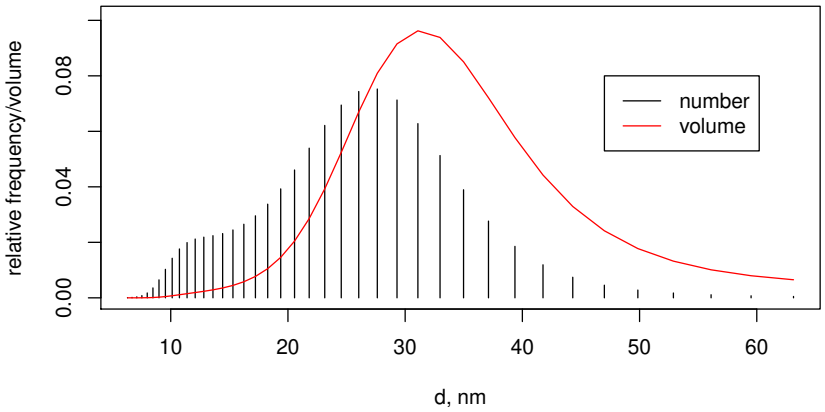

Figure A.2: Nanoparticle size distribution (magnetic phase) in ferrofluid FF 13-04 as relative frequency and fraction of volume

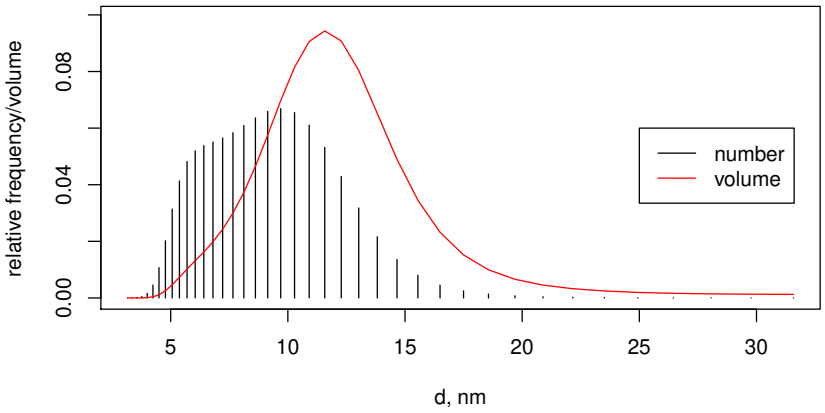

Figure A.3: Nanoparticle size distribution (magnetic phase) in ferrofluid U5 as relative frequency and fraction of volume

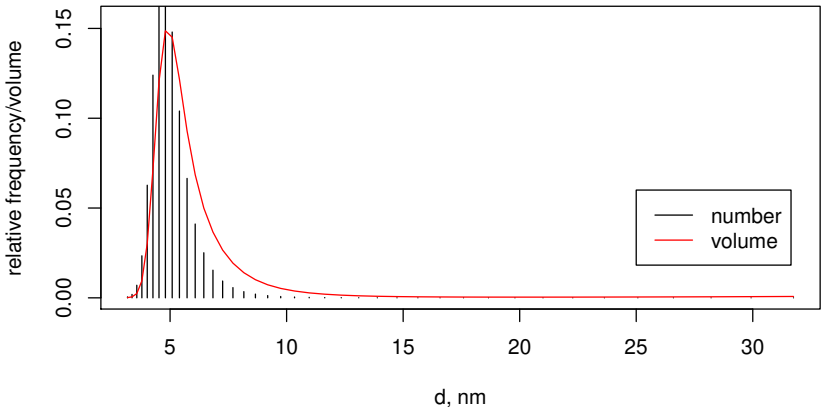

Figure A.4: Nanoparticle size distribution (magnetic phase) in ferrofluid S-1 as relative frequency and fraction of volume

Appendix B

Interpreting surfactant redistribution in thermoosmosis experiments

Provided here is an attempt to interpret results of thermoosmosis of a tetradecane - oleic acid mixture, given in chapter 7. The analysis given here should be treated as accompanying the conclusions presented in sect. 7.4.

With the observed effects of surfactant concentration on $d_{T,eff}$ having failed to provide much insight in the phenomena of interest, we turn our attention to possible mechanisms behind the changes in $d_{T,eff}$. The purpose of this investigation is attempting to determine the mechanism behind both reduction of thermoosmotic coefficient in thermoosmosis experiments and the increasingly thermophilic behavior of colloidal particles in thermophoresis experiments - both phenomena emerging as increasing amounts of surfactant are added to the fluid.

For this purpose, we try to relate effects of surfactant on thermoosmosis to surfactant molecule redistribution under a temperature gradient. In sect. 7.2, we made the assumption that all thermally induced motion of the fluid that is driven by surfactant is embodied in the coefficient d_T^*. To offer an interpretation for the results of thermoosmosis experiments, we make a further assumption that, in pressure mode experiments, the mechanism of surfactant molecule thermal transport can be expressed in the general shape of the Soret effect, as given in sect. 1.5:

$$\nabla c_s = -c_s(1-c_s)S_{T,eff}\nabla T \tag{B.1}$$

$c_s, \%$	$d_{eff}S_{T,eff}^{normalized}$	$\pm dS_{T,eff}^{normalized}$
0.5	1.00	0.20
1.0	1.59	
1.5	1.36	
2.5	0.66	

Table B.1: Dependence of normalized product of effective osmotic coefficient and Soret coefficient on surfactant volume concentration

Where $S_{T,eff}$ is the effective Soret coefficient of oleic acid molecules in the porous environment. Now, eq. B.1 can be inserted in eq. 7.1, and arrive at flow equation in the form:

$$\vec{j} = -\frac{K}{\nu}\nabla p - d_{eff}c_s(1-c_s)S_{T,eff}\nabla T + d_T\rho\nabla T \tag{B.2}$$

Here, d_{eff} is an effective osmotic coefficient of tetradecane in the tetradecane-oleic acid mixture. Equation B.2 can be rewritten as:

$$\vec{j} = -\frac{K}{\nu}\nabla p + (d_T - d_{eff}c_s(1-c_s)S_{T,eff})\rho\nabla T \tag{B.3}$$

By analogy with eq. 7.4, d_T^* would be defined as:

$$d_T^* = -d_{eff}c_s(1-c_s)S_{T,eff} \tag{B.4}$$

We therefore attempt to characterize d_T^*, which embodies the contribution of surfactant related effects to thermally induced flow of carrier fluid - surfactant mixture, as proportional to an effective Soret coefficient of oleic acid molecules in the porous environment, to an effective osmotic coefficient of the carrier fluid in a carrier fluid - surfactant mixture, and to concentration of the surfactant.

Knowing the surfactant concentration values, we calculate $d_{eff}S_{T,eff}$ from d_T^*, arriving at positive values with order of magnitude $\sim 10^{-10}\frac{m^2}{s\cdot K}$. The values are normalized to $d_{eff}S_{T,eff}(c_s = 0.5\%)$ - the lowest surfactant concentration we have data from. Results of this analysis are presented in table B.1.

Splitting of $d_{eff}S_{T,eff}$ is not possible without additional experimental work. It could be assumed that d_{eff} is positive - that is, to assume that carrier fluid would flow towards higher surfactant concentration, which would

be the case is carrier fluid flow would be driven by an osmotic process. In this case, value of effective Soret coefficient for surfactant molecules would also be positive in the experimentally investigated range of oleic acid concentration - surfactant transport directed to lower temperatures. Then, thermophilic behavior of colloidal particles would correspond to motion of those particles away from higher surfactant concentration.

If carrier fluid flow would instead be driven by Marangoni effect on pore walls, it would be directed towards a lower surfactant concentration, implying negative values for d_{eff} and effective coefficient of proportionality between surfactant concentration and temperature (replacing S_T). Following the same considerations as before, we would now conclude that colloidal particles of the ferrofluid moving towards higher temperatures move towards a higher surfactant concentration. The body of experimental data at hand does not enable us to identify the transport mechanism here. It must therefore be admitted that, while the addition of oleic acid does influence thermally induced flow of tetradecane beyond the effect of increased viscosity, our options to determine either the mechanism through which this influence is exerted or the implications it would have on colloidal particle thermophoresis are exhausted without arriving to a clear conclusion.

Bibliography

[1] E. Blums, A. Cebers, and M. Maiorov, *Magnetic Fluids*. Walter de Gruyter, 1997.

[2] S. Odenbach, "Ferrofluids—magnetically controlled suspensions," *Colloids and Surfaces A: Physicochemical and Engineering Aspects*, vol. 217, no. 1, pp. 171 – 178, 2003. Symposium C of the E-MRS 2002 Spring Meeting in Strasbourg, France.

[3] E. Shojaeizadeh, F. Veysi, and K. Goudarzi, "Heat transfer and thermal efficiency of a lab-fabricated ferrofluid-based single-ended tube solar collector under the effect of magnetic field: An experimental study," *Applied Thermal Engineering*, vol. 164, p. 114510, 2020.

[4] M. Vasilakaki, I. Chikina, V. B. Shikin, N. Ntallis, D. Peddis, A. A. Varlamov, and K. N. Trohidou, "Towards high-performance electrochemical thermal energy harvester based on ferrofluids," *Applied Materials Today*, vol. 19, p. 100587, 2020.

[5] J.-H. Kim, H.-S. Seo, and Y.-J. Kim, "Thermal-flow characteristics of ferrofluids in a rotating eccentric cylinder under external magnetic force," *Micromachines*, vol. 9, no. 9, p. 457, 2018.

[6] S. Wiegand, "TOPICAL REVIEW: Thermal diffusion in liquid mixtures and polymer solutions," *Journal of Physics Condensed Matter*, vol. 16, pp. R357–R379, mar 2004.

[7] P. Geelhoed, J. Westerweel, S. Kjelstrup, and D. Bedeaux, *Thermophoresis*, pp. 3305–3309. 01 2015.

[8] R. Piazza and A. Parola, "Thermophoresis in colloidal suspensions," *Journal of Physics: Condensed Matter*, vol. 20, p. 153102, mar 2008.

[9] R. Lanfranco, F. Giavazzi, M. Salina, E. D. Nicolò, and M. Buscaglia, "Optical Detection of Surfactants by Means of Reflective Phantom Interface Method," in *Sensors. Lecture Notes in Electrical Engineering* (D. Compagnone, F. Baldini, C. D. Natale, G. Betta, and P. Siciliano, eds.), vol. 319 of *Lecture Notes in Electrical Engineering*, pp. 33–37, Springer, 2015.

[10] P. Costesèque, T. Pollak, J. K. Platten, and M. Marcoux, "Transient-state method for coupled evaluation of soret and fick coefficients, and related tortuosity factors, using free and porous packed thermodiffusion cells: Application to cuso4 aqueous solution (0.25m)," *Eur Phys J E Soft Matter*, vol. 15, no. 3, pp. 249–253, 2004.

[11] B. Elhajjar, A. Mojtabi, P. Costesèque, and M.-C. Charrier-Mojtabi, "Separation in an inclined porous thermogravitational cell," *International Journal of Heat and Mass Transfer*, vol. 53, no. 21, pp. 4844 – 4851, 2010.

[12] D. Melnikov and V. Shevtsova, "Separation of a binary liquid mixture in compound system: Fluid–porous–fluid," *Acta Astronautica*, vol. 69, no. 7, pp. 381 – 386, 2011.

[13] E. Blums, G. Kronkalns, M. M. Maiorov, and A. Mezulis, "Thermoosmotic transfer of sterically stabilized ferrofluid particles in non-isothermal capillary porous layer," *J. Magn. Magn. Mat.*, vol. 289, pp. 275–277, 2005.

[14] G. Mèriguet, G. Demouchy, E. Dubois, R. Perzynski, and A. Bourdon, "Experimental determination of the soret coefficient of ionic ferrofluids influence of the volume fraction and the ionic strength," *Journal of Non-Equilibrium Thermodynamics,*, vol. 32, pp. 271–279, 2007.

[15] M. Sarkar, J. C. Riedl, G. Demouchy, F. Gélébart, G. Mériguet, V. Peyre, E. Dubois, and R. Perzynski, "Inversion of thermodiffusive properties of ionic colloidal dispersions in water-dmso mixtures probed by forced rayleigh scattering," *Eur Phys J E Soft Matter*, vol. 42(6), no. 72, 2019.

[16] T. Voelker and S. Odenbach, "Thermodiffusion in ferrofluids in the presence of a magnetic field," *Physics of Fluids*, vol. 17, no. 3, p. 037104, 2005.

[17] E. Blums, "New transport properties of ferrocolloids: magnetic soret effect and thermomagnetoosmosis," *Journal of Magnetism and Magnetic Materials*, vol. 289, pp. 246 – 249, 2005. Proceedings of the 10th International Conference on Magnetic Fluids.

[18] E. Blums, V. Sints, A. Mezulis, and G. Kronkalns, "New problems of mass transport in magnetic fluids," *Magnetohydrodynamics*, vol. 49, no. 3-4, pp. 360 – 367, 2013.

[19] R. E. Rosensweig, *Ferrohydrodynamics*. Courier Corporation, 1997.

[20] M. Doi, *Soft Matter Physics*. Oxford, New York: Oxford University Press, 2013.

[21] J.-C. Bacri, R. Perzynski, D. Salin, V. Cabuil, and R. Massart, "Ionic ferrofluids: A crossing of chemistry and physics," *Journal of Magnetism and Magnetic Materials*, vol. 85, no. 1, pp. 27 – 32, 1990.

[22] C. Scherer and A. M. F. Neto, "Ferrofluids: Properties and applications," *Brazilian Journal of Physics*, vol. 35, no. 3A, pp. 718–727, 2005.

[23] L. Zhang, R. He, and H.-C. Gu, "Oleic acid coating on the monodisperse magnetite nanoparticles," *Applied Surface Science*, vol. 253, no. 5, pp. 2611–2617, 2006.

[24] D. Susan-Resiga, V. Socoliuc, T. Boros, T. Borbáth, O. Marinica, A. Han, and L. Vékás, "The influence of particle clustering on the rheological properties of highly concentrated magnetic nanofluids," *Journal of Colloid and Interface Science*, vol. 373, no. 1, pp. 110 – 115, 2012. The 1st International Symposium on Colloids and Materials: New Scientific Horizons.

[25] V. Buzmakov and A. Pshenichnikov, "On the structure of microaggregates in magnetite colloids," *Journal of Colloid and Interface Science*, vol. 182, no. 1, pp. 63 – 70, 1996.

[26] A. Hoell, M. Kammel, A. Heinemann, and A. Wiedenmann, "Solvent dependent arrangement of shell molecules in ferrofluids studied by small-angle scattering with polarized neutrons," *J. Appl. Cryst.*, vol. 36, pp. 558–561, 2003.

[27] M. M. Maiorov, D. Zablotsky, E. Blums, and A. Krumina, "Model colloids to study surface – ligand interactions in nanosized Fe_3O_4," *IOP Conf. Ser.: Mater. Sci. Eng.*, vol. 503, p. 012029, 2019.

[28] H. B. Callen, *Thermodynamics and an introduction to thermostatistics; 2nd ed.* New York, NY: Wiley, 1985.

[29] S. J. Blundell and K. M. Blundell, *Concepts in Thermal Physics (Second edition).* Oxford, New York: Oxford University Press, 2009.

[30] P. Mazur and S. R. de Groot, "On onsager's relations in a magnetic field," *Physica*, vol. 19, no. 1–12, pp. 961–970, 1953.

[31] N. V. Churaev, *Physical Chemistry of Heat and Mass Transfer Processes in Porous Media.* Moscow: Himiya, 1990. In Russian.

[32] E. Blums, G. Kronkalns, A. Mezulis, and V. Sints, "Non–isothermal mass transfer of ferrocolloids through porous membrane," *J. Magn. Magn. Mat.*, vol. 323, no. 10, pp. 1334–1337, 2011.

[33] A. Würger, "Do thermal diffusion and dufour coefficients satisfy onsager's reciprocity relation?," *European Physical Journal E*, vol. 37, no. 10, p. 96, 2014.

[34] P. Costesèque, A. Mojtabiab, and J. K. Plattenc, "Thermodiffusion phenomena," *Comptes Rendus Mecanique*, vol. 339, no. 5, pp. 275–279, 2011.

[35] A. Würger, "Is soret equilibrium a non-equilibrium effect?," *Comptes Rendus Mécanique*, vol. 341, no. 4, pp. 438–448, 2013. 10th International Meeting on Thermodiffusion.

[36] P. Geelhoed, R. Lindken, and J. Westerweel, "Thermophoretic separation in microfluidics," *Chemical Engineering Research and Design*, vol. 84, no. 5, pp. 370–373, 2006. International Conference on Sustainable (Bio)Chemical Process Technology.

[37] A. L. Sehnem, R. Aquino, A. F. C. Campos, F. A. Tourinho, J. Depeyrot, and A. M. Figueiredo Neto, "Thermodiffusion in positively charged magnetic colloids: Influence of the particle diameter," *Phys. Rev. E*, vol. 89, p. 032308, Mar 2014.

[38] R. Piazza, "Thermophoresis: moving particles with thermal gradients," *Soft Matter*, vol. 4, no. 9, p. 1740, 2008.

[39] H. Brenner, "Navier–stokes revisited," *Physica A: Statistical Mechanics and its Applications*, vol. 349, no. 1, pp. 60 – 132, 2005.

[40] S. N. Semenov and M. E. Schimpf, "Molecular thermodiffusion (thermophoresis) in liquid mixtures," *Phys. Rev. E*, vol. 72, p. 041202, Oct 2005.

[41] K. I. Morozov, "On the Theory of the Soret Effect in Colloids," in *Thermal Nonequilibrium Phenomena in Fluid Mixtures* (W. Köhler and S. Wiegand, eds.), vol. 584 of *Lecture Notes in Physics*, p. 38, Springer-Verlag, 2002.

[42] E. Ruckenstein *J. Colloid Int. Sci.*, vol. 83, p. 77, 1981.

[43] B. V. Derjaguin and G. P. Sidorenkov *Dokl. Acad. Nauk SSSR*, vol. 32, p. 622, 1941.

[44] J. Villaluenga, B. Seoane, V. Barragán, and C. Ruiz-Bauzá, "Thermo-osmosis of mixtures of water and methanol through a nafion membrane," *Journal of Membrane Science*, vol. 274, no. 1, pp. 116 – 122, 2006.

[45] A. P. Bregulla, A. Würger, K. Günther, M. Mertig, and F. Cichos, "Thermo-osmotic flow in thin films," *Phys. Rev. Lett.*, vol. 116, p. 188303, May 2016.

[46] A. Parola and R. Piazza, "Particle thermophoresis in liquids," *Eur Phys J E Soft Matter*, vol. 15, no. 3, pp. 255–263, 2004.

[47] S. Iacopini, R. Rusconi, and R. Piazza, "The "macromolecular tourist": Universal temperature dependence of thermal diffusion in aqueous colloidal suspensions," *Eur Phys J E Soft Matter*, vol. 19, pp. 59–67, 2006.

[48] S. Iacopini and R. Piazza, "Thermophoresis in protein solutions," *Europhys. Lett.*, vol. 63, p. 247, 2003.

[49] I. Dueramae, M. Yoneyama, N. Shinyashiki, S. Yagihara, and R. Kita, "Thermal diffusion of aqueous solution of acetylated dextran: The effect of hydrophobicity using optical beam deflection technique," *Inter-*

national Journal of Heat and Mass Transfer, vol. 132, pp. 997 – 1003, 2019.

[50] S. A. Putnam, D. G. Cahill, and G. C. L. Wong, "Temperature dependence of thermodiffusion in aqueous suspensions of charged nanoparticles," *Langmuir*, vol. 23, no. 18, pp. 9221–9228, 2007. PMID: 17655335.

[51] R. Kita, G. Kircher, and S. Wiegand, "Thermally induced sign change of soret coefficient for dilute and semidilute solutions of poly(n-isopropylacrylamide) in ethanol," *The Journal of Chemical Physics*, vol. 121, no. 18, pp. 9140–9146, 2004.

[52] H.Davarzani, M.Marcoux, and M.Quintard, "Theoretical predictions of the effective thermodiffusion coefficients in porous media," *Int. J. Heat Mass Transfer*, vol. 53, no. 7-–8, pp. 1514–1528, 2010.

[53] H. Davarzani, M. Marcoux, P. Costeseque, and M. Quintard, "Experimental measurement of the effective diffusion and thermodiffusion coefficients for binary gas mixture in porous media," *Chemical Engineering Science*, vol. 65, no. 18, pp. 5092–5104, 2010.

[54] A. Ahadi, C. Giraudet, H. Jawad, F. Croccolo, H. Bataller, and M. Saghir, "Experimental, theoretical and numerical interpretation of thermodiffusion separation for a non-associating binary mixture in liquid/porous layers," *International Journal of Thermal Sciences*, vol. 80, pp. 108 – 117, 2014.

[55] J. Colombani, G. Galliéro, B. Duguay, J.-P. Caltagirone, F. Montel, and P. A. Bopp, "A molecular dynamics study of thermal diffusion in a porous medium," *Phys. Chem. Chem. Phys.*, vol. 4, no. 2, pp. 313–321, 2002.

[56] V. Yasnou, A. Mialdun, D. Melnikov, and V. Shevtsova, "Role of a layer of porous medium in the thermodiffusion dynamics of a liquid mixture," *International Journal of Heat and Mass Transfer*, vol. 143, p. 118480, 2019.

[57] J. K. Platten and P. Costeseque, "The soret coefficient in porous media," *Journal of Porous Media*, vol. 7, no. 4, 2004.

[58] J. L. Anderson, "Colloid transport by interfacial forces," *Ann. Rev. Fluid Mech.*, vol. 21, pp. 61–99, 1989.

[59] E. Blums, V. Sints, G. Kronkalns, and A. Mezulis, "Non-isothermal separation of ferrofluid particles through grids: Abnormal magnetic soret effect," *Comptes Rendus Mécanique*, vol. 341, no. 4-5, pp. 348–355, 2013.

[60] T. A. Franklin, "Ferrofluid flow phenomena," Master's thesis, Massachusetts Institute of Technology, 2003.

[61] J.-C. Bacri, A. Cebers, A. Bourdon, G. Demouchy, B. M. Heegaard, B. Kashevsky, and R. Perzynski, "Transient grating in a ferrofluid under magnetic field: Effect of magnetic interactions on the diffusion coefficient of translation," *Phys. Rev. E*, vol. 52, pp. 3936–3942, Oct 1995.

[62] A. O. Tsebers, "Thermodynamic stability of magnetofluids," *Magnetohydrodynamics*, vol. 18, no. 2, pp. 137–142, 1982.

[63] R. G. Larson, *The Structure and Rheology of Complex Fluids*. Oxford, New York: Oxford University Press, 11 1998.

[64] M. Abareshi, S. H. Sajjadi, S. M. Zebarjad, and E. K. Goharshadi, "Fabrication, characterization, and measurement of viscosity of α-Fe_2O_3-glycerol nanofluids," *Journal of Molecular Liquids*, vol. 163, no. 1, pp. 27–32, 2011.

[65] J. Tothova, J. Kovac, P. Kopcansky, M. Rajnak, K. Paulovicova, M. Timko, and A. Jozefczak, "Viscosity dependence of a magnetic fluid nanoparticles concentration," *Acta Physica Polonica A*, vol. 126, no. 1, pp. 278–279, 2014.

[66] J. Yang, H. Yan, Z. Hu, and D. Ding, "Viscosity and sedimentation behaviors of the magnetorheological suspensions with oleic acid/dimer acid as surfactants," *J. Magn. Magn. Mat.*, vol. 417, pp. 214–221, 2016.

[67] E. Blums, M. M. Maiorov, and G. Kronkalns, "Thermomagnetic properties of ferrofluids containing chemically coprecipitated mn-zn ferrite particles," *IEEE Transaction on magnetics*, vol. 29, no. 6, p. 3267, 1993.

[68] G. Kronkalns, "Formation and magnetic properties of mn-zn ferrites nanoparticles," *Magnetohydrodynamics*, vol. 39, no. 2, pp. 215–233, 2003.

[69] G. Kronkalns, M. Kodols, and M. M. Maiorov, "Structure, composition and magnetic properties of ferrofluid nanoparticles after separation," *Latv. J. Phys. Tech. Sci.*, vol. 50, no. 4, pp. 56–61, 2013.

[70] Z. Zarnegar and J. Safari, "Modified chemical coprecipitation of magnetic magnetite nanoparticles using linear –dendritic copolymers," *Green chemistry letters and reviews*, vol. 10, no. 4, pp. 235–240, 2017.

[71] R. Tadmor, R. E. Rosensweig, J. Frey, and J. Klein, "Resolving the puzzle of ferrofluid dispersants," *Langmuir*, vol. 16, no. 24, pp. 9117–9120, 2000.

[72] O. Petrichenko, A. Plotniece, K. Pajuste, V. Ose, and A. Cebers, "Formation of magnetoliposomes using self-assembling 1,4-dihydropyridine derivative and maghemite γ-Fe_2O_3 nanoparticles," *Chem. Heterocycl. Compd.*, vol. 51, no. 7, pp. 672–677, 2015.

[73] K. K. Tan, Y. M. Tan, and T. S. Y. Choong, "Onset of natural convection induced by bottom–up transient mass diffusion in porous media," *Powder Technology*, vol. 191, pp. 55–60, 2009.

[74] V. Sints, E. Blums, M. Maiorov, and G. Kronkalns, "Diffusive and thermodiffusive transfer of magnetic nanoparticles in porous media," *Eur Phys J E Soft Matter*, vol. 38, no. 5, p. 119, 2015.

[75] A. Mahidjiba, M. Mamou, and P. Vasseur, "Onset of double-diffusive convection in a rectangular porous cavity subject to mixed boundary conditions," *Int. J. Heat Mass Transfer*, vol. 43, no. 9, pp. 1505–1522, 2000.

[76] A. Mezulis, *Mass Transport Phenomenon in Non-Isothermic Magnetic Colloids*. PhD thesis, University of Paris 7, France, and Institute of Physics, University of Latvia, Latvia, 1997.

[77] D. O. Smith, "Development of a vibratingcoil magnetometer," *Rev. Sci. Instrum.*, vol. 27, no. 5, pp. 261–268, 1956.

[78] M. M. Maiorov, E. Blums, and K. Raj, "Inverse task for evaluation of particle size distribution of polydisperse magnetic fluids," *Physics Procedia*, vol. 9, pp. 74–77, 2010.

[79] V.Sints, E.Blums, G.Kronkalns, K.Erglis, and M.M.Maiorov, "Experimental research of surfaced nanoparticle thermal transport in a porous medium," *Int. J. Heat Mass Transfer*, vol. 125, pp. 580–588, 2018.

[80] J. Chen and K. J. Stebe, "Surfactant-induced retardation of the thermocapillary migration of a droplet," *Journal of Fluid Mechanics*, vol. 340, p. 35–59, 1997.

[81] E. Guyon, J.-P. Hulin, L. Petit, and C. D. Mitescu, *Physical Hydrodynamics*. Oxford, New York: Oxford University Press, 6 2001.